4-17-2019

Characterization of Graphene Oxide

Harish Kumar
University of Connecticut - Storrs, harish.kumar@uconn.edu

Characterization of Graphene Oxide

Harish Kumar, Ph.D.

University of Connecticut, 2019

Abstract

The conversion of graphite to graphene oxide (GO) is an effective and widely used method for solubilizing and exfoliating graphite. However, the oxidation is not uniform, and wide variations in the degree of oxidation exist between and within batches of GO. In this dissertation, we introduce an approach to both quantify the global degree of oxidation in GO and to separate GO into fractions, each with more uniform extents of oxidation. Using the formation of GO-stabilized oil-in-water emulsions, GO is separated into an emulsion fraction and a water fraction. The results find that the GO sheets that stabilize the emulsion droplets are less oxidized than sheets suspended in water as shown by multiple characterization techniques. The use of successive fractionation allows not only for the preparation of GO fractions with more narrowly defined properties but also provides a method for characterizing GO batches. Further, this fractionation method is applied to statistically determine the distribution of oxidation within a GO batch and used to calculate a number called oxidation dispersity (OD). Various properties of these GO fractions, such as optical, electrochemical, electrical, mechanical, and biocompatible were also investigated. Another study is focused on the changes occurring in GO sheets in different environments, like water

or air, with time. The degree of oxidation and Raman defects appear to be changing as the GO ages. This phenomenon affects the outlook for GO applications and provides a better understanding of GO kept for storage. This fractionation method and aging study promise to provide the field with some critical missing pieces: a straightforward and standard method for the global characterization and comparison of GO made by different procedures, and the effects aging has on GO and its most important properties.

Characterization of Graphene Oxide

Harish Kumar

Integrated 5-Year M.Tech., Indian Institute of Technology Roorkee, 2011

A Dissertation

Submitted in Partial Fulfillment of the

Requirements for the Degree of

Doctor of Philosophy

at the

University of Connecticut

2019

2019

APPROVAL PAGE

Doctor of Philosophy Dissertation

Characterization of Graphene Oxide

Presented by

Harish Kumar, M. Tech.

Major Advisor

_____

Prof. Douglas H. Adamson

Associate Advisor

_____

Prof. Richard S. Parnas

Associate Advisor

_____

Prof. Yao Lin

University of Connecticut

2019

Acknowledgements

This work could not have been accomplished without the help and support of my advisor, colleagues, friends, and family. First, I would like to thank my major advisor Prof. Douglas Adamson who served as a mentor for my graduate studies and provided funding for the research and opportunities to travel to various meetings and conferences. He encouraged me to step out of my comfort zone into the fields of physical chemistry, colloids, and graphene-based materials, which make up virtually the entirety of this dissertation. His doors were always open for ideas or inputs on my research work and manuscript writing.

I would also like to thank Prof. Richard S. Parnas for being an excellent mentor. I took his three graduate courses that helped me a lot in understanding and resolving a number of problems related to materials science during my experimental research. I am very fond of his teaching skills which made complicated topics look very simple and easier to understand. I am very thankful to Prof. Yao Lin for going beyond the role of an associate advisor. Also, I learned a lot about materials characterization as a student and later as a TA from Prof. Yao Lin's Characterization-I course. I learned both theoretical and experimental parts of XRD, Raman, FTIR, and thermal analysis techniques in his mentorship which helped me in the characterization of graphene oxide fractions very quickly in the first year of my Ph.D. studies. I am thankful to Prof. Mu-Ping Nieh and Prof. Stefan Schaffoener for attending my Ph.D. defense talk despite having a very busy schedule.

I would also like to thank Prof. Schniepp and his Research Group for providing support in the optical analysis of GO samples, Prof. Asandei Research and his Research Group for allowing me to carry out experiments in his lab, Prof. Gregory Sotzing and his Research Group for their help with lab instruments.

Also, much thanks to the staff in the IMS especially Laura Pinatti for countless hours of help, arguments and discussion on a wide variety of topics, Gary Lavigne for his help learning and using various spectroscopic instruments, Jack Gromek and Daniela Morales for helping me with X-Ray analysis, and Lichun Zhang for his training and help with obtaining beautiful SEM pictures.

I would also like to thank everyone in my research group for working and dealing with me for all these years, especially Chinthani Leliyang and Elizabeth Brown with whom I have worked very closely on a number of projects. Whenever I was stuck with a problem, someone from my group was happy to help me out. I also need to thank my undergraduate student Thomas Francis who worked to help me run numerous experiments that I could not have carried out single-handedly. I am very grateful to Peter Kerns and Veronica Hayes in UConn Chemistry, Laura Fajardo in UConn Pharmacy, Alessandro Palmieri in UConn Engineering, Vignesh Vasu, Mengfang Li, Huseini Patanwala and Sneh Sinha in UConn-Polymer Program, Sudeep Bapat in UConn-Statistics, and William Dickinson in The College of William & Mary for helping me with their excellent skillsets in different areas.

I also have to give a great deal of thanks to my parents, Sh. Vijay Pal Singh and Smt. Sushila Devi, for instilling in me a curiosity for mathematics and science in the first place as well as for the love and support they have given me throughout my life. Lastly, I owe perhaps the greatest amount of gratitude to my wife, Khushboo, for her love, support, and, most importantly, patience throughout my graduate career. She encouraged me, motivated me, and most of all stood by me through these grueling years of my life.

Table of Contents

List of Figures

List of Tables

Chapter 1: Introduction to Graphene and Graphene Oxide

1.1 Graphene

Graphene oxide (GO) is an oxidized product of graphite and is sometimes referred to (incorrectly) as graphene due to its exfoliated nature.[1,2,3] In order to understand the importance of GO, it is necessary to first know about graphene. Graphene is a two-dimensional sheet of sp^2-hybridized carbon atoms arranged in a honeycomb lattice. The combination of two equivalent sub-lattices of carbon atoms gives rise to a graphene honeycomb lattice. These carbon atoms are bonded together with sigma bonds in this honeycomb lattice, as shown in Figure 1-1a.[4] The π orbital of each carbon atom in the lattice contributes to the delocalization of electrons and is essential for the excellent properties of graphene.[1] Monte Carlo simulations[4] and transmission electron microscopy (TEM) studies address the presence or absence of freely suspended graphene has 'intrinsic' ripples.[5] A lateral dimension of about 8-10 nm and a height displacement of about 0.7 to 1 nm were estimated in the microscopic corrugations (Figure 1-1b).[4]

Graphene has been described as "the mother of all carbon allotropes," as it can be wrapped into zero-dimensional fullerenes, rolled into one-dimensional carbon nanotubes, or stacked into three-dimensional graphite.[1] Until its discovery in 2004 by

Novoselov et al., it was thought that a two-dimensional carbon material was thermodynamically unstable[6] and could only serve to form three-dimensional structures. Geim and Novoselov were the first to successfully isolate and experimentally determine the properties of a single layer of graphene,[7] which eventually earned them the Nobel Prize in physics in 2010.

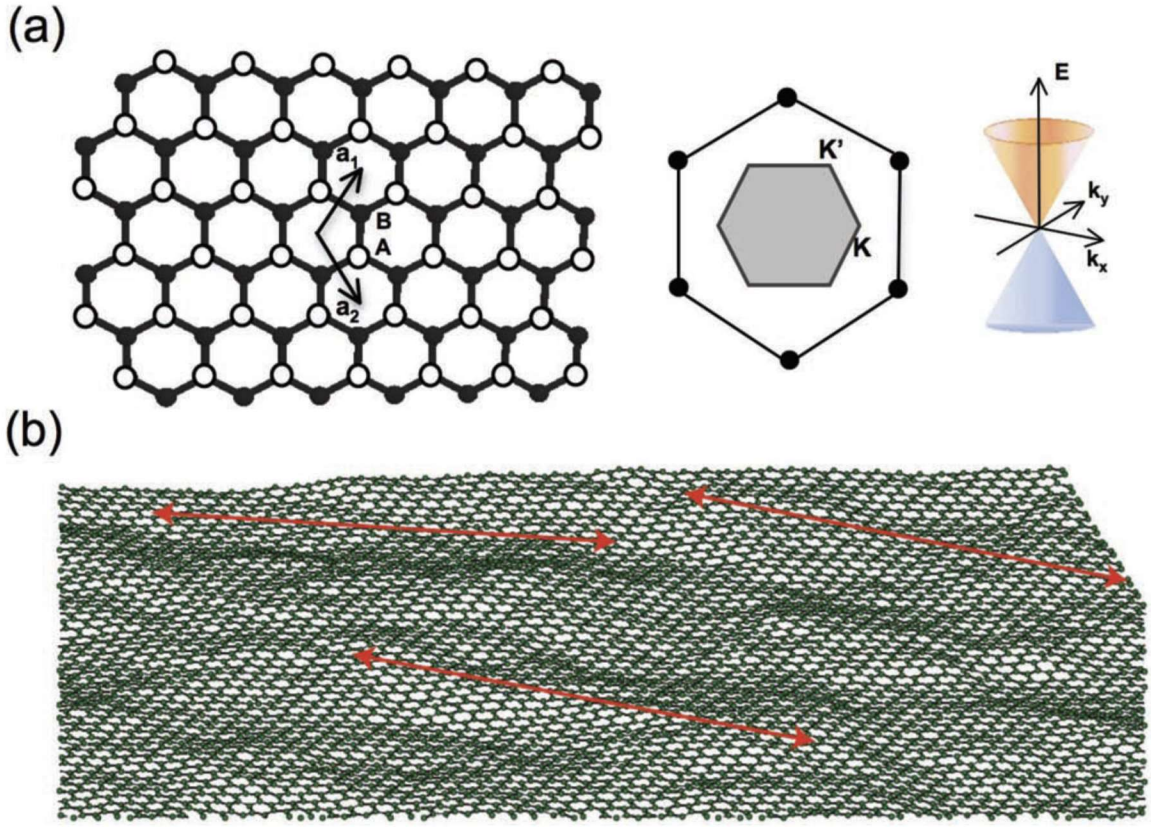

Figure 1-1. (a) Schematics of the crystal structure, Brillouin zone and dispersion spectrum of graphene; (b) 'Rippled graphene' from a Monte Carlo simulation. The red arrows are ~ 8 nm long.[4] Reproduced with permission from Nature Publishing Group.[4]

Ever since the initial isolation of graphene, its unique chemical, electronic and physical properties have become the focal point of considerable research. Graphene has a tensile modulus of 1 TPa,[8] a thermal conductivity of 5,000 W m^{-1} K^{-1},[9] a specific surface area of 2,630 m^2 g^{-1},[10] an electron mobility of 250,000 cm^2 V^{-1} s^{-1}, [11] good chemical stability,[12] transmittance of 97.7% of visible light,[9] and is very sensitive to electrical perturbations.[13] These properties of graphene sheets make it an attractive material for a variety of applications. For example, graphene can be used as a transparent conductive material,[14–17] supercapacitor,[18–20] for hydrogen storage,[21,22] and for chemical sensors.[13,23]

1.2 Outline

This dissertation focuses on exploring the structure/property relationships and synthesis mechanism of graphene oxide. In the past, most efforts in the graphene oxide (GO) community have focused on optimizing the performance of GO-based materials in applications rather than fundamental studies of the material itself. The first part of this dissertation investigates existing studies of GO synthesis. It introduces some common characterization techniques that are used for studying graphene oxide. Chapter 3: describes a method to cheaply and efficiently vary the properties of graphene oxide without carrying out a physical or chemical reaction. This method uses oil and water emulsion systems to produce various grades of GO material different from each other in terms of the degree of oxidation, and size. Chapter 4: contains a closer look at the distribution of oxidation of graphene oxide within a GO sample. A

fractionation method is used to define this qualitatively and quantitatively. Chapter 5: looks at the various properties of graphene oxide fractions, i.e. contact angle, transmission through films, fractions size variations, biocompatibility of polymer and GO-based materials, mechanical properties of polymers and GO fraction-based nanocomposites and electrochemical applications of the GO fractions. Chapter 6 defines two new generations of GO materials with unique properties where one is obtained from fractionation processes with no chemical reaction involved, the other is produced by physical modifications during the oxidation reaction for GO synthesis. Chapter 7: presents an aging study of graphene oxide. GO has been used for about two decades, but no research has been done on the effect of long term storage on GO. This study shows how aging has a very significant effect on GO materials.

1.3 Graphene Oxide

1.3.1 Structure of Graphene Oxide

Graphene oxide's structure, unlike graphene, is not identical when produced in different batches, with the oxygen functional groups uniquely distributed on each GO sheet.[24,25] Therefore, it is important to study and understand the underlying features of this material.

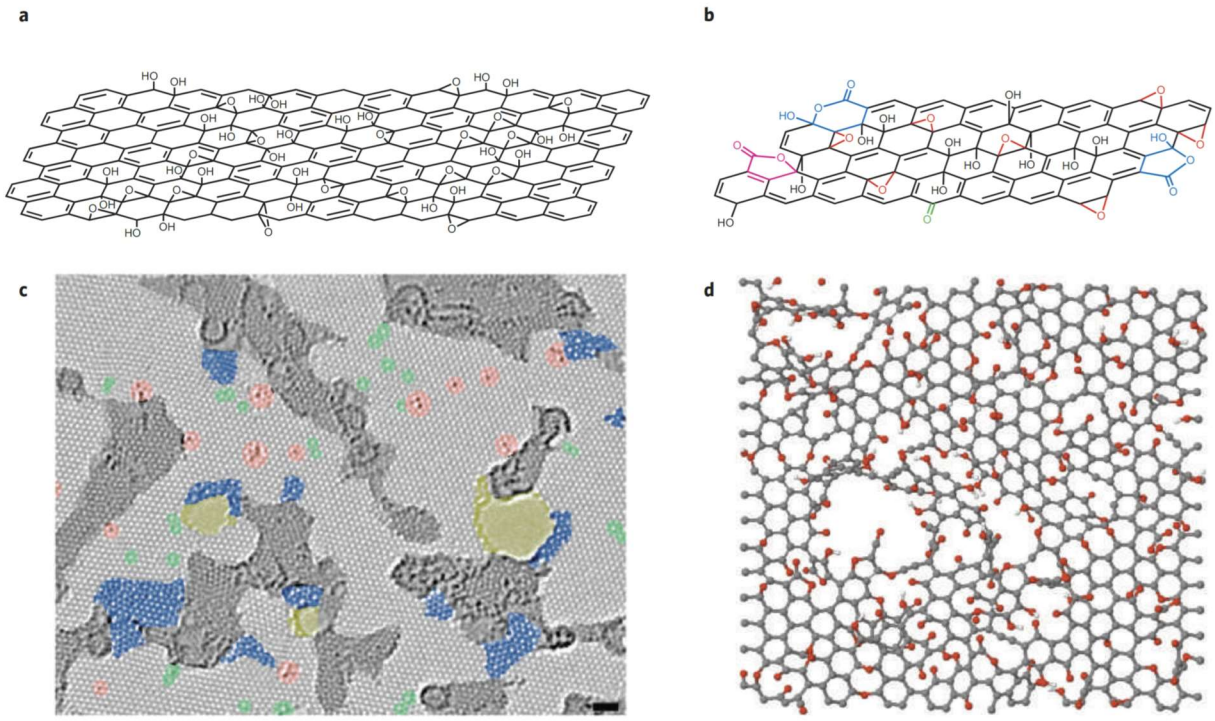

Figure 1-2. Description of molecular and atomic structures of Graphene Oxide (GO) and Reduced Graphene Oxide.[24] **a**, Lerf–Klinowski model describing the structure of single sheet structure of graphene oxide.[26] **b**, GO chemical structure described by Gvao and colleagues in 2009.[27] **c**, Atomic resolution, aberration-corrected high-resolution transmission electron micrograph of a single-layer rGO membrane.[28] Color scheme highlights the different structural features: dark grey, contaminated regions; blue, disordered single-layer carbon networks or extended topological defects; red, individual adatoms or substitutions; green, isolated topological defects; yellow, holes and their edge reconstructions. Scale bar: 1 nm.[28] **d**, Atomic model schematically illustrating disordered rGO basal plane consisting of holes, topological defects, and remnants of oxygen groups.[29]

The distance between adjacent layers in stacked GO sheets is known as the interlayer distance.[24] This interlayer distance, i.e. intrinsic thickness of GO flakes, is ~0.6 to 0.9 nm, from diffraction studies on dehydrated samples.[24,30] This distance is a

range for multiple reasons. It can vary depending upon the type of synthesis methods, dehydration method used, hydration due to storage, inherent properties of the precursor graphite used, i.e. synthetic or natural, size if GO sheets, etc. The GO flake size or lateral dimensions can range between a few nanometers to hundreds of micrometers.[31,32] A major reason behind this is the size of the starting graphite material. Also, the oxidation process breaks the sheets apart and changes the sheet size. Different synthesis methods can lead to different flake sizes. The Lerf–Klinowski model is one of the first widely accepted pictures for the structure of graphene oxide,[26] as shown in Figure 1-2a. It was supported by several investigators experimentally and represents a single atomically thin layer of GO with hydroxyl and epoxy groups.[24,33] However, chemically the reality different. Later, Gao and co-workers brought a new and better chemical structure of graphene oxide with 5 and 6-membered ring lactols present on the edges of the sheets. In-plane esters of tertiary alcohols are a majority in their model (Figure 1-2b).[27]

Gómez-Navarro and coworkers[28] reported a detailed high-resolution transmission electron micrograph of reduced graphene oxide (rGO).[34] This method has revolutionized the atomic scale topological studies of two-dimensional materials, especially graphene and derivatives as shown in Figure 1-2c.[28] For the first time, they showed the various defects in rGO structure at a very small (sub-nanometer) scale with various highlighted regions. This study has shown the groups of holes, Stone-Wales and other defects descriptively. In contrast with GO, very few calculated models have been proposed for reduced GO. Using first principles and molecular dynamics calculations, Bagri and coworkers[29] have shown the evolution of the atomic structure

of graphene oxide as a function of the extent of reduction of the material.[24] This study proposed a disordered picture of reduced graphene oxide which consists of holes in the basal plane as shown in Figure 1-2d. These holes appear due to the evolution of CO_2 and CO during the reduction process. The appearance of the holes is confirmed by the HR-TEM as demonstrated in Figure 1-2c. One other important piece of information that is obtained from this study[29] is that the oxygen functionalities present in GO are not identically attached in terms of stability. After the reduction process, there are some functionalities (residual oxygen is 7—8% of total rGO weight) that are still attached to the structure. They are highly stable carbonyl and ether groups that cannot be further removed unless the entire graphene plane is destroyed. This fact will be discussed more in the experimental sections in Chapter 7: where the GO loses oxygen functionalities with aging in natural dry storage environment but not much in an aqueous environment. This has a lot to do with the highly disproportionate stability of these functional groups.

1.4 Characterization Methods for Graphene Oxide

In addition to difficulties in the formation of single GO sheets, there are multiple problems associated with characterizing GO. A single layer of graphene absorbs only 2.3% of light, therefore is difficult to detect optically. Silicon wafers 100 nm or 300 nm in thickness can be used to visually observe monolayer graphene.[35] Two of the most commonly used methods are scanning probe microscopy[36–38] and Raman spectroscopy[39–41] in case of graphene and its derivatives like GO and rGO. These methods are used to identify the quantity and quality of graphene material.

1.4.1 Raman Spectroscopy

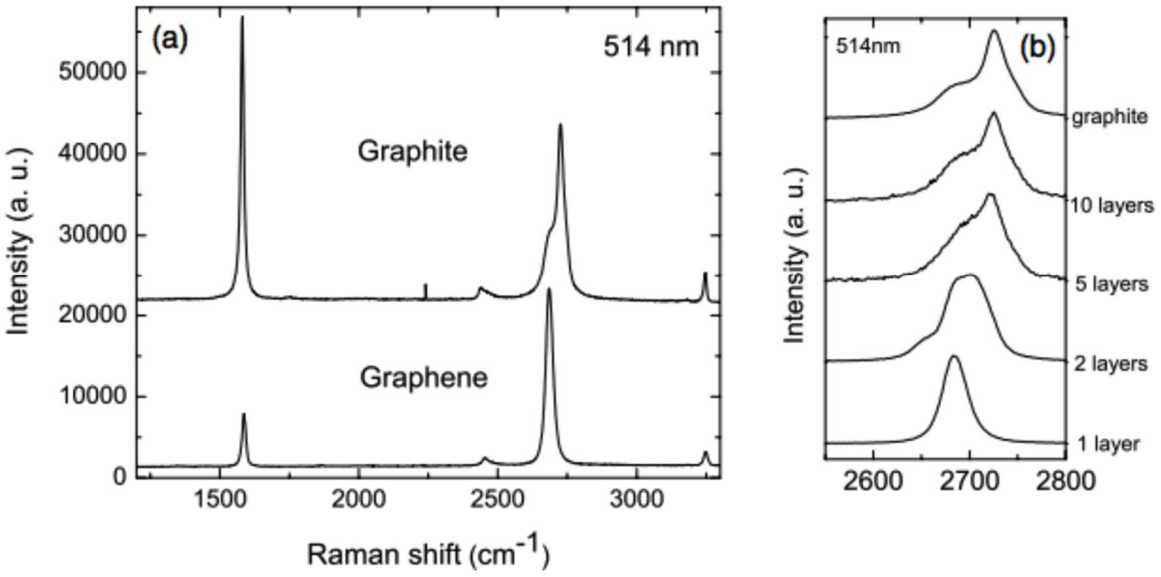

Figure 1-3. Raman spectra showing (a) the difference in peak intensities between the G peak at 1580 cm-1 and the 2D peak at ~2700 cm-1 for graphite compared to graphene and (b) the ability of the 2D peak to identify the number of graphene layers.[37] Copyright 2006 by The American Physical Society

The key peak of interest is known as either the 2D or the G' peak. It is located at approximately 2700 cm^{-1} and, like the G-peak, is present in all graphene samples. This peak is a result of a second order, two-phonon mode in the so called fingerprint region. The fingerprint region peak is used to determine the number of layers in graphite based on its location and shape (as shown in Figure 1-3b). Though Raman spectroscopy can provide a great deal of information regarding graphene sheets, additional characterization is necessary to identify the types and chemistries of the defects involved.[39,40]

Raman spectroscopy provides high-throughput quantitative data. It identifies the number of layers as well as the quality of sheets quickly with little need for sample preparation, which are limiting factors for SPM. The data obtained from Raman spectroscopy shows that changing the laser wavelengths has very little effect on the resulting spectra for graphene,[39] whereas other carbon materials such as carbon nanotubes exhibit wavelength-dependent peaks.[42] Spectra of graphene typically contain three main peaks of interest (see Figure 1-3a). The two primary peaks occur at approximately 1370 cm^{-1} and 1580 cm^{-1} and are referred to as the D and G peaks, respectively. The D-peak at around 1370 cm^{-1} corresponds to a radial breathing mode of the hexagons, which only arise when defects within the material are present. The G-peak is indicative of sp^2 hybridized carbon stretching and is constantly present. It will also shift and broaden depending on the chemical environment surrounding the graphene. For our Raman studies, a Renishaw System 2000 Raman microscope at λ= 514 nm using 50X objective lens was used. Samples were prepared by drying suspensions on a glass slide.

1.4.2 X-Ray Diffractometer

XRD analysis indicates the spacing of the stacked sheets, with the smaller peak at 2θ =26.6 arising from the 0.33 nm graphite stacking and the larger peak at 2θ=10-13.5 arising from the increased spacing due to the oxidation of the graphene sheets[43–46] A 2D X-Ray Diffractometer (XRD) (Bruker D2 Phaser) with radiation of wavelength =1.54 Å was used. The sample was prepared by drop casting a GO and water suspension onto a glass slide.

To compare all the XRD patterns of different GO's and GO fractions, we used the ratio r= A_{GO}/(A_{GO}+ A_G) where A_G is XRD graphite peak area (A_G), and A_{GO} is XRD GO peak area.[25] XRD GO, and G peak areas were calculated using the XRD instrument software.

1.4.3 Electrical Conductivity measurements

Dried GO films of size 2 cm x 1 cm x 190 μm were fabricated by drop-casting and their thickness was measured by a vernier caliper. The electrical conductivity of the dried GO film was calculated using a Fluke 25 Multimeter.

1.4.4 Optical Microscopy

Optical Microscopy is used to look at the size distribution of GO sheets. Due to the limited resolution available, the defect profile on GO sheets and the exfoliation details cannot be seen through this technique. Optical microscopy pictures were taken from a Nikon Diaphot Microscope.

1.4.5 Fourier Transform Infrared Spectroscopy

The large peak at 3400 cm^{-1} shows the O-H stretching vibrations in the GO samples. C=O stretching vibrations (1720cm^{-1}), C=C stretching vibrations (1580-1630cm^{-1}) in the GO plane, and C-O stretching vibrations (1250 cm^{-1}) were identified in the GO samples[4748]. FTIR spectra of GO is done using a Nicolet Magna 560 instrument.

1.4.6 Scanning Probe Microscopy

One of the benefits of scanning probe microscopy (SPM) is the ability to measure electronic properties at the surface of a material. Atomic force microscopy (AFM) is

the most common method of SPM associated with graphene. AFM requirements for scanning, sample preparation, and testing conditions are much more flexible than those of SPM techniques. With this method, a cantilever tip scans across an area of the sample while a laser measures subtle movement that translates into differences in height or attraction. Measurements are taken either in contact mode or tapping mode. Contact mode requires that the tip is dragged across the surface of the sample. Tapping mode oscillates the cantilever at a set frequency, and any changes detected in the oscillation height denote different interactions with the sample. The study of graphene through AFM has also revealed that observed height can vary from 0.6nm to 1nm depending on the type of substrate used and its interaction with the graphene sheets.

The other type of SPM is surface tunneling microscopy (STM); this technique brings a conductive tip in close proximity to the surface of a conductive material to measure the voltage difference between the two surfaces. An STM scan of graphite only shows three of the six carbons in a hexagonal arrangement.[49] This is due to electron density differences when the graphene sheets that make up graphite are stacked in an offset fashion. However, all six carbons of single layer graphene will be visible in STM scans. Additionally, any defects in the atomic structure can be visualized and quantified to determine the quality of the graphene.

1.4.7 X-ray photoelectron spectra (XPS)

The most commonly used method for elemental analysis of GO material is XPS. The instrument we used is PHI model Quantum 2000 spectrometer with scanning ESCA multiprobe (F Physical Electronics Industries Inc.), using Al Ka radiation

(l=1486.6 eV) as the radiation source. The spectra were recorded in the fixed analyzer transmission mode with pass energies of 187.85 eV and 29.35 eV for recording survey and high-resolution spectra, respectively. The thin film samples were pinned to a sample stage with a washer and screw then placed in the analysis chamber. The main chamber was pumped down to ultrahigh vacuum ($1x10^{-9}$ torr) before data acquisition. Binding energies (BE) were measured for C KLL, C 1s, and O 1s. The XPS spectra obtained were analyzed and fitted using CasaXPS software (version 2.3.16). Measurements take into account only the top 5nm depth of the samples. Beam diameter is 100μm.

Chapter 2: Conversion of graphite to graphene oxide

2.1 Introduction

GO will be used as an abbreviation for graphene oxide or graphite oxide throughout this dissertation. The chemical oxidation of graphite produces graphite oxide, which can then be exfoliated to single or few layered sheets called graphene oxide. These two materials are chemically the same, but graphite oxide refers to a stack of graphene oxide layers.

Graphene oxide is a two-dimensional sheet, though it can have topological defects due to oxidation and the breakage of sp^2 hybridization. These defects dramatically alter the properties of GO from its sister compound, graphene. Oxidation turns graphite into an insulating material and can double the inter-sheet spacing, depending on the reaction and environmental conditions. These property variations are attributed to the presence of oxygen functionalities, which cause chemical changes that enable GO to be water dispersible. The decreased electrical properties initially resulted in fewer applications of GO. However, electrical conductivity increases after reduction of GO, resulting in reduced graphene oxide (rGO). Exfoliation and reduction of the GO (thermally or chemically) results in a large percentage of oxygen functional groups being removed from the sheets and the individual graphene sheet-like properties

partially return. It is not possible for the rGO sheets to be completely flawless; defects are still present due to residual functionalities. These rGO flakes have increased conductivities and are no longer dispersible in water, one of the differences between GO and rGO.

2.2 Synthesis, Structure, and Modifications

2.2.1 Methods of Oxidation

The modified Hummers' method is the most popular and commonly used methods for the oxidation of graphite. But before discussion of this method, it is important to know the history behind GO synthesis. The term graphene oxide came into the picture after 2004, but oxidation of graphite existed long before that. In 1859, Benjamin Brodie first reported the oxidation of graphite while conducting research at the University of Oxford.[50] Brodie attempted to determine the molecular weight of carbon and determine differences between various graphite sources. His reaction method is currently one of the most common ways to produce graphene sheets through oxidation and reduction of graphite. There are three basic approaches for the oxidation of graphene: Brodie's synthesis, Staudenmaier's synthesis[51] and Hummers' synthesis,[1] developed in 1859, 1898, and 1958, respectively. All three methods use a strong acid and a strong oxidizing agent to complete the reaction. A comparison of these methods and their resulting materials is shown in Table 2-1.

Table 2-1. A comparison of different methods commonly used to synthesize graphene oxide.[1,50,51,52]

	Brodie	Staudenmaier	Hummers	Modified Hummers	
Year	1859	1898	1958	1999	2004
Oxidants	$KClO_3$, HNO_3	$KClO_3$ (or $NaClO_3$), HNO_3, H_2SO_4	$NaNO_3$, $KMnO_4$, H_2SO_4	Pre-ox: $K_2S_2O_8$, P_2O_5, H_2SO_4 ox: $KMnO_4$, H_2SO_4	$NaNO_3$, $KMnO_4$, H_2SO_4
C:O ratio	2.16	1.85	2.25	1.3	1.8
Reaction time	3-4 days	10 days	2 h	6 hr pre-ox + 2 h ox	5 days
Interlayer spacing [Å]	5.95	6.23	6.67	6.9	8.3

A typical oxidation reaction involves addition and dispersion of graphite in an acid followed by the addition of an oxidizing agent. Due to the exothermic nature of the reaction, the flask is constantly stirred while the temperature is controlled by an ice bath. In some cases, the reaction is allowed to proceed for up to five days.

The oxidation process permeates the graphitic structure and adds various oxygen functionalities to the graphene sheets, which breaks up the sp^2 hybridization and

increase the interlayer distance. This increased spacing reduces the van der Waals forces between layers, thus lowering the energy requirement to exfoliate to single layers. Additionally, the presence of oxygen functionalities enhances the hydrophilic nature of the sheets by making them dispersible in water when sonicated.

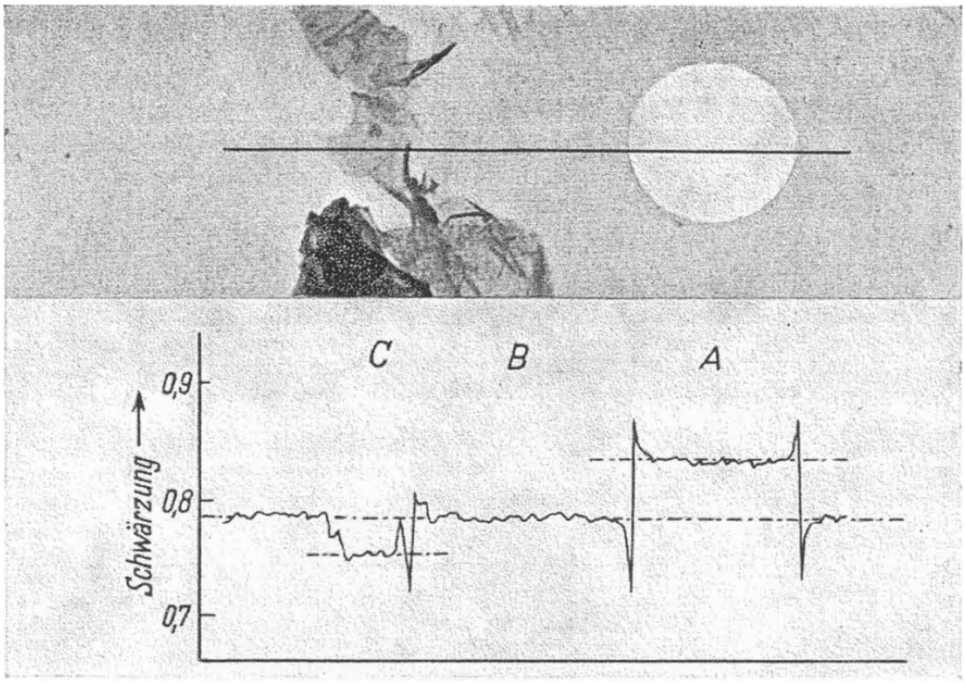

Figure 2-1. (Top) TEM image of graphene oxide cast from water onto a nitrocellulose film with holes. (Bottom) Transparency corresponding to the line through top indicating a single graphene layer.[53]

Hanns-Peter Boehm studied variations in layer spacing of graphite oxide based on the swelling medium used and published this study in 1961.[53] He showed that at low concentrations in 0.01M NaOH, the graphite oxide sheets become completely separated from one another. His work also studied the reduction effects of hydrazine

hydrate and showed that it decreased the interlayer spacing of graphite oxide to almost to that of graphite. Boehm used an early TEM to study graphene flakes on a ~100 Å nitrocellulose film and observed that the intensity on the photographic plate could be used to determine the thickness of the sheets. Figure 2-1 shows a single layer of graphene oxide extracted through this method. X-ray diffraction and methylene blue surface area measurements show that the average thickness of the sheets is two to three layers. This is widely believed to be the first discovery of single layered graphene or at least the first observation of single layer graphene.[54]

2.2.1 Modified Hummers' Oxidation

Unless stated, the oxidation of graphite was performed via a modified Hummers' method throughout this dissertation.[1] Twenty-five milliliters of sulfuric acid (Fisher Scientific, ACS Plus) and 500 mg of sodium nitrate (Acros Organics, 99%+, ACS Reagent) were added to a round bottom flask and stirred until dissolved. One gram of natural flake graphite (Asbury Mills, Grades 3243 and 2299) was then added to the flask and mixed until dispersed. When graphite is added, the solution turns black with a viscosity similar to that of water. Finally, 3 g of potassium permanganate (EM Sciences, GR ACS) is slowly added to the reaction flask to avoid overheating the system, but quickly enough so that the system does not thicken first. Addition of the oxidizing agent initially changes the solution to a dark red, which then rapidly converts to dark green color with an increase in viscosity. The solution temperature can rise above 80 ˚C, and as the reaction continues past an hour, the temperature begins to drop slightly.

Once all reagents are combined, the reaction proceeds under constant stirring for two hours before it is quenched. In order to study mechanisms for oxidation, sample aliquots were taken at specified times after the addition of the oxidizer. The times recorded were 0 minutes, 5 min, 10 min, 15 min, 30 min, 1 hour, 2 hours, and 4 hours. To quench the reaction, 200 mL of de-ionized (DI) water and 25 mL of hydrogen peroxide (Acros Organics, 35 wt. %) were rapidly added to the reaction vessel. Adding the water caused the solution temperature to rise with a vigorous effervescence caused by the addition of hydrogen peroxide. After the effervescence slowed to a minor bubbling, 25 mL of hydrochloric acid (Sigma Aldrich, 37% A.C.S. reagent) was added to solubilize residual salts.

After quenching the solution, it becomes an olive-green color and is filtered through a Büchner apparatus and repeatedly washed with DI water. Additional washing methods include centrifugation at 4,000 rpm until the supernatant is clear. The supernatant is then removed, and fresh DI water is added to resuspend the graphite via bath sonication. The process is repeated until the solution attains a pH value above 6.0. Another method for removal of residual reagents and salts is dialysis of the graphite oxide in a Spectra/Por Dialysis Membrane (50,000 molecular weight cutoff) and daily water changes. Cleaned graphite samples are then dried, ground into a powder, and stored in a vacuum oven to prevent absorption of water.

2.2.2 Structure: Atomistic Simulations and Sketching Models

The oxidation of graphite is a heterogeneous reaction. As a result, GO structure is not predictable and difficult to control. Due to the variations in position and distribution

of oxygen functionalities in the GO plane, researchers have shown a lot of interest in its simulation studies to propose various models.[55,56,57] Figure 2-2 shows atomistic simulations of graphene oxide.[55,56] Various spectroscopic techniques have demonstrated that epoxide and hydroxyl groups are the two major functional groups on the GO basal plane.

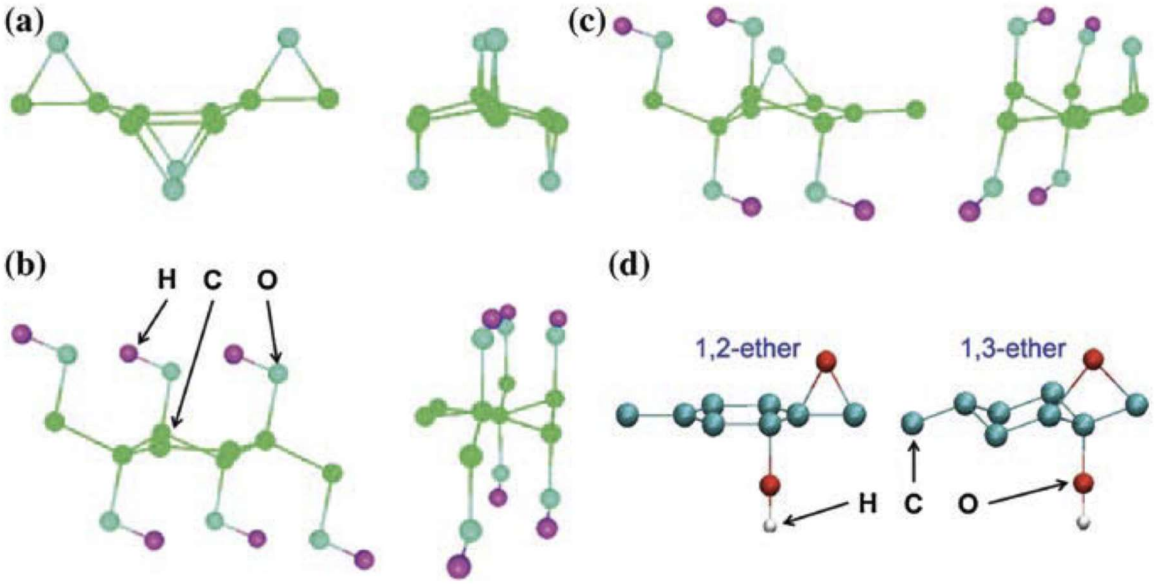

Figure 2-2. The most stable configurations of GO with epoxide groups only (a), hydroxyl groups only (b), and both epoxide and hydroxyl groups (c). Carbon, oxygen, and hydrogen atoms are shown in green, blue, and violet, respectively. Reprinted with permission from American Chemical Society.[55] (d) Schematic to show configurations of 1,2-ether and 1,3-ether epoxide groups, respectively. Reprinted with permission from American Physical Society.[56]

Single-layered GO has a thickness of ~7.8 Å when both epoxide and hydroxyl groups are placed on the carbon plane. From DFT computations, Boukhvalov and Katsnelson[55] have published three types of GO structure atomistic models: first with

epoxides only (Figure 2-2a), second with hydroxyls only (Figure 2-2b), and the third one with both epoxide and hydroxyl groups (Figure 2-2c). These studies have found that the oxygen functionalities are present on both sides of graphene. Also, the hydroxyls are energetically favorable to be attached to neighboring carbon atoms from opposite sides of the graphene. Among the three models of GO in question, the third model containing both epoxide and hydroxyl groups is more stable than the other two with either epoxide or the hydroxyl functional group.

In 2009, Lahaye et al.[56] published a model by analyzing the epoxide in detail. This study showed that the presence of 1,3-ether oxygen in GO is not energetically favorable as shown in Figure 2-2d. On the other hand, 1,2-ether oxygen is more stable. This study further proposes that GO structure with the 1,2-ether oxygen has dominated and is closely arranged. However, hydroxyl molecules located on the opposite sides of the graphene plane leads to more stability. With a few variations, this arrangement repeats along the carbon network of the GO plane and leads to a random pattern when the oxidation over a macroscopic region appears.

To date, a variety of sketching models have been proposed and are summarized in Figure 2-3. Over the years many experimental and theoretical studies have been used to further understand the structure of graphite oxide, yet no definitive results have been proven, and it is still an ongoing field of study.[58-59] In 1939, Holst and Hofmann proposed a model in which only epoxy groups exist as chemical functionalities on the graphite.[58] Additionally, these groups attached to neighboring carbons (1,2 ether) had no effect on the sheet morphology. These functionalities are randomly attached throughout the basal plane, leading to a molecular formula of C_2O. Years later, Ruess

proposed that the sheets were, in fact, not planar, an idea still present in current theories.[60] He theorized that the sheet was decorated with hydroxyl and 1,3 ether functionalities instead of epoxy functionalities. Hofmann et al. modified this structure slightly by adding the concept of enol- and keto-type functionalization to explain the acid-like properties of GO.[61] In 1969, Scholz and Boehm disputed the idea of epoxy and ether groups altogether and proposed a structure completely consisting of hydroxyl and carbonyl groups.[62] Shortly after this, Nakajima and Matsuo proposed a similar theory with hydroxyls, except they proposed that the sheets were connected into a 3-dimensional network via epoxy linkages.[63]

Later, Szabo and Dakeny incorporated the functional groups from both the Ruess and Sholz-Boehm models into their model.[57] Currently, the most widely accepted model is that proposed by Lerf et al. in 1998.[59] Using NMR, they assigned shifts to 1,2 ethers and hydroxyls and proved the existence of these structures on the GO. Additional studies have used X-ray photoelectron spectroscopy to identify the existence of carboxyl and carbonyl peaks that are located on the sheet edges.[64]

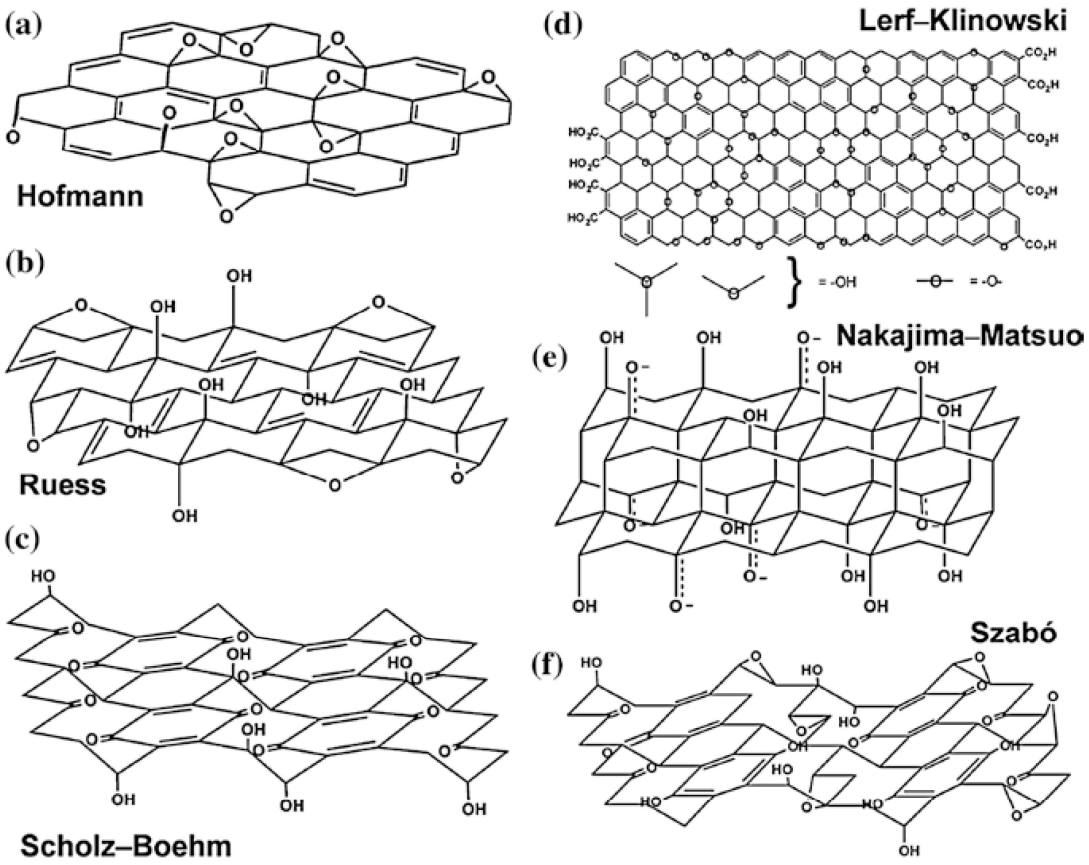

Figure 2-3. Schematics of various common models of the structure of graphene oxide. Reproduced with permission from American Chemical Society.[57]

Another newly introduced model supports the Lerf model but claims that the number of functional groups on the graphene sheets is much lower than previously claimed. This work by Rourke et al. claims that instead of being highly oxidized sheets, the majority of the graphite oxide has only minor oxidation and that oxidative debris interact very strongly to this graphite oxide.[65] It is interpreted that these highly oxidized debris moieties act as a surfactant to stabilize the non-reacted graphene layers. It is also proposed in the study that the oxidative debris is stripped from the surface of the graphite oxide through base washing the system. The remaining graphite oxide

regains electrical conductivity (due to low oxidation extent and high delocalization of planar electrons) but loses the ability to be dispersed in water.

All of the previous models of graphite oxide structure investigated a static structure for the functional groups, which many believe is incomplete. Current research focuses on identifying a dynamic structure, which can interact with its surroundings to form functional groups in solution. The most prevalent of these theories is by the Tour group. According to this theory, graphene oxide initially consists of epoxy and hydroxyl groups, but with prolonged exposure to water, a reaction takes place that cleaves a carbon-carbon bond, thus forming a carboxylic acid.[66]

In addition to the chemical nature of GO, morphology is another area of current research interest. As mentioned before, graphite oxide has an increased interlayer spacing, and the sheets have a puckered or wrinkled morphology. Additionally, chemical functionalization is not uniform throughout the sheet. This allows for some regions of the sheet to retain their sp^2 hybridization while other regions are more highly reacted and can even have holes in the sheets (see Figure 1-2c). These differences in sheet morphologies and surface chemistries drastically vary the majority of pristine graphene properties.

2.2.3 Reduction and Chemical Modification

Due to the very low conductive nature of GO relative to graphene, it has limited uses in industrial applications until after reduction when its electrical properties have been partially restored. Reducing GO by thermal and chemical routes is relatively easy to achieve and has helped to make GO a popular source of graphene-like sheets.

Reduction of GO typically happens by removal of hydroxyl and epoxy groups from the basal plane, though some mechanisms may additionally remove carboxyl groups.

Chemical reduction normally involves sonication of GO to exfoliate and disperse it in a polar solvent, typically water. A reducing agent is then added to the colloidal dispersion of the oxidized flakes. Ruoff *et al.* were able to show the reduction mechanism of GO with hydrazine hydrate at 100 ˚C.[64] The solution turns from a typical yellow-brown dispersion of GO to a black precipitate, indicating the loss of the stabilizing oxygen functionalities and the return of long-range conjugation. A variety of other reducing agents like sodium borohydride,[67] ascorbic acid,[68] and hydroquinone[69] can also be used to form rGO.

Schniepp *et al.* developed a one-step thermal reduction mechanism in which GO powder is rapidly heated in an argon environment to 1050 ˚C to remove functional groups and exfoliate the sheets simultaneously.[70] The use of an inert or reducing atmosphere is key because the presence of oxygen during the reduction process would cause GO to decompose completely.

The reduction of GO results in the loss of water dispersibility. A variety of mechanisms have been developed to increase the water dispersibility of rGO. One of the first methods for suspension in water was achieved by chemical reduction of GO in water and poly (sodium 4-styrenesulfonate) (PSS). PSS serves as a surfactant in the system with its hydrophobic backbone interacting with the rGO, while its side chains serve to stabilize the system in solution.[71] Additionally, direct chemical modification of the sheet can increase its solubility with only minor loss of properties. Si and Samulski used diazonium salt chemistry to add sulfonic acid groups to the

basal plane of an rGO sheet that resulted in the water dispersibility of the flakes.[67] Stankovich *et al*. showed the addition of isocyanate functionalities allows for the dispersion of GO sheets in organic solvents.[72] Functionalization of graphene allows for fine-tuning its properties for both specific applications as well as increasing processing efficiency.

2.3 Properties and Applications

The chemical treatment of graphene also has an effect on the mechanical properties of single layer graphene. A single layer of pristine graphene has a reported Young's modulus of 1.0 TPa,[8] while the Young's modulus of GO is reported as 207.6 GPa.[73] The Young's modulus value for GO is five times less than that of pristine single sheet graphene but is approximately the same value as that of steel. This signifies that although GO is not as mechanically strong as pristine graphene, it still maintains excellent mechanical integrity.

The presence of various functional groups allows graphene oxide to exhibit a variety of interesting customizable mechanical, electronic, and optical properties. The electronic properties of a material depend strongly on its chemical and atomic structure. Graphene's sp^2 hybridization allows for excellent electron transport throughout the sheet. Therefore the presence of sp^3 hybridized carbon and other functional groups serve as inhibitors to its electronic properties. In general GO sheets have been shown to be insulating materials with a band gap in the density of states[55] and a sheet resistance of about 10^{12} Ω □$^{-1}$ or higher.[74] The high resistance correlates with an insulating material, as there is no percolation of conductive sites throughout the material. Reduction to rGO reinstates these electronic properties with

conductivities in the order of 1000 Sm^{-1}.[75] The ability to control graphene oxidation and tailor the electronic properties has been studied theoretically but has not yet been performed experimentally.[76]

The unique surface chemistry and aspect ratio of GO presents numerous biological and stabilizing applications. Unlike carbon nanotubes, which exhibit high cytotoxicity due to their one-dimensionality, the two-dimensional sheets of graphene oxide have been shown to be much more biocompatible and show only mild to no cytotoxicity levels with excellent antibacterial properties.[77] The sheets can be modified into drug carriers for water-insoluble compounds such as various cancer treatments.[78] The ability to attach nanoparticles to GO sheets enables these composite materials to carry multiple drugs at a time[79] or to function as a potential candidate for photothermal treatments where nanoparticles can be grown from the sheet and then irradiated with a laser.[80]

The ability of graphene to be chemically functionalized to either GO or rGO and then exfoliated into single layers allows for the materials to be successful as hydrogels,[75] catalysts, and energy sources. In all of these applications, the high specific surface area of exfoliated sheets is important, as well as the ability to control the chemistry. The large aspect ratio of GO leads to uses in composites and also the formation of graphene oxide paper. By filtering a solution of graphene oxide flakes, a self-supporting paper can be formed. These papers still retain insulating properties but provide the ability to use graphene oxide in a bulk fashion where it exhibits a tensile modulus of 32 GPa.[81]

A few properties of GO can be improved by its reduction to obtain rGO. Dispersing rGO in organic solvents and then casting it as a thin film for use as a transparent conducting material has been proposed as a potential organic substitute for Indium Tin Oxide (ITO) and other oxide layers. This interest is due to both the expense and brittleness of indium. Films made by spin-coating rGO have been reported to exhibit a transparency of 87% (sheet resistance = 1.1×10^4 Ω □$^{-1}$),[82] compared to graphene grown by CVD on nickel with 76% transparency (sheet resistance = 280 Ω □$^{-1}$).[16]

Chapter 3: Fractionation of Graphene Oxidation

3.1 Why Fractionation?

The oxidation of graphite to graphite oxide (GO) is a widely used approach for the exfoliation and dispersion of graphitic sheets in water[83] with thousands of research articles describing research utilizing GO. Despite the enormous amount of attention, however, there is currently no routine method for the global characterization or fractionation of the highly disperse material produced by the oxidation of graphite. In this chapter, we present such a method based on our finding that the degree of oxidation of graphene sheets has a direct correlation to their ability to stabilize oil-in-water emulsions. Inspired by the early work in the polymer field to quantify the polydispersity of polymers by fractionation[84,85], we introduce a fractionation approach to quantify the dispersity found in the degree of oxidation within batches of GO.

The oxidation of graphite was first reported over 150 years ago by Brodie in an attempt to determine the atomic weight of carbon.[50] The approach has changed and been improved over the years,[51,1,3,86,59,57] but the mechanism of oxidation is still an active area of research[86]. Two things are clear about GO however: it is a very polydisperse material in terms of the level of oxidation of individual sheets,[3,59] and every batch of GO has a unique distribution of oxidized sheets.[3,57] The oxidation process requires the use of harsh conditions, often involving sulfuric acid and

potassium permanganate, and produces sheets with a wide range of oxidation levels, with some sheets highly oxidized and others having nearly no oxidation. This is problematic, as different synthetic approaches, and even the same approach but with different batches, can give GO with very different extents of oxidation, and thus different properties, making the characterization of the batches a critical need for GO-based research. The availability of more uniform and better characterized GO would be of great utility for controlling the chemical, physical, electrical, and thermal properties of GO and accelerating the pace of GO utilization in medical devices[87], nanoelectronics[88], electromechanical systems[89], sensors[13], composites[90], catalysis[91], energy storage devices[92], and optics[24].

Currently, the characterization of GO batches is done by methods that look at individual sheets, such as AFM or electron microscopy, that require time-consuming and tedious work to obtain any global data, or by methods that give an overall average of the batch. Although knowing the overall average degree of oxidation is useful, it does not give any information as to how the oxidation is distributed: is the GO batch composed of a few highly oxidized sheets or do all the sheets have roughly the same level of oxidation? The answer to that question has a significant impact on understanding the properties of devices and materials made with that batch of GO.

3.2 Fractionation of Graphene Oxide

3.2.1 Fractionation Procedure

For a typical procedure, 20 mg of GO was added to 5 ml of DI water in a 20 ml scintillation vial. The mixture was then bath sonicated for 1 minute. After sonication,

the GO was dispersed, and the suspension appeared black. Next, 5 ml of chloroform was added to the suspension. This GO in a chloroform/water system was then mixed for 1 minute using a Kinematica Brinkmann Polytron Homogenizer mixer (Model PT 10-35), leading to the formation of a stable emulsion. As the oil phase is chloroform, with a density greater than water, the spheres were seen at the bottom of the vial (GOe fraction). The top region (containing GOw) consisted of a uniformly black water/GO suspension. Other organic solvents, such as heptane and benzene, form water and emulsion phases as well, but the emulsion phase is the top layer in those cases.[25]

3.2.2 Nomenclature of GO fractions

The nomenclature used is as follows: the region the fraction is taken from (w for water and e for emulsion) is used following the GO to denote the route from the original GO to the current fraction. For instance, if GO is fractionated by separating the water and emulsion phases, the material obtained from the water phase is denoted GOw and the material isolated from the emulsion phase is denoted GOe. If the GOe material is then fractioned, the sample from the water phase is GOew, and the sample fom the emulsion phase is GOee.

3.2.3 Characterization of GO fractions

Before starting characterization, the following are details about GO materials other than Modified Hummers' GO samples that will be used for experiments.

CabGO. Sample preparation is proprietary.

Improved GO[3]. A 9:1 mixture of H_2SO_4/H_3PO_4 (360:40 mL) was added to a mixture of 3.0 g graphite flakes (Asbury Mills grade 3243, avg sheet size 50 μm) and 18.0 g

$KMnO_4$. After 15 min of stirring, the reaction was heated to 50 °C and stirred for an additional 12 h. The reaction was allowed to cool to room temperature and poured onto 400 mL ice and 3.0 mL 30 % H_2O_2. The filtrate was centrifuged (5000 rpm for 3 hrs), and the supernatant was decanted off. The remaining solid material was then washed in succession with 200 mL of water, 200 mL of concentrated HCl, and two additional centrifugations, removing the supernatant each time. The final pH was observed to be 6.5. The solid obtained on the filter was vacuum-dried overnight at room temperature.

We have previously found that pristine (never oxidized) graphene sheets behave as two-dimensional surfactants in stabilizing the high energy interface between immiscible oil and water phases to form water-in-oil emulsions.[93,94] Likewise, when GO is agitated in a water/oil mixture, we and others[95] have found that oil-in-water emulsions can be stabilized. However, we also find that the more intact, less oxidized sheets in the GO batch are better at stabilizing the interface and give rise to a stable emulsion phase, while the more oxidized sheets partition to the water phase. Separating these two phases fractionates the GO into a more and a less oxidized sheet population. Such an emulsion, with an upper water phase and lower emulsion phase, is shown in Figure 3-1a. Although oil phases such as heptane and toluene also give rise to emulsions, having the emulsion as the lower phase is advantageous for separating the phases and is thus the system used in all of our reported investigations.

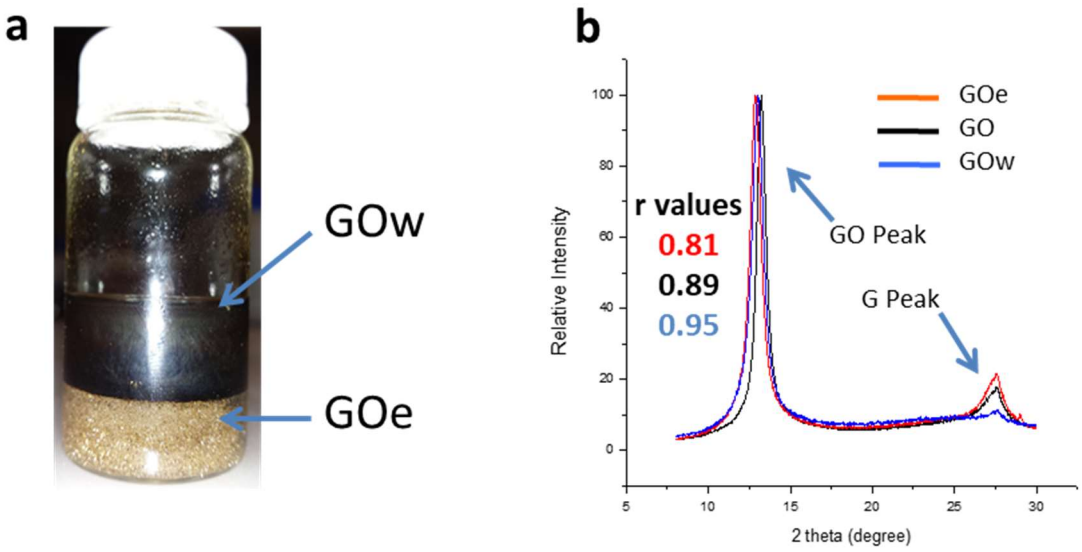

Figure 3-1. (a) Image of fractionated GO. The upper phase contains GO suspended in water (GOw) and the lower region contains GO at the interface of a chloroform-in-water emulsion (GOe). (b) Overlaid XRD spectra of the original GO sample (black), the GOw from the water phase (blue), and GOe from the emulsion phase (red).

After forming two phases the water phase, termed the GOw phase, is separated from the emulsion phase, termed the GOe phase, and both are analyzed. Figure 3-1b compares the XRD spectra of the original GO and the GOw and GOe fractions. XRD analysis indicates the spacing of the stacked sheets, with the smaller peak at 2θ =26.6 arising from the 0.33 nm graphite stacking and the larger peak at 2θ=10-13.5 arising from the increased spacing due to the oxidation of the graphene sheets[43–46] To quantify the observed differences, we use the area of the peak assigned to graphite stacking, A_G, and the area of the peak assigned to GO stacking, A_{GO}, to calculate the value of r [where $r = A_{GO}/(A_{GO}+ A_G)$].

Table 3-1. Experimental results for Orginal GO and its different fractions. The Original GO is the graphene oxide sample from which other GO fractions are isolated using fractionation process.

Sample	XRD r value $[A_{GO}/(A_{GO}+A_G)]$	Carbon to Oxygen weight ratio	Electrical Conductance ($x10^{-6}$ S)
GOeee	0.49	2.28	2.49
GOe	0.81	1.86	1.42
Original GO	0.89	1.71	0.73
GOw	0.95	1.43	0.52

We find the value of r decreases in the order of GOw > GO > GOe, indicating an increasing fraction of graphitic spacing in the samples going from water-soluble fractions to original material to emulsion fraction. Table 3-1 shows the values, as well as the value for GOeee, a sample in which the emulsion fraction was fractionated two additional times. The closeness of the value of r for GOeee to 1 indicates that the fraction contains very little material that shows GO spacing.

XRD, however, does not directly measure the extent of oxidation. For that, elemental analysis of the fractions was obtained, and the results are shown in the second column of Table 3-1. The ratio of carbon to oxygen is observed to directly correlate with the trend seen by XRD, with the C/O ratio increasing from GOw to GO to GOe to GOeee. This same trend is also observed in measurements of the electrical conductance of films made with each fraction with the most oxidized material, the GOw, showing the

least conductance. This is to be expected, as oxidation is known to disrupt the conjugation in graphene responsible for electrical conductivity.[96]

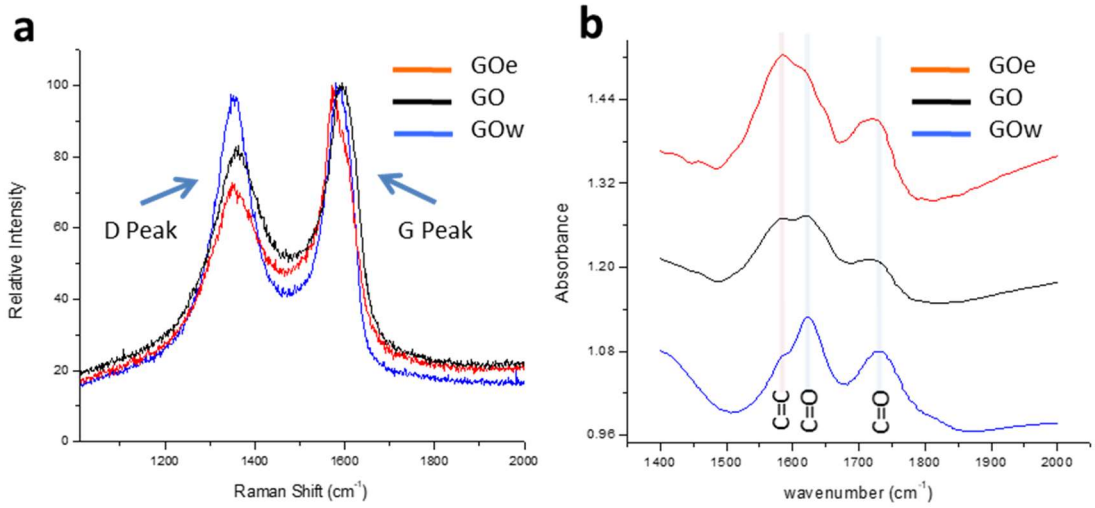

Figure 3-2. (a) Overlaid Raman spectra of GO (black), GOw (blue), and GOe (red) showing the G and D peaks. (b) Overlaid FTIR spectra of GO (black), GOw (blue), and GOe (red) highlighting changes in relative intensities of peaks at 1580 cm^{-1} (sp^2-hybridized C=C), 1620 cm^{-1} (ketone C=O), and 1730 cm^{-1} (carboxyl C=O).

This disruption can be seen as well by Raman spectroscopy, where the ratio of the D and G peaks is often used as an indication of the degree of conjugation in graphene.[97] The Raman spectra of GO contains G and D peaks where the G peak at ~1580 cm^{-1} is the result of bond stretching of sp^2 hybridized carbons and the D peak at ~1340 cm^{-1} is the result of defects in the graphene sheets.[39,93] These defects correspond to disorder in the sample that can be a result of oxygenated functionalities in the graphene plane. Shown in Figure 3-2a, the ratio of the D and G peaks indicate

a trend from less ordered to more ordered moving from GOw to GO to GOe. This is the same trend observed for the XRD, elemental analysis and conductivity studies.

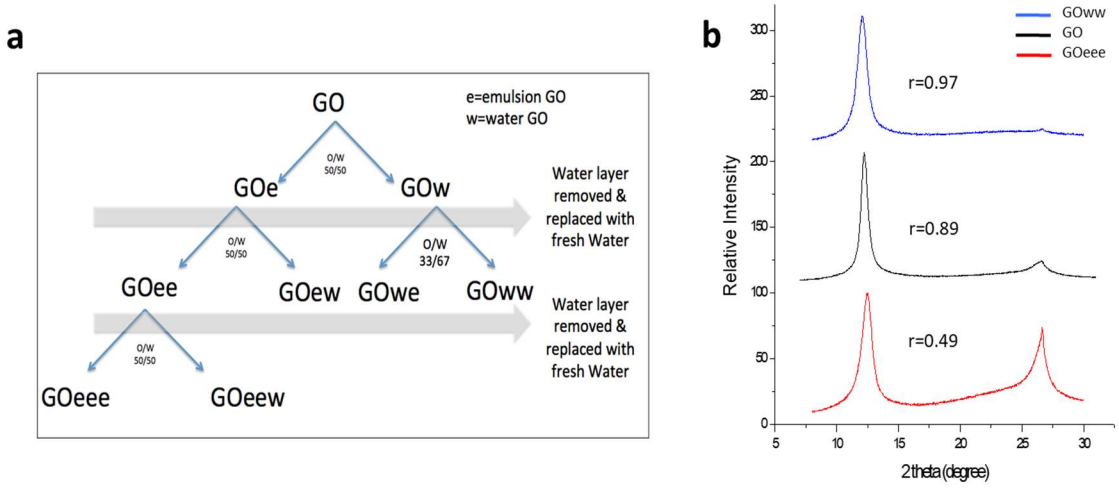

Figure 3-3. (a) Schematic illustration of stepwise GO fractionation and nomenclature. (b) XRD spectra of original GO, GOww and GOeee fractions showing the substantial increase of material displaying pristine graphite spacing with multiple emulsion fractions. All samples originated from the same batch of GO.

These results indicate that the GOw fraction contains the more highly oxidized material, and the GOe contains more lightly oxidized material. The GOe has some degree of oxidation, however, as indicated by the aforementioned analysis as well as from the observation that the emulsions are oil-in-water, while pristine graphene forms water-in-oil emulsions. The hydrophilicity imparted by the low level of oxygen functional groups is enough to flip the emulsion with respect to pristine graphene. Additionally, Appendix (Figure 10-1) shows the FTIR spectra of the three GO samples and fractions in question. To simplify and quantify the characterization of GO fractions, we focus on the peaks at 1580 cm^{-1} (sp^2-hybridized C=C), 1620 cm^{-1} (ketone C=O),

and 1730 cm^{-1} (carboxyl C=O) as shown in Figure 3-2b.[3,47] FTIR analysis shows that the chemical differences in different fractions exist as well. In the order of GOw to GO to GOe, the peak at 1620 cm^{-1} (ketone C=O) loses intensity relative to the peak at 1580 cm^{-1} (sp^2-hybridized C=C). This shows how oxidation functional group changes are taking place at the molecular level.

3.3 Need for universal characterization

3.3.1 Differences between look-alike

Like the fractionation of polymers done in the early days of polymer science, it is possible to fractionate the fractions of GO. Figure 3-3a shows a general outline of the multiple fractionations. Comparing the XRD of triply and doubly fractionated materials with GO in Figure 3-3b shows a much greater difference in the XRD r values than is seen after a single fractionation. In decreasing order of graphitic content by XRD we find Geee, > GOe > GO > GOw > GOww. This trend shows the emulsion fraction always prefers the less oxidized, or more graphitic, population of the available GO in the system. Again, like for the fractionation of polymers, this fractionation can be repeated as many times as desired to create fractions with ever narrower distributions of oxidation levels. In addition to allowing the formation of less dispersed samples of GO, fractionation can also be used to characterize batches of GO produced by different synthetic approaches. As an example, we compare three different GO batches: one synthesized via a standard Hummers method,[1] one by a recently introduced improved GO method (IGO)[3] and one sample (CabGO) obtained from industry (the preparation method is proprietary).

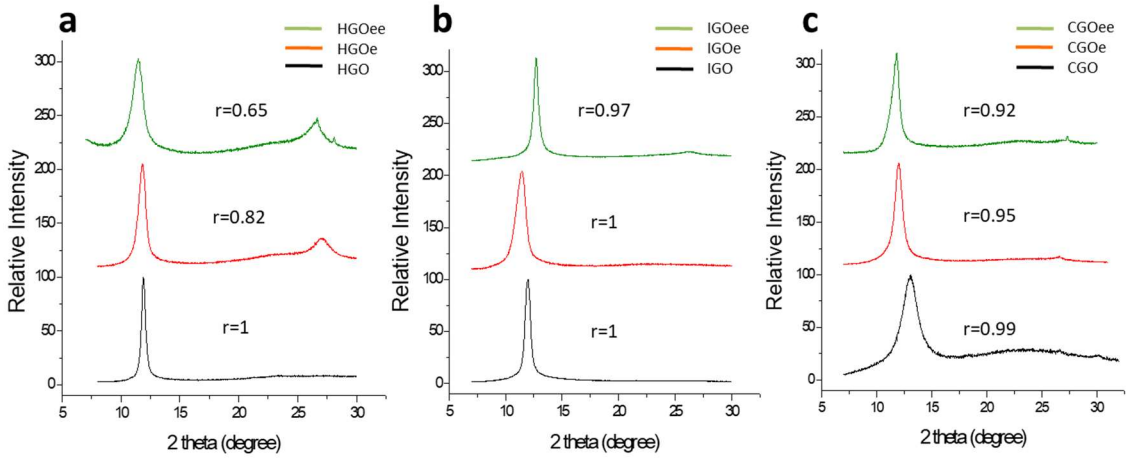

Figure 3-4. (a) XRD patterns of Hummers GO and its emulsion fractions, (b) XRD patterns of Improved GO (IGO) and its emulsion fractions, and (c) XRD patterns of CabGO (CGO) and its emulsion fractions.

Shown in Figure 3-4 are the XRD spectra of each GO type, with the lower black curve being from the unfractionated. They initially appear similar, with a prominent peak arising from oxidized material, and no visible graphitic peak. However, after a single fractionation, there is a clear difference. The GOe and GOee fractions of the Hummers GO, Figure 3-4a, show a clear increase in the area of the graphitic peak, indicating a significant population of material with pristine graphite stacking. Figure 3-4b shows that the IGO material contains no significant graphitic peak in the GOe fraction and only a very small graphitic peak in GOee fraction, indicating that the less oxidized material contains only trace amounts of the original stacking. Lastly, in Figure 3-4c, the CabGO is shown to have a small but measurable amount of residual graphite stacking.

3.3.2 Instruments and techniques

X-Ray Diffraction- A 2D X-Ray Diffractometer (XRD) (Bruker D2 Phaser) with radiation of wavelength =1.54 Å was used. The sample was prepared by drop casting GO water suspension onto a glass slide. To compare all the XRD patterns of different GO's and GO fractions, we used the ratio $r = A_{GO}/(A_{GO}+ A_G)$ where A_G is XRD graphite peak area (A_G), and A_{GO} is XRD GO peak area. XRD GO, and G peak areas were calculated using the XRD instrument software.

Raman Spectroscopy- A Renishaw System 2000 Raman microscope at λ= 514 nm using 50X objective lens was used. Samples were prepared by drying suspensions on a glass slide.

Elemental Analysis- Elemental analysis experiments were performed by Galbraith Laboratories, Inc. Samples were dried overnight before the experiments.

Electrical Conductivity measurements- Dried GO films of size 2 cm x 1 cm x 190 μm were fabricated by drop-casting and their thickness was measured by a vernier caliper. Electrical conductivity of dried GO film was calculated using a FLUKE 25 Multimeter.

Optical Microscopy- Emulsion phase pictures were taken from Nikon Diaphot Microscope.

Fourier Transform Infrared Spectroscopy- Figure S4 shows the FTIR spectra of three GO samples (GO, GOe and GOw) using a Nicolet Magna 560 instrument. The large peak at 3400 cm^{-1} shows the O-H stretching vibrations in the GO samples. C=O stretching vibrations (1720cm^{-1}), C=C stretching vibrations (1580-1630cm^{-1}) in the GO plane, and C-O stretching vibrations (1250 cm^{-1}) were identified in the GO samples.[47].

3.4 Different Features of Fractionation

3.4.1 Emulsion region analysis.

Optical microscope images of spheres in the emulsion system (containing water as the continuous phase) were observed by putting the spheres on a glass slide as shown in

Figure 3-5. The size distribution of these emulsion spheres was found to be from

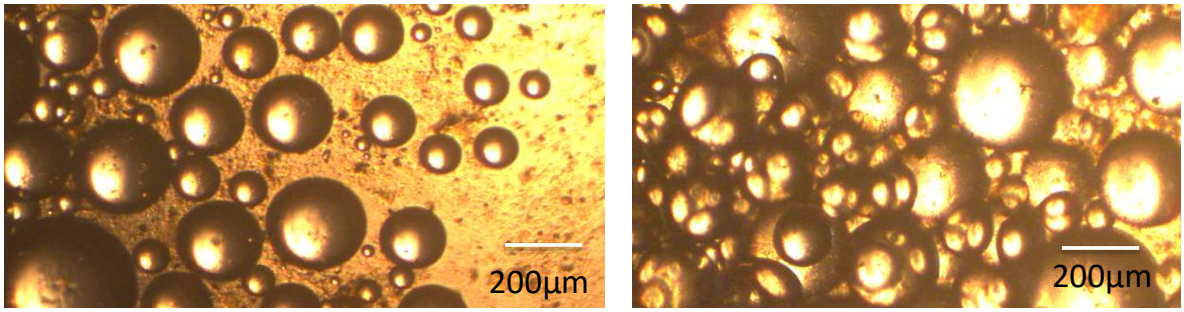

40-400 µm.

Figure 3-5. Optical microscopic pictures of emulsion region spheres as observed on a glass slide. Spheres were observed in a dilute continuous water phase (left) and concentrated continuous water phase (right).

Energy dispersive X-ray spectroscopy (EDX) analysis of GO fractions- EDX of GOe and GOw fractions are shown in Figure 3-6 and demonstrate the presence of salt impurities in the GO samples. As expected, GOw fractions contain more impurities than do GOe fractions.

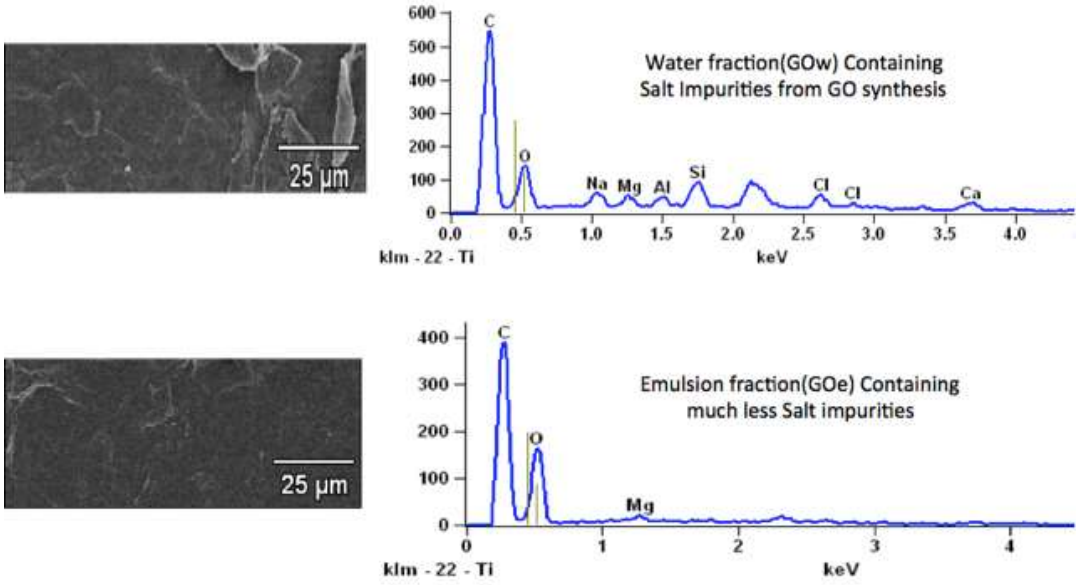

Figure 3-6. EDX of water region (top) and emulsion region (bottom) GO fractions.

Stable Emulsion Formation and Settling- After mixing GO with chloroform and water, the emulsion region volume was observed to change with time, with a stable emulsion region was attained after a few minutes. Appendix (Figure 10-2) shows a plot of the sphere region volume versus time, showing that after about 5 minutes the sphere region volume becomes stable. Fractions were collected only after achieving this 5-minute steady state condition.

To see the effect of changing solvents, toluene and dichloromethane were compared to chloroform. Table 3-2 shows that changing solvents changed the size of the emulsion regions and changed the oxidation extent of GO sheets in the GOe fraction. Thus the fractionation method, if used for characterization, depends to some extent on the organic solvent chosen. As stated previously, we used chloroform for all data presented.

Table 3-2. Different GO fractions obtained by using different solvents with water

Oil phase in oil water emulsion system	Original GO used for fractionation	XRD r value for Emulsion GO fraction	XRD r value for Water GO fraction	Volume of sphere region
Toluene	2mg/ml	0.86	0.96	~75% of total V
Dichloromethane	2mg/ml	0.83	0.96	~65% of total V
Chloroform	2mg/ml	0.81	0.95	~60% of total V

So far, the main focus of our fractionation studies has been to obtain GO fractions with lower extents of oxidation. This was done by collecting emulsion region GO fraction (e.g. GOe, or GOee) and fractionating it again. As shown in Appendix (Figure 10-3), fractionation can also be used to obtain highly oxidized GO. The more fractions obtained from the water phase, the more oxidized is the product, i.e., GOwww is more oxidized than GOw.

3.5 Conclusion

The fractionation of GO results from the less oxidized material's ability to stabilize oil-in-water emulsions preferentially to more oxidized material and allows for the preparation of narrowly defined samples. These studies demonstrate the utility of the fractionation method, as originally all three samples appeared the same but were shown to be significantly different after analyzing the emulsion fractions. Studies done

with each of these samples would be expected to provide very different results, yet common methods for GO analysis would indicate no differences in the GO.

Repeated fractionations were shown to increase the enrichment of GO fractions in either higher or lower levels of oxidized material, and this enrichment was shown by XRD, Raman spectroscopy, FTIR, and elemental analysis; all analytical techniques commonly used for GO. We have also demonstrated that important physical properties, such as electrical conductivity, are directly correlated with the degree of oxidation in each fraction.[98] It is anticipated that this approach will lead to more reproducible results in GO material research and enable a more fundamental understanding of GO-based applications.

Chapter 4: Distribution of Oxidation of Graphene Oxide Flakes

4.1 Oxidation distribution

4.1.1 Introduction

Researchers routinely use graphene oxide (GO) for a number of applications without knowing the dispersity of oxidation (DO) within a GO sample or the effect of DO variations on the performance of various GO based application.[99-107] GO synthesis, done using the same or different methods, leads to variation in oxidation,[25,108,109] but the distribution of oxidation of GO within a given sample has never been calculated. We use GO fractionation and classical statistical methods to calculate DO values for a GO sample and show that the changes in GO synthesis methods give rise to different DO numbers. Going further, our experimental results reveal a significant improvement in performance of GO-based applications in (but not limited to) mechanical, optical, electronic, sensor, biomedical areas for low or high DO and XRD r values of GO. These findings will help thousands of research and industrial facilities improve the performance of their materials by informing their choice of DO and oxidation degree (oxidation r value) saving money, time, and effort.

Graphene and Graphene oxide are household names in the material research community, possessing excellent material properties and large abundance. Each year, 1000's (and the number is increasing) of articles[52] mention and discuss new properties and applications replacing other expensive, less abundant, and relatively low performing materials.[110,111] Researchers in academia and industry still use graphene oxide without keeping in mind the graphene oxide's non-uniform oxidation distribution. A reliable standard experimental method to qualitatively observe or quantitatively calculate this dispersity of oxidation is not available, and so the effect of degree and dispersity of oxidation of hundreds of different applications of GO is unknown.

As already been discussed, the XRD r value is a function of the area of GO and G peaks in XRD. This is an indirect measure of GO interlayer distance relative to the G interlayer distance and not the oxidation. We are taking inspiration from other scientific techniques which use indirect measurement to calculate a parameter, e.g., GPC is used to calculate the molecular weight (MW) and polydispersity of a polymer. GPC never calculates MW directly but through the hydrodynamic radius of the polymer chain by fractionating it. Despite a vast difference between the actual parameters calculated (radius depending upon factors like solvent) and the final parameter (MW), GPC is widely used due to the ease of doing the experiment and clear method of quantification.

Using statistical tools with this method, we find w_i , the weight of different GO fractions (with different oxidation degree), corresponding to their oxidation extent, r_i. We further use this w_i vs. r_i comparison for a given GO sample to calculate the value

of polydispersity of oxidation (DO number) of a given GO sample and open the gates to a consistent and better performance of GO in different applications without changing other variables e DO number for a given GO sample.

4.2 Calculation of dispersity of oxidation

4.2.1 Choice of GO fractions

Figure 4-1 shows the fractionation process chosen for the statistical studies to calculate the dispersity of oxidation values for the GO samples. The final GO fractions obtained for the study from this fractionation process are shown as highlighted.

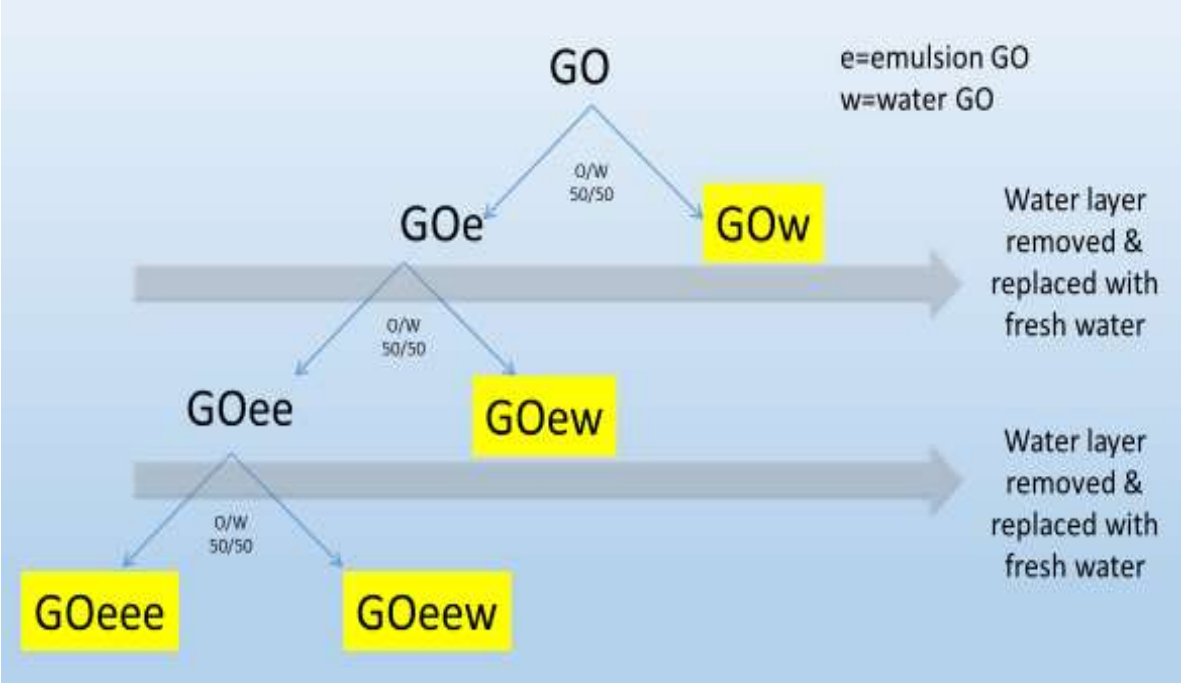

Figure 4-1. Scheme illustrating the method to obtain GO fractions to be used for calculation of polydispersity of oxidation.

It is seen that a major portion of oxidized GO comes out in the GOw fraction (mostly highly oxidized sheets)[25] which is a relatively uniform oxidized material and further fractionation of GOw will not result in a broad range of XRD r ratios. On the other hand, fractionation of GOe (not oxidized completely) results in fractions (GOeee, GOeew, and GOew) that fall in broad range of XRD r ratios. This specific combination of GO fractions (GOw, GOew, GOeew, and GOeee) is chosen for calculation of dispersity of oxidation because they are easier to obtain, they represent the distribution of oxidation of GO in a broad oxidation range, and they are helpful in distinguishing two different given samples quantitatively and qualitatively.

4.2.2 Experimental conditions

The oil/water GO system used an oil to water ratio of 50/50 by volume with a GO concentration of 2 mg/ml. The experiment was carried out using 10 ml water and 10 ml chloroform. The three constituents were mixed for a minute manually, and then various factions were obtained as illustrated in Figure 4-1. The XRD r value and weight fraction of the obtained GO fractions were then calculated. To avoid confusion, it is important to note that the word 'fraction' is used in two references here, one denotes the GO fraction$^{(a)}$ (concrete noun, usually followed by 'GO', e.g. GOe and GOw are GO fractions$^{(a)}$) obtained from fractionation process, and the other denotes weight fraction$^{(b)}$ (abstract noun, usually followed by 'weight', mathematically showing the proportion of weight compared to the whole GO material, e.g. weight fraction$^{(b)}$ of GOe is 0.40). For the i^{th} GO fraction$^{(a)}$, the weight fraction$^{(b)}$ is w_i and XRD r value is r_i. For qualitative analysis, w_i is plotted against r_i. Three GO samples, GO1, GO2, and GO3,

which are different in terms of oxidation, are chosen for this experiment. XRD diffraction patterns of GO1, GO2, and GO3 are shown in Figure 4-2. GO1 and GO2 are obtained from Modified Hummers oxidation[1] for 1 hour and 2-hour oxidation respectively while GO3 is obtained by IGO method[3] where the oxidation reaction took place for 12 hours. Clearly, there is a difference in terms of graphitic content of these samples as indicated by the relative intensity of G peak at 27° 2θ-value.

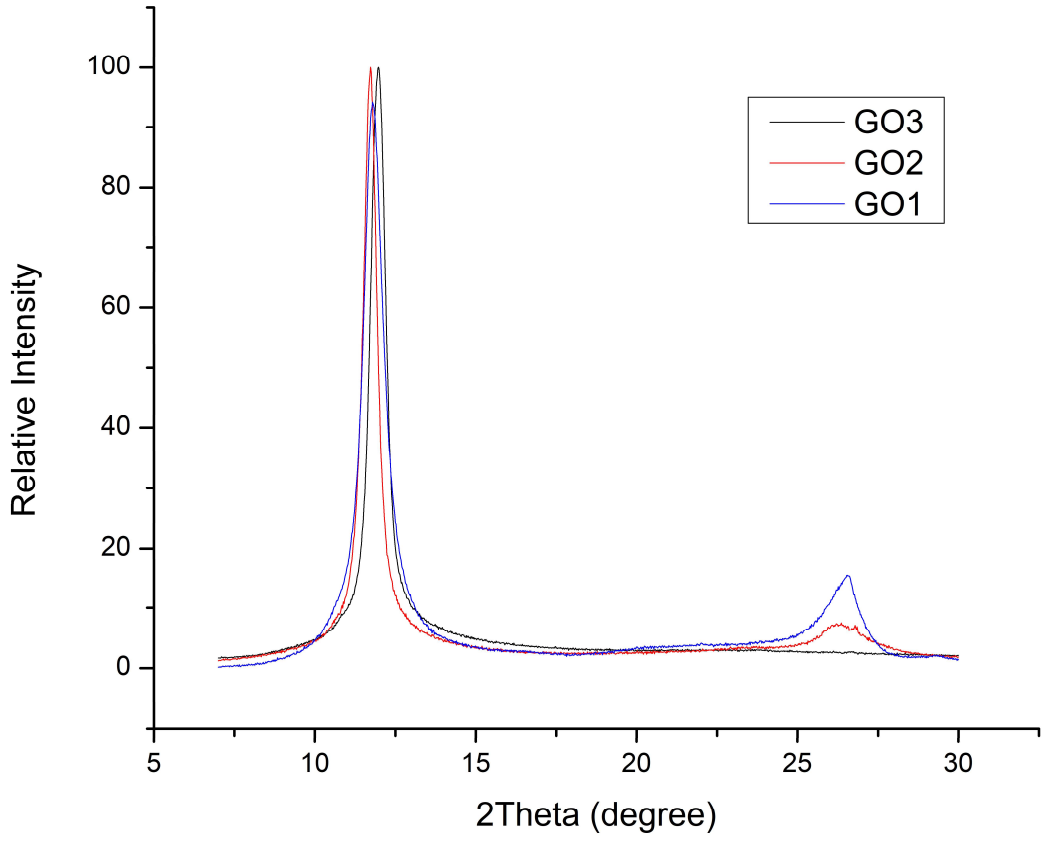

Figure 4-2. XRD diffraction patterns for GO1, GO2 and GO3. GO1 and GO2 are obtained from Modified Hummers oxidation for 1 hour and 2 hours oxidation respectively. GO3 is obtained by IGO method where the oxidation reaction took place for 12 hours.

In Figure 4-3, w_i is plotted against r_i. It is clear from the plots that more oxidation leads to less dispersity of oxidation as depicted by the comparison of the spread of points in Figure 4-3a, Figure 4-3b and Figure 4-3c corresponding to GO1, GO2, and GO3 respectively.

4.2.3 Weight fractions versus XRD r value plots

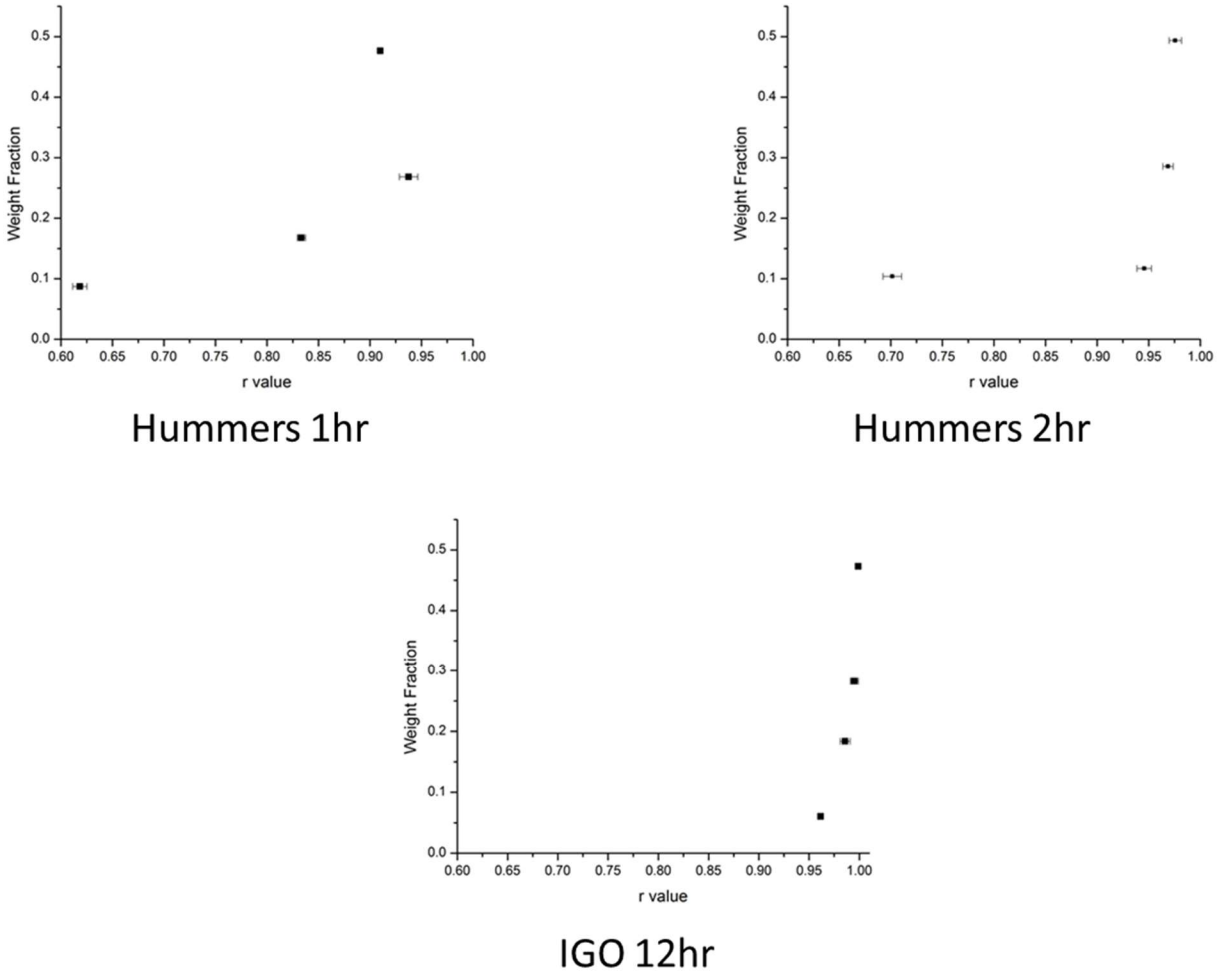

Figure 4-3. Plots comparing weight fraction of GO fractions vs. their corresponding XRD derived r-values obtained from a) GO oxidized by hummers method for 1 hour (GO1), b) GO oxidized for 2 hours (GO2), and c) GO oxidized using IGO method[3] (GO3).

It should be noted that we have chosen three different kinds of GO samples in Figure 4-3 to cover the most common GO oxidation spectrum used nowadays. Although the nature of w vs. r curve can be different from the three GO examples used here depending upon the material's distribution of oxidation and should not be limited to what is shown in this study.

Numbered mean (Rn) and weighted mean (Rw) of XRD r value are calculated using the following equations.

$$Rw = \frac{\sum (r_i^2 . w_i)}{\sum (r_i . w_i)}$$

$$Rn = \frac{\sum (r_i . w_i)}{\sum w_i}$$

Further, the ratio of Rw and Rn is referred as DO'.

$$DO' = \frac{Rw}{Rn}$$

DO' is then numerically modified to obtain the dispersity of oxidation number (DO) of a GO sample as shown in the following equation.

$$DO = [(DO'-1)x100]+1$$

Table 4-1 shows the oxidation methods for GO1, GO2 and GO3 and their respective DO values calculated from the w_i vs r_i data. There is a difference between the dispersity of oxidation in case of Hummers reaction for 1 hour and 2 hours. Oxidation time decreases the distribution of oxidation among the GO sheets from DO= 1.9904

to DO=1.7637. Further, the improved GO synthesis method[3] with 12 hours of reaction time in different reaction environment than Hummers' gives rise to a GO material that is near to monodisperse with a value of 1.0089. Relatively this value is much lower than that of GO1, and GO2 clearly indicates a GO material with a large oxidation dispersity.

Table 4-1. Table mentioning the dispersity of oxidation (DO) for three given GO batches has been calculated. GO1 and GO2 are oxidized using Modified Hummers' method, and GO3 is oxidized via the IGO Method.

	Graphite	GO1	GO2	GO3
Oxidation	No reaction	1 hour Modified Hummers	2 hour Modified Hummers	12 hour IGO Method
DO	1	1.9904	1.7637	1.0089

In order to understand the DO number better, a study to compare graphite and GO DO numbers can be done. Since Rw will always be greater or equal compared to Rn, the minimum theoretical value of DO' is 1. Due to this, a minimum possible value for DO is where all the r_i values obtained are the same.[85,112] It is noted here that the r value provides the degree of oxidation that depends upon how much the GO is oxidized. So, there is a huge difference between graphite and GO3 where the r value for graphite with no GO peak is 0 and r value for GO3 appears to be near to 1. However, DO value does not indicate oxidation of GO sheets, but it shows how widely distributed the oxidation of the GO batch is. That's why the DO number for graphite

and GO3 is 1. In other words, graphite is monodisperse in terms of oxidation; however its oxidation is nearly zero. GO3 has a DO number close to 1 which is closer to graphite DO value than GO1 and GO2.

4.3 Factors affecting DO value

Large variations in temperature can change the surface tension of the solvents. This changes the emulsion formation and GO fractionation system, i.e., different weights of GO fractions are obtained at large temperature differences. This is why all the measurements are carried out at near 20 ˚C. Concentrations of the aqueous or organic phase of the emulsion system can change the volume of the final emulsion region and hence affect the GO fractions obtained.

Figure 4-4 shows that the emulsion becomes stable as the pH of the fractionation system increases from 3 to 8. The emulsions did not form beyond pH= 8 with the given concentration of GO, water, and chloroform. All the fractionation experiments were carried out at pH= 6. Thus control over pH is required to be sure of the consistency in the process to obtain GO fractions. An inconsistent weight or r-value data due to variations in pH of the fractionation emulsion system can affect the DO number.

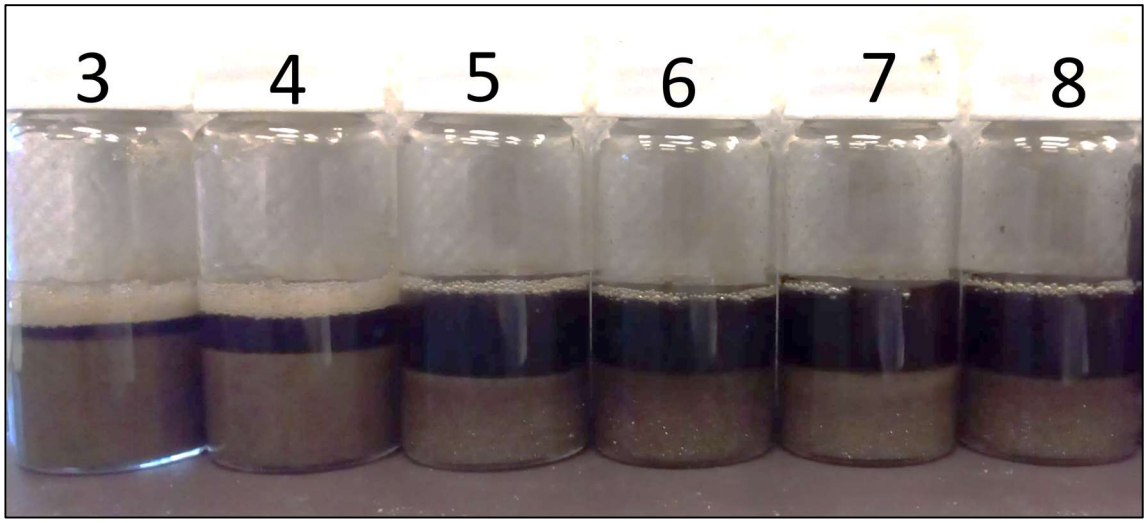

Figure 4-4. Investigation of the pH effect on emulsion formation. Increasing pH decreases the volume of the emulsion (lower phase). The number indicates pH of the vial constituents.

4.4 Statistical analysis

The DO findings can be statistically analyzed. In order to do that, we have analyzed 4-point data (referring to 4 fractions) for the DO calculation. Later, the accuracy of this 4-point data is analyzed by comparing it with 8-point data obtained for the same sample and by using identical method. In order to analyze both extremes of polydispersity (DO) we have chosen GO1 (x1 vs. y1) and GO3 (x2 vs. y2) samples.

4.4.1 Analysis of GO1

More data provides better accuracy in DO calculation, however, collecting 8-point data rather than 4-point data from GO fractionation experiment is more work. To see if the extra work is necessary, we gather results for our r value vs. weight fraction for four different fractions. The data in Table 4-2 shows the dependency between the two

variables ‘x’ and ‘y’. The variable ‘x’ refers to the r value for a fraction and y refers to the weight fraction of that fraction.

Table 4-2. r value versus weight fraction 4-point data for GO1 sample.

X1 r value	Y1 Weight Fraction
0.268456	93.75
0.47651	90.99099
0.167785	83.33333
0.087248	61.83206

Although we only have 4 data points, one can see an exponential relationship. We will now try to find a model which will best describe this relationship. Next we analyze three different relationships namely, linear, quadratic, and exponential and find out the best fitting distribution. Following is the analysis:

Linear association: $\boldsymbol{y = a + bx}$

Coefficients:

	Estimate	Std. Error	t value	Pr(>|t|)
(Intercept)	-0.4643	0.4588	-1.012	0.418
x	0.8661	0.5500	1.575	0.256

Multiple R-squared: 0.5536,Adjusted R-squared: 0.3304

Quadratic association: $\boldsymbol{y = a + bx + cx^2}$

Coefficients:

	Estimate	Std. Error	t value	Pr(>|t|)
(Intercept)	0.926	6.118	0.151	0.904
X	-2.857	16.315	-0.175	0.890
x2	2.415	10.570	0.228	0.857

Multiple R-squared: 0.5757,Adjusted R-squared: -0.2729

$Y= 0.926 -2.857x + 2.415x^2$

Exponential association: $\boldsymbol{y = ab^x}$

Coefficients:

	Estimate	Std. Error	t value	Pr(>|t|)

(Intercept)	-5.215	1.353	-3.853	0.0612
x	4.419	1.622	2.724	0.1125

Multiple R-squared: 0.7877, Adjusted R-squared: 0.6815

Table 4-3. r value versus weight fraction 8-point data for GO1 sample. Actual weight fraction (y1) is calculated experimentally and extrapolated weight fraction (y1') is calculated from the exponential model obtained from 4-point data.

X1 r value	Y1 Actual Weight Fractions	Y1' Extrapolated Weight Fractions
0.96988	0.154362	0.394908
0.915254	0.114094	0.310214
0.958159	0.261745	0.374975
0.880952	0.214765	0.266583
0.937107	0.107383	0.341665
0.803922	0.060403	0.189670
0.857143	0.053691	0.239959
0.559471	0.033557	0.064396

On analyzing the above models, one can compare the R^2 (coefficient of determination) or the adjusted R^2 values for each model. The exponential association proves to be the best, giving a very high R^2 value. The model, or the distribution connecting x and y, is thus found to be:

$$\mathbf{log}(\boldsymbol{y}) = \mathbf{-5.215 + 4.419}\boldsymbol{x}.$$

The question now is that whether it is possible to extend this model and extrapolate it to a higher magnitude? In order to corroborate further, we now extend our discussion to 8-point data. The 8-point data results from the same sample GO1 but for 8 different fractions. Table 4-3 shows the extrapolated weight fraction (y1') that is calculated from the exponential model obtained from 4-point data.

One can again sense an exponential relationship between the two variables. If we analyze the exponential model, the following are the results:

Coefficients:

	Estimate	Std. Error	t value	Pr(>|t|)
(Intercept)	-5.937	1.148	-5.170	0.00207 **
x	4.246	1.321	3.214	0.01828 *

Multiple R-squared: 0.6326, Adjusted R-squared: 0.5713

The R^2 value is again medium to high, confirming a decent fit.

Our last step is to extrapolate the weight fractions with the 8-point data using the model from the 4-point data and comparing them with the available 8-point weight fractions. Table 4-3 the shows the extrapolated y1' values.

All the values are closer and there doesn't seem to be a significant error when comparing y values in Table 4-3. The correlation between the two sets of values is 0.68 which is medium to high.[113,114] We can also check for "equality of means" between the two groups using a "Mann-Whitney U Test".[115] This is useful since it doesn't assume any form of a distribution and is non-parametric. The hypotheses are:

H0: The two means are equal. Ha: The two means are not equal

A Mann-Whitney U Test gives a p-value of 0.0104 which suggests that one should accept the null hypothesis at 1% level. This supports the fact that, statistically, the two sets of data are significantly close and comparable at 1% level, suggesting that if one uses the model described above to extend the results to any number of points further, it should produce good results.

4.4.2 Analysis of GO3

Similar to the case of GO1 (x1 vs. x2), Table 4-4 shows the 4-point data of GO3 (x2 vs. y2).

Table 4-4. r value versus weight fraction 4-point data for GO2 sample.

X2 r value	Y2 Weight Fraction
0.473094	0.999001
0.282511	0.995025
0.183857	0.985915
0.060538	0.961538

Although we only have 4 data points, one can clearly see an exponential relationship between the two. We will now try to find a model which will best describe this relationship. We analyze three different relationships namely, linear, quadratic and exponential and find out the best fitting distribution. Following is the analysis:

Linear association: $\boldsymbol{y = a + bx}$

Coefficients:

	Estimate	Std. Error	t value	Pr(>|t|)
(Intercept)	-8.861	3.271	-2.709	0.114
x	9.246	3.319	2.786	0.108

Multiple R-squared: 0.7951,Adjusted R-squared: 0.6927

Quadratic association: $\boldsymbol{y = a + bx + cx^2}$

Coefficients:

	Estimate	Std. Error	t value	Pr(>|t|)
(Intercept)	431.8	257.7	1.675	0.343
x	-890.8	526.4	-1.692	0.340
x2	459.5	268.7	1.710	0.337

Multiple R-squared: 0.9478,Adjusted R-squared: 0.8434

Exponential association: $\boldsymbol{y = ab^x}$

Coefficients:

	Estimate	Std. Error	t value	Pr(>|t|)
(Intercept)	-52.223	5.894	-8.860	0.0125
x	51.347	5.981	8.585	0.0133

Multiple R-squared: 0.9736,Adjusted R-squared: 0.9604

On analyzing the above models, one can compare the R^2 (coefficient of determination) or the adjusted R^2 values under each model. The exponential

association proves to be the best giving a very high R^2 value. The model or the distribution connecting x and y is thus:

$$\mathbf{log}(\boldsymbol{y}) = -\mathbf{52.223} + \mathbf{51.347}\boldsymbol{x}.$$

Similar to the GO1 analysis, we further use 8-point data results as shown in Table 4-5 to look into GO3.

Table 4-5. r value versus weight fraction 8-point data for GO3 sample. Actual weight fraction (y2) is calculated experimentally and extrapolated weight fraction (y2') is calculated from the exponential model obtained from 4-point data.

X2 r value	Y2 Actual Weight Fractions	Y2' Extrapolated Weight Fractions
0.999001	0.280269	0.395622
0.996016	0.192825	0.339403
0.996678	0.179372	0.351138
0.97561	0.103139	0.119033
0.990991	0.114350	0.262216
0.967742	0.069507	0.079471
0.972973	0.042601	0.103959
0.931973	0.017937	0.012664

Analyzing the exponential model, we find the following results:

Coefficients:

	Estimate	Std. Error	t value	Pr(>|t|)
(Intercept)	-39.39	5.13	-7.678	0.000255
x	37.83	5.24	7.219	0.000358

Multiple R-squared: 0.8968, Adjusted R-squared: 0.8796.

The R^2 value is again high, confirming a good fit.

Our last step is to extrapolate the weight fractions with an 8-point data set using the model from the 4-point data and comparing them with the available 8-point weight fractions data as shown in Table 4-5. All the values seem to be close across the board, and there doesn't seem to be a significant error. The correlation between the two sets of values is 0.93, which is also very high.[113,114]

We also check for "equality of means" between the two groups using a "Mann-Whitney U Test".[115] This is useful since it doesn't assume any form of a distribution and is non-parametric.

The hypotheses are:

H0: The two means are equal. Ha: The two means are not equal

A Mann-Whitney U Test gave a p-value of 0.2786 which suggests that one should accept the null hypothesis even at 10% level. This supports the fact that, statistically, the two sets of data are closer but at the same time, higher GO oxidation distribution in GO3 rose this level to 10% than 1% in case of GO1.

This suggests that if one uses the model described above to extend their results to any number of points further, it should produce accurate results.

4.4.3 Statistical analysis conclusion

Table 4-6 shows the summary of the statistical analysis. GO fractionation is done to produce 4 fractions in first set and 8 fractions in second set to look into the distribution of oxidation. Data obtained from 8 GO fractions is much closer to the obtained statistical models than that of the 4 fractions study. GO1 and GO3 samples were

chosen for this statistical study because these are the two extreme samples available on the basis of distribution of oxidation (DO) values. Various statistical models (linear, quadratic, and exponential) are analyzed corresponding 4-point data for GO1 and GO3. GO fractions seem to follow an exponential association among the three methods applied due to very high multiple and adjusted R^2 values. R^2 values of exponential model for 8-point data are also found to be better than other two models.

Table 4-6. Various DO models & Statistical analysis for two graphene oxide samples GO1 and GO3. Different statistical models used 4-point data unless specified as 8-point data.

Sample	**Model**	**R^2 (coefficient of determination)**		**Correlation**[113]	**p-value (from Mann-Whitney U Test)**[115]
		Multiple	**Adjusted**		
GO1	Linear	0.5536	0.3304	0.68 (exponential model)	0.0104
	Quadratic	0.5757	-0.2729		
	Exponential	0.7877	0.6815		
	Exponential for 8-point	0.6326	0.5713		
GO3	Linear	0.7951	0.6927	0.93 (exponential model)	0.2786
	Quadratic	0.9478	0.8434		
	Exponential	0.9736	0.9604		
	Exponential 8-point	0.8968	0.8796		

Further, this exponential model is then used to get the model w_i values (obtained from proposed exponential model and not the experimental data) as shown in Table 4-3 and Table 4-5. Correlation for 8-point experimental data and 4-point exponential model data is calculated to be 0.68 (medium to high) for GO1 and 0.93 (very high) for GO3 respectively, suggesting exponential model's reproducibility in both the

cases.[113,114] To test the effect of DO values on extrapolation, a Mann-Whitney U Test was done.[115] Due to its higher p-value, GO3 with low DO (1.0089) will have very small errors when extrapolated using the suggested model as compared to GO3 having higher DO (1.9904).

Chapter 5: Properties and Applications of GO Fractions

5.1 Hydrophilicity Control with Fractionation

Surface characteristics are one of the most important properties of graphene oxide. These sheets are generally hydrophilic in nature due to the presence of oxygen functional groups. The most significant method to determine the hydrophilicity and surface roughness of the GO sheets is through contact angle measurements. The picture of the water droplet allows for the determination of contact angle as shown in Appendix (Figure 10-4) where the substrate is the GO film on a glass slide. The measurement shows the solid-liquid interaction between GO and water.[116] The variations in contact angle values due to the roughness of the film are accounted for by multiple experiments and eventually through the error bars in the results.

Figure 5-1 shows the contact angles for different GO fractions. GO (org) is the original GO that was used to produce other GO fractions, i.e., GOw, GOew, and GOee. The fraction obtained from water region (GOw) shows a significant loss in contact angle value due to the presence of a relatively larger number density of oxygen functionalities. GOee shows increased value of the contact angle. Interestingly GOew shows a value which is in between GO and GOee. It is important to note the error bar that signifies the presence of graphene oxide sheets that are varied in terms of the number density of functional groups. GOew is the water fraction obtained from

fractionation of GOe, i.e., it is obtained from both emulsion and water phases of the two-step fractionation process. In other words, the distribution of oxidation on these sheets appears to be more than that of the other GO fractions because of the involvement of the two phases of fractionation. Appendix (Figure 10-5) shows the variation in the contact angle with different oxidation methods, i.e., by Modified Hummers'[1] and Improved Graphene Oxide (IGO)[3] synthesis methods. It shows a vast difference between the two contact angles where IGO appears to have a very low value of contact angle due to the large oxidation time of 12 hours.

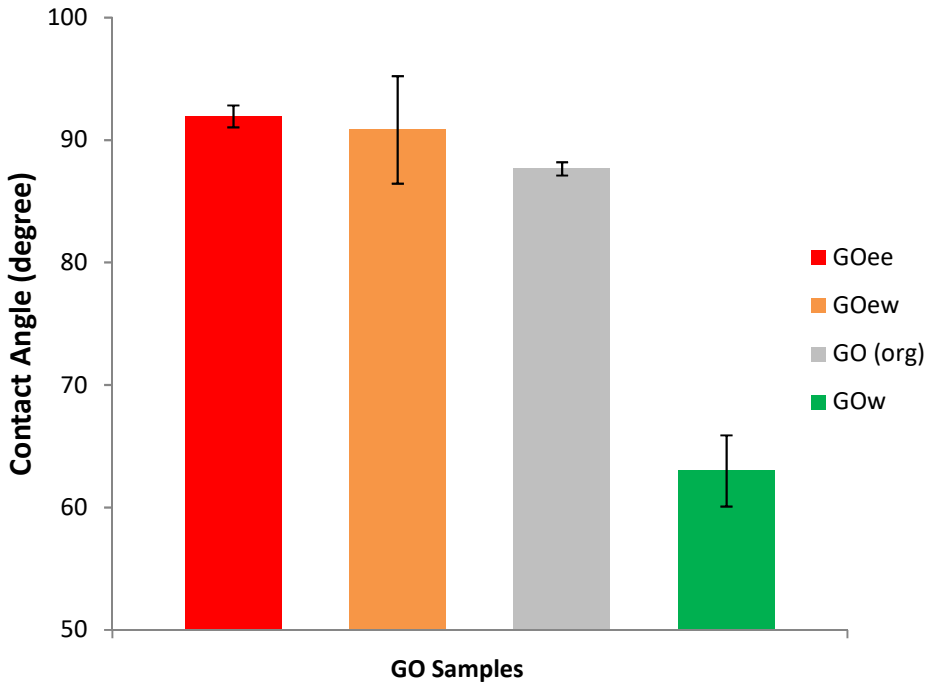

Figure 5-1. Contact angle values for different GO fraction samples starting from the emulsion phase and moving to the water pahse.

5.2 Optical Properties of Graphene Oxide Films

In order to look into the optical properties of GO and its fractions, films were formed on a glass substrate. The process was started from film fabrication on a glass slide using GO, GOw, GOee, and GOew fractions. The first batch of films formed with 0.12mg/cm^2 surface density of GO and named as film-t. The second batch formed with double the surface density of GO (0.24mg/cm^2) is named as film-2t. Film-MW-2t is obtained from microwave reduction[117] of film-2t for 2 minutes.

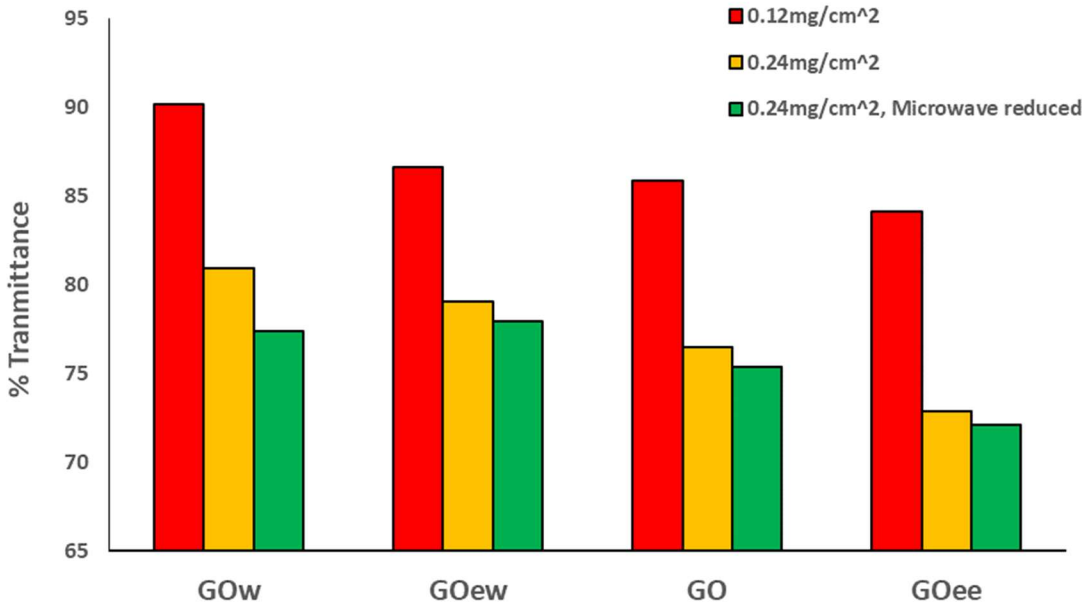

Figure 5-2. Transmittance (%) of light (wavelength, λ= 550nm) for GO fractions coated on a glass slide.

As shown in Figure 5-2 and Table 5-1, transmittance (%) is calculated for all the GO films. As a reference, wavelength value that is generally considered for transmittance (%) is λ= 550nm.[118,74] For example, UV-vis spectra of the films from appendix (Figure

10-6) is used to calculate the transmittance (%) of film-2t by referring to the corresponding values at λ= 550nm.

Table 5-1. Average values of transmittance of light (wavelength, λ= 550nm) for different GO films formed from different GO fractions. The surface density of GO on films named as film-t, and film-2t (thickness twice of film-t), are 0.12mg/cm^2 and 0.24mg/cm^2 respectively. MW-2t is the microwave-reduced film-2t. Glass is the substrate for all GO films.

GO Films	GO Fractions			
	GO	GOw	GOew	GOee
t	85.87	90.15	86.65	84.11
2t	76.50	80.91	79.07	72.89
%change [(t-2t)/t]*100	10.91	10.24	8.74	13.33
MW-2t	75.37	77.4	77.94	72.11
%change [(2t-MW2t)/2t]*100	1.47	4.33	1.42	1.07

No significant effect is observed on doubling the surface density of GO to form film-2t as shown in Figure 5-2. However, microwave reduction affects the GO fractions differently. The change in transmittance of GOw-film-2t after microwave reduction is three times the change in that of GO-film-2t. There is more effect of microwave reduction on the water region GO fractions than that of emulsion GO fractions, which is around 1-1.5%. This phenomenon is partly attributed to the fact that there are more oxygen functionalities in GOw than in emulsion region fractions (GOee and GOew). The most important reason for this significant effect of reduction on GOw is likely due

to the difference in the nature of functional groups in between the water region (GOw) and emulsion region GO fractions.[99,74,119] GOw has the lowest degree of conjugation, and GOe has the highest among GOw, GO, and GOe.

Appendix (Figure 10-7) shows the thickness distribution of GO films made from 0.24mg/cm^2 surface density of GO material on a glass substrate. Synthesis methods for GOa[1] and GOb[3] are different. It shows that the thickness distribution of the GO films made from totally different types of GO materials remain similar. Hence, it is important to note that the transmittance results are significantly affected by the nature of the GO material and mildly affected by thickness of its films.

5.3 Size Distribution of GO fractions

While it is instructive to study the functional groups and degree of oxidation in different GO fractions,[25,109] one other feature that determines the properties of GO material is the flake size and flake size distribution. The optical imaging and image analysis procedure used in our system to obtain the data for sheet size and exfoliation consisted of: imaging, removal of inhomogeneities, conversion of brightness to sheet thickness, and recognition of individual sheets. The substrate carrying the GO sheets was observed under a microscope with a 20X objective, which is a good compromise between spatial resolution and the number of sheets imaged at a time.[120]

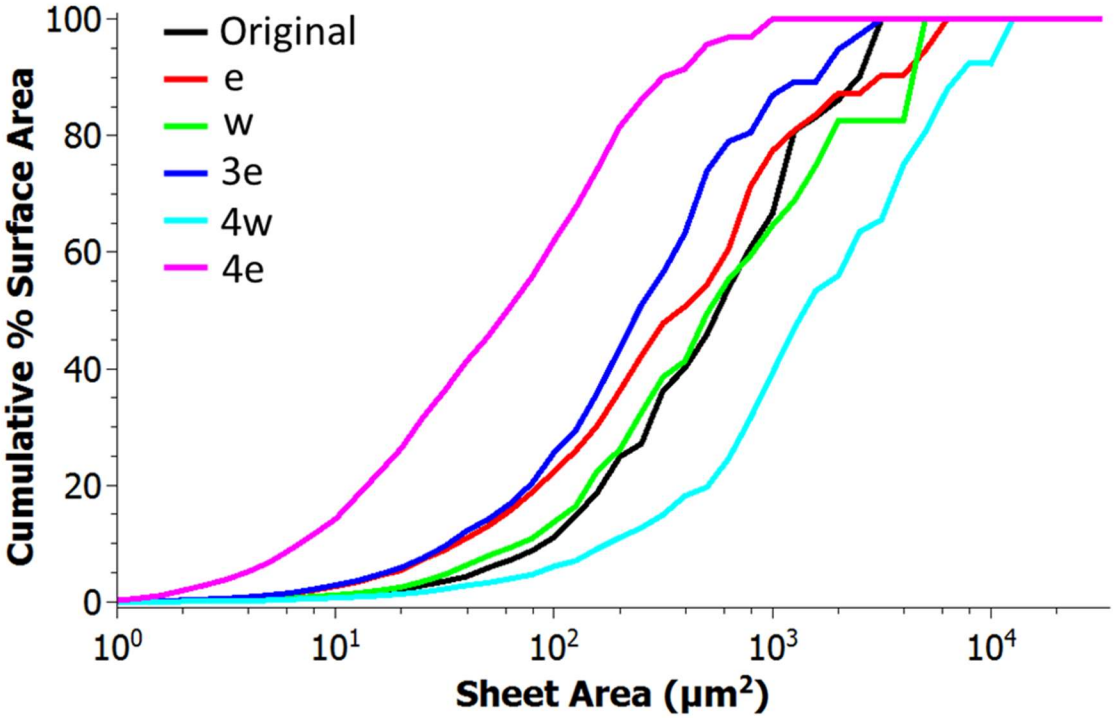

Figure 5-3. Microscopic study of various Graphene Oxide fractions showing cumulative percentage of total sheet surface area as a function of average layer number.

A recent technique to calculate the high-throughput optical thickness and size characterization of 2D materials was used to determine the size and exfoliation (number of layers stacked) of the GO fractions.[120] With the help of this technique, it was observed that the fractionation method was selective for both sheet size and layer number as shown in Figure 5-3 and Figure 5-4. The sheets in the emulsion region fractions (e.g., GOe) were systematically smaller and thinner compared to the original GO solution; accordingly, the water region fractions (e.g., GOw) systematically retained sheets that were larger and had greater layer numbers. GO4w and GO4e are the extreme fractions with highest and lowest oxidation extent and are also the best

examples of this observation. This was most apparent in the layer number distributions of the original GO and GOw (water region GO fraction) samples before and after a few layers mark (less than five layers) and in the convergence of size distributions of these samples after the initial separation in the smaller sheet regime.

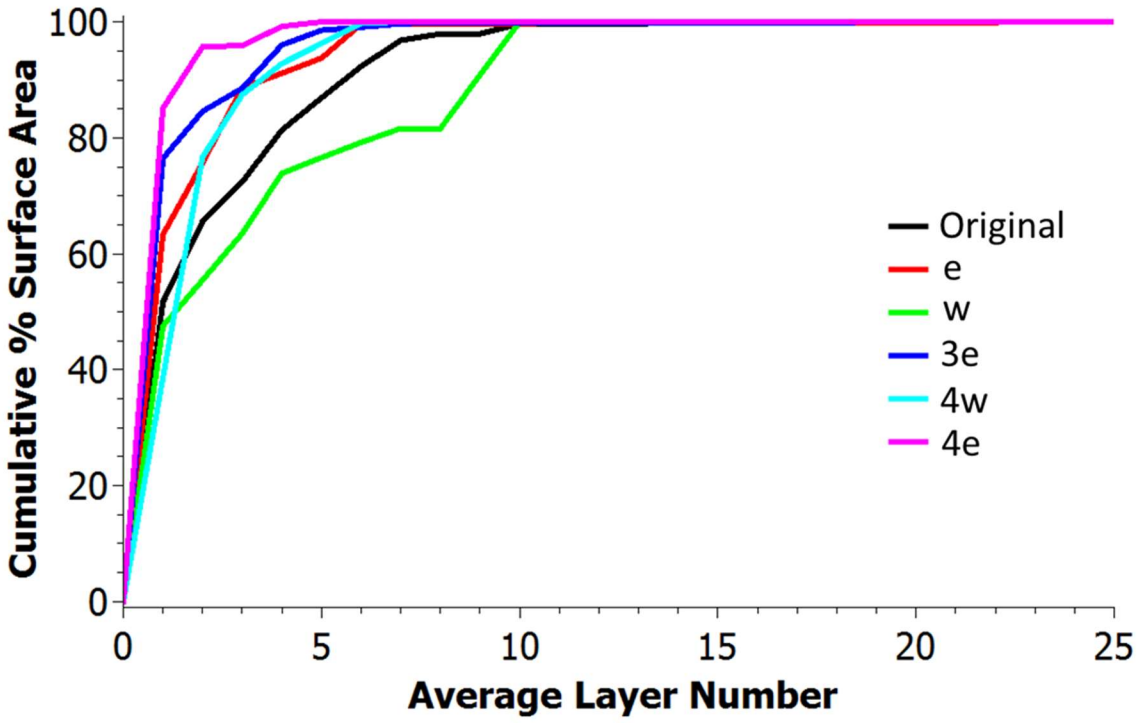

Figure 5-4. Cumulative percentage of total sheet surface area of different GO fractions as a function of sheet area.

Interestingly, all water region GO fraction samples, but not the emulsion region fractions, featured correlated spikes in their layer number distributions at different positions. The fact that both GO and water region fractions independently showed these peaks, while they are absent in the emulsion region GO fractions sample, suggests that these sizes and thicknesses were already overrepresented in the original graphite.

It is interesting to compare this correlation between larger sheet dimensions and higher oxidation levels with the work of Dimiev and Tour, who showed that the oxidation of graphite into graphite oxide during the Hummers' method is controlled by the diffusion rate of the oxidizing agent.[121] This could possibly lead one to expect that larger sheets would be less oxidized than smaller ones. At first glance, the results appear to contradict this expectation, although this is not the case. Rather, the more hydrophobic, nearly un-oxidized graphite in the GO sample went to the oil/water interface, which has been shown to drive exfoliation.[25] The more hydrophilic, highly oxidized material, in contrast, remained in the aqueous phase and thus did not exfoliate and; therefore, remained larger and on average more stacked. This was seen in the difference in the distribution of sheets with an average layer number less than four in Figure 5-4.

It has been shown that oxidation of graphene changes its optical properties.[24] Consequently, we were interested whether different degrees of oxidation found in the various GO fractions would lead to a noticeable difference in the brightness versus thickness curves for different materials. Therefore a linear fit was applied to the brightness values for the first layer (Layer 1) for each sample as shown in Figure 5-5. The brightness change per layer was determined from the slope of this fit for each material and showed a surprisingly strong and significant change as a function of the r value (Figure 5-5).

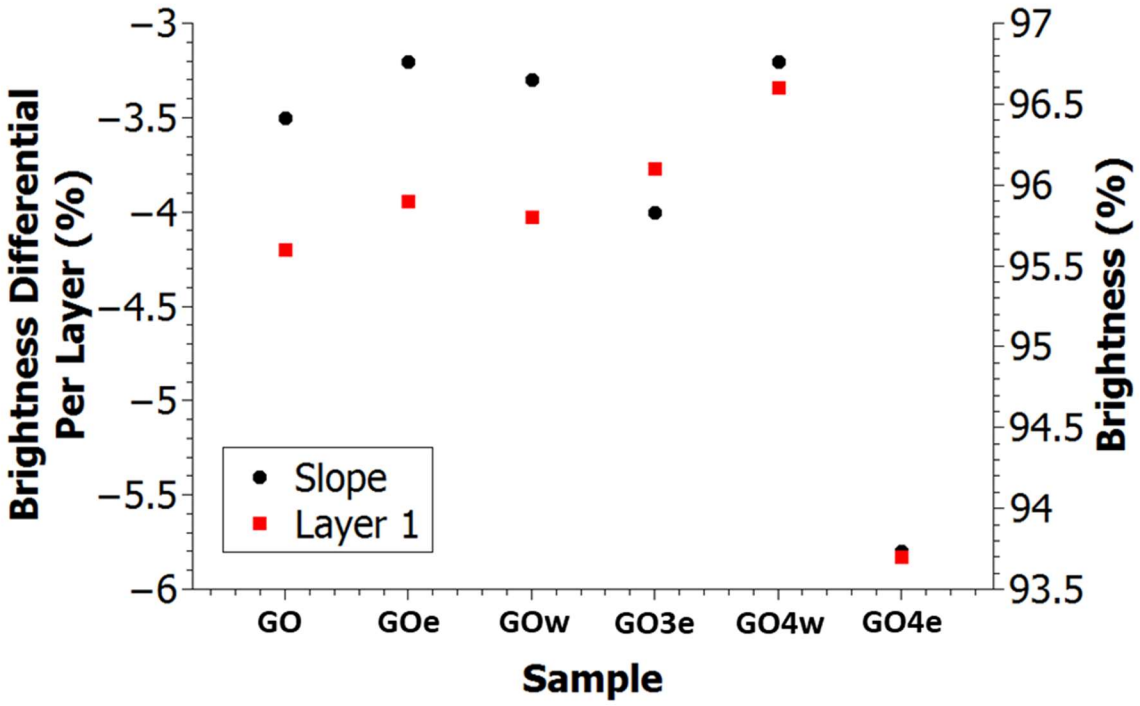

Figure 5-5. Brightness values (right y-axis) for the first layer for each of the samples, with linear fits. Brightness differential per layer in left y-axis (slope of the linear fits from brightness) plotted against the corresponding GO fractions.

As the change in brightness for a given nanosheet layer number is dependent on the dielectric constant of the material,[122] these analysis experiments provide a surprisingly powerful way to assess optical properties of a population; in principle, one could calculate the optical constants of the material using this method.

Also, Appendix (Figure 10-8) shows that the size distribution of the GO sheets is polydisperse and also signals towards different degrees of stacking for the GO sheets governed by the varied brightness of these sheets in the picture.

5.4 GO-Polymer Biocompatibility

Biomaterials like bio-nano interfaces are combinations of nanomaterials and biomolecular assemblies, such as protein complexes or lipid membranes.[123] By tuning the characteristics of these biomaterials, a myriad of nanomaterial functionalities can be realized for biomedical applications in biosensing, drug delivery, neuroscience, imaging, and tissue engineering.[124] There are a very few nanomaterials based drug delivery systems available for aromatic, water-insoluble drugs. PEG is one of the most common candidates used in drug delivery applications however it can't be combined with graphene due to lack of functionalization sites on its structure. On the other hand, GO is one of the most favorable nanomaterials that is used to get various classed of bio-nanomaterials.[31]

PEG (molecular weight = 3.4 Kg/mol, Sigma Aldrich) was combined with various GO fractions in order to look at the effects of fractionation on the viability of these systems. To make the experiments easier but effective, we used a high concentration of GO to PEG to carry out cell viability experiments. 100 µl of 20mg/ml PEG solution is added to 2 ml of 0.5 mg/ml GO (or GO fractions) solution. DI water was the solvent for both solutions. This gives us a 2:1 ratio of PEG and GO material by weight.[31,124] Cell viability results at two different dilutions (original concentration is 25000 of A549 cells per ml) of polyethyleneglycol (PEG) in combination with GO, GOe, GOew, and GOw graphene oxide samples at 7.4 pH are shown in Figure 5-6.

5.4.1 Cell Culture Procedure

A549 cells (adenocarcinomic human alveolar basal epithelial cells) were seeded in a 96 well plate at a concentration (termed as 1/1 dilution) = 25 000 cells/ml.[125] The cells were incubated overnight at 37 °C and 5% CO_2. Absorption of the microplate (with background correction) at 540 nm was measured using a UV-Vis plate spectrophotometer. The pH of a dilution 1/5 of each sample was adjusted to 7.4.

A further dilution 1/10 from the initial 1/5 dilution was made to get a final dilution of 1/50. Subsequent dilutions of ½ from the 1/50 dilution were made (1/100, 1/200, 1/400) to test their effect on cell viability. All the dilutions were made in DMEM cell culture media with antibiotics. Table 5-2 provides the descriptive quantitative look at all these concentrations.

Samples were added to the cells followed by incubation at 37 °C and 5% CO_2 for 24 hours. Then the samples were removed from the cells, and the cells were washed with 100 ul of PBS. This step was repeated twice. 100 ul of the MTT reagent was the added to each sample, and cells were incubated for 4 hours at 37 °C and 5% CO_2.

The MTT reagent was removed, and 200 µl of DMSO was added to each sample. Absorption at 540 nm was measured using a UV-Vis plate spectrophotometer. Cell viability Figure 5-6 is expressed as a percentage of the control that was not exposed to any sample.

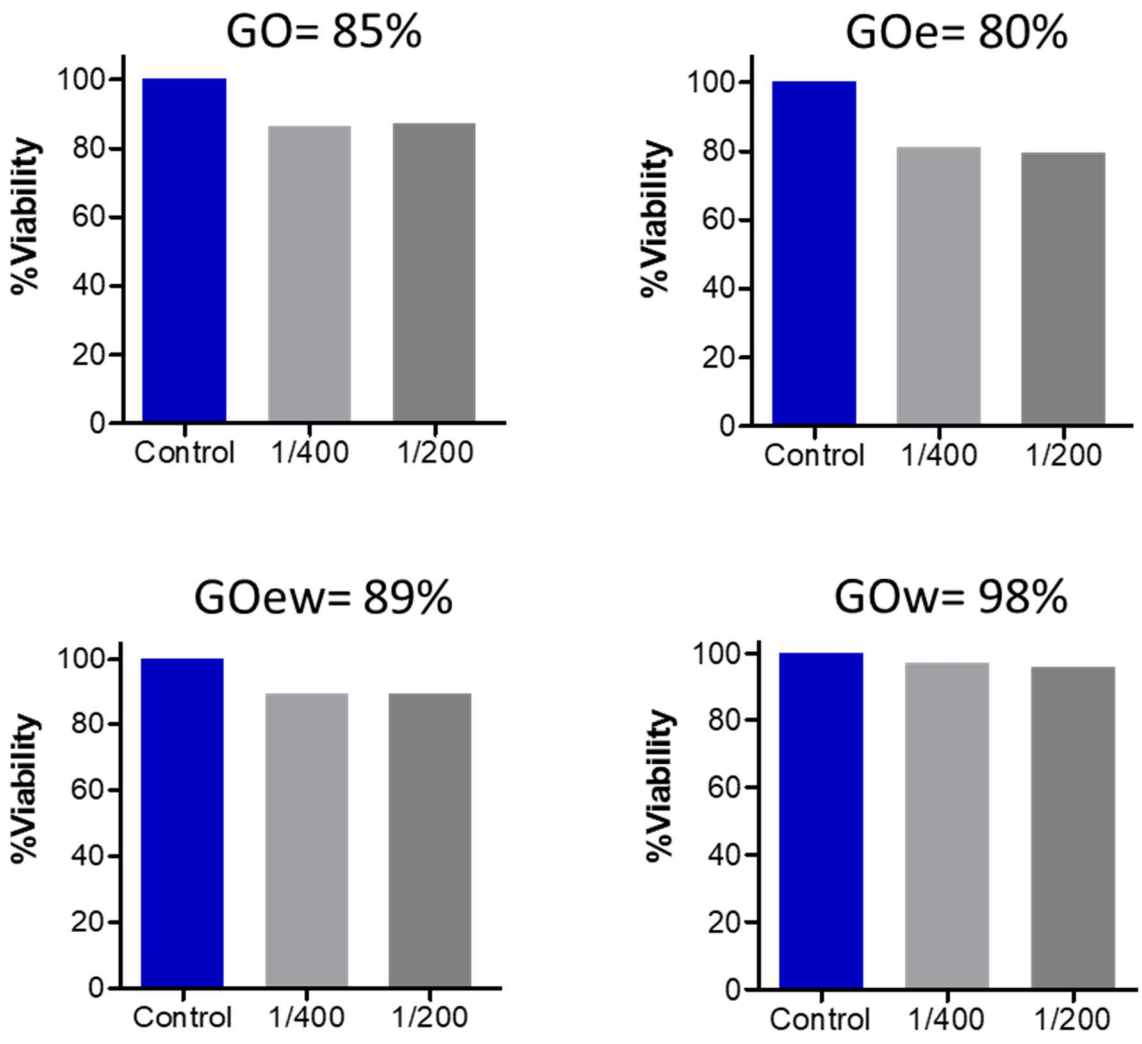

Figure 5-6. In vitro cell viability at 1/200 and 1/400 dilutions (original concentration is 25000 of A549 cells per ml) of Polyethyleneglycol in combination with GO, GOe, GOew, and GOw graphene oxide samples respectively at 7.4 pH. In all the bar graphs, x-axis corresponds to the concentration and y-axis is the % cell viability.

5.4.2 Observations of In vitro cell viability

The % cell viability analysis was done considering a % viability lower than 80% as a real cytotoxic effect. From the pictures in Appendix (Figure 10-9) taken at the lower concentration of nanoparticles, no evidence of cell cytotoxicity was observed. Sample

GO and GOw did not affect the viability of A549 cells at low concentrations. However, at the highest concentrations (1/100 and 1/50) some cytotoxicity was observed. Sample GOe produced a slight decrease in the viability of A549 cells at almost all the evaluated dilutions (except 1/400). This effect was not concentration-dependent however. Sample GOew did not affect the viability of A549 cells at any of the tested dilutions.

Table 5-2. Results and analysis for in vitro cell viability tests for various GO fractions with PEG. Data consistans of %viability average, standard deviation (SD), variance(VC), and values relative to control sample (100%).

GO						
	Blank	Control	1/400	1/200	1/100	1/50
	0.0343	0.8372	0.7411	0.7066	0.5989	0.7946
	0.0289	0.9139	0.7044	0.7891	0.5433	0.6652
	0.033	0.7633	0.8157	0.8218		0.5688
	0.034	0.73		0.7279	0.5193	0.5032
	0.0305	0.9832				
	0.0287	1.0301				
		0.9091				
		0.7738				
Average	0.0316	0.8676	0.7537	0.7614	0.5538	0.6330
SD	0.0025	0.1090	0.0567	0.0534	0.0408	0.1267
VC	8.0034	12.5640	7.5246	7.0081	7.3726	20.0096
Average - blank	0.0000	0.8360	0.7222	0.7298	0.5223	0.6014
% Control		100.0	86.4	87.3	62.5	71.9

GOe						
	Blank	Control	1/400	1/200	1/100	1/50
	0.0343	0.8372	0.6452	0.7626	0.6073	0.7626
	0.0289	0.9139	0.6598	0.7133	0.6076	0.7133
	0.033	0.7633	0.7432	0.6741	0.5983	0.6741
	0.034	0.73	0.788	0.6277	0.6359	0.6277
	0.0305	0.9832				
	0.0287	1.0301				
		0.9091				
		0.7738				
Average	0.0316	0.8676	0.7091	0.6944	0.6123	0.6944
SD	0.0025	0.1090	0.0681	0.0574	0.0163	0.0574
VC	8.0034	12.5640	9.6006	8.2596	2.6672	8.2596
Average - blank	0.0000	0.8360	0.6775	0.6629	0.5807	0.6629
% Control		100.0	81.0	79.3	69.5	79.3

GOew						
	Blank	Control	1/400	1/200	1/100	1/50
	0.0343	0.8372	0.7249	0.8592	0.7881	0.9589
	0.0289	0.9139	0.6527	0.8166	0.6402	0.8047
	0.033	0.7633	0.7375	0.6666	0.7268	0.7941
	0.034	0.73	1.0087		0.7657	
	0.0305	0.9832				
	0.0287	1.0301				
		0.9091				
		0.7738				
Average	0.0316	0.8676	0.7810	0.7808	0.7302	0.8526
SD	0.0025	0.1090	0.1564	0.1012	0.0651	0.0922
VC	8.0034	12.5640	20.0221	12.9569	8.9189	10.8191
Average - blank	0.0000	0.8360	0.7494	0.7492	0.6986	0.8210
% Control		100.0	89.6	89.6	83.6	98.2

GOw						
	Blank	Control	1/400	1/200	1/100	1/50
	0.0343	0.8372	0.8547	1.0409	0.5977	0.7849
	0.0289	0.9139	0.7693	0.833	0.513	0.5986
	0.033	0.7633	0.848	0.7875	0.634	0.5414
	0.034	0.73	0.9078	0.6726	0.569	
	0.0305	0.9832				
	0.0287	1.0301				
		0.9091				
		0.7738				
Average	0.0316	0.8676	0.8450	0.8335	0.5784	0.6416
SD	0.0025	0.1090	0.0571	0.1539	0.0511	0.1273
VC	8.0034	12.5640	6.7565	18.4597	8.8319	19.8441
Average - blank	0.0000	0.8360	0.8134	0.8019	0.5469	0.6101
% Control		100.0	97.3	95.9	65.4	73.0

With the results from Figure 5-6, Table 5-2, and Appendix (Figure 10-9), it is clear that the water region GO fractions should be chosen to improve the cell interactions with GO-based bio-nanomaterial systems.

5.5 GO-Reinforced Polymer Composites

A variety of uses have been envisioned or demonstrated for graphene and GO in the past decade, and their use as a composite filler has attracted considerable interest.[73,105,126,127] While polymer nanocomposites incorporating GNP fillers continue to be a significant research focus, recent work has largely focused on the use of graphene-based filler materials derived from GO. GO-derived fillers can exhibit high electrical conductivities (on the order of thousands of S/m), high moduli and can be functionalized to tailor their compatibility with the host polymer.[102] The reported values of stiffness and electrical conductivity of GO-derived filler materials can be higher than those reported for nano-clays, but generally lower than those reported for single-walled carbon nanotubes (SWNTs).

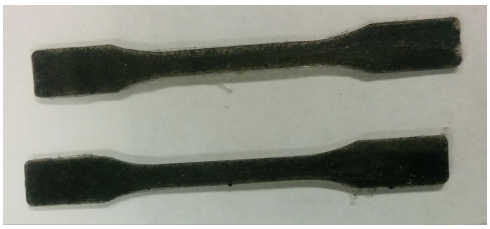

Figure 5-7. Dog-bone shaped ASTM D638 mechanical testing 1% GO-PP samples.

The mechanical properties of GO can be improved by various modifications before or during the nancomposite processing.[128-131] However, the intrinsic mechanical properties and electrical and thermal conductivities of SWNTs may be comparable to those of pristine graphene. Moreover, the two-dimensional platelet geometry of graphene and graphene-based materials may offer certain property improvements

that SWNTs cannot provide when dispersed in a polymer composite, such as improved gas permeation resistance of the composite. [105,102]

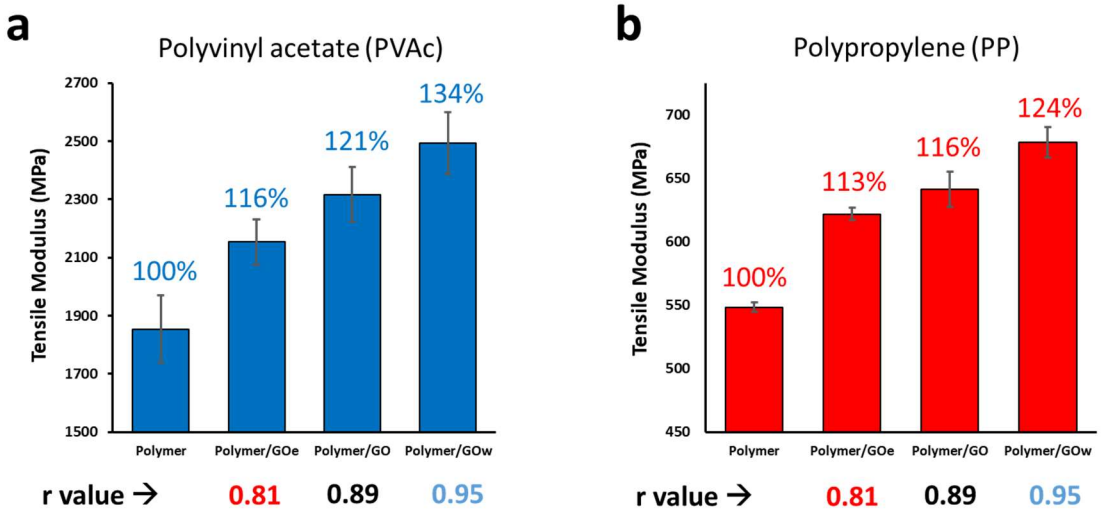

Figure 5-8. Comparison of tensile moduli of (a) hydrophilic PVAc and (b) hydrophobic PP composites made with 1% loading of different GO fractions. Polymer represents the control experiment and % represents the increase of modulus relative to control.

Two types of polymer matrices, isotactic polypropylene (PP, Mol. Wt.= 250K) and polyvinyl acetate (PVAc, Mol. Wt.= 500K) were obtained from Sigma Aldrich. The choice of polymers is based on the variation in the chemical nature of the two. PP is a hydrophobic polymer, and PVAc is hydrophilic. While PVAc will have an affinity towards GO oxygen functional groups, it was interesting to see how the PP and GO interaction takes place and how graphene oxide impacts the mechanical properties of PP.

For processing of polymer composites, a calculated amount of polymer matrix with 1% by weight concentrations of GO, GOe and GOw respectively were prepared and mixed using a rotating mixer at 36 rpm for 30 mins. The blend was dried in a vacuum oven at 100 °C for 24hrs. The dried mixture was loaded into a co-rotating Haake Minilab II micro-compounder at 200 °C and mixed efficiently for 7mins at 50 rpm, by passing through recirculation channels.

After the processing operation was complete, the melt was diverted out of the channel, and the collected melt chopped into fine granules. The granules were fed into a Microinjection Molding Haake Minijet, and the injection molding samples were prepared following the ASTM D638 (Type V) at 200 °C at a pressure of 760 bar. Figure 5-7 shows the mechanical testing dog-bone samples obtained from PP matrix reinforced with original GO filler.

Table 5-3. Tensile modulus with % error values of PVAc and PP reinforced by different types of GO fractions as fillers.

	PVAc		PP	
	Tensile Modulus	%Error	Tensile Modulus	%Error
Polymer	1854.1	6.3	548.4	0.6
Polymer/GOe	2153.2	3.6	621.7	0.8
Polymer/GO	2316.0	4.1	641.1	2.1
Polymer/GOw	2492.8	4.3	678.4	1.8

The tensile testing was done following the ASTM D638 test method. The compounded materials were evaluated at the rate of 5mm/min. The width and thickness of the samples were measured to make sure of the accuracy of ASTM standards. Figure 5-8 shows the tensile modulus for polymer control and GO or GO fractions- reinforced polymer composites. Table 5-3 shows the value of the tensile modulus with an error below 6 % in all the cases. This error value makes the modulus values comparable.

The tensile modulus of the polymer increases with the addition of GO, or its fractions. In general, mechanical loads that are being applied to the composite material are being supported by the reinforcing fillers, i.e., GO in the present case. The function of the matrix bonded to the GO transfers the load.

An interesting aspect that has never been seen previously is that just 1% GOw (water fraction of GO) reinforces the polymer matrix to increase its modulus by 34%, more than corresponding GO or GOe in the present set of polymer composites. The tensile properties depend on the movement of polymer chains over other polymer chains and GO surface.[132] In addition, there are some other factors that play an important role in the mechanical behaviour of polymer composites, e.g. the orientation of plane of α-form PP, and extent of GO acting as β-nucleating agent for PP.[132,133] GO reinforces the hydrophilic polymer to a greater extent than that of hydrophobic polymers resulting in higher value of % tensile modulus increase for Polymer/GOw composites. Also, due to the higher resistance to movement of polymer chains and GOw sheets, corresponding GOw composites reinforce more than that of the GO and GOe composites. Higher resistance is because of the presence of OH, COOH, CO

and other oxygen functionalities on GO sheet surface that establish adhesion with the hydrophilic polymers but not with the hydrophobic polymer that well.

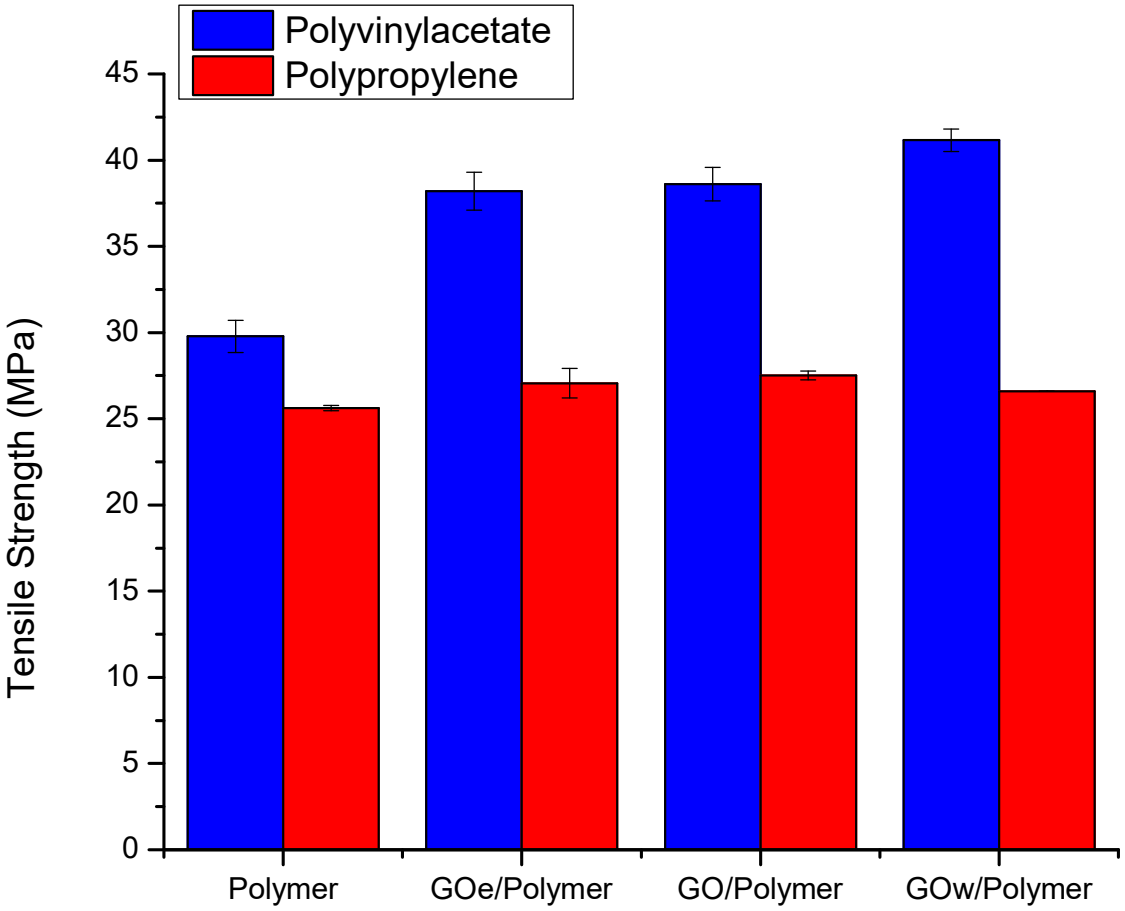

Figure 5-9. Comparison of tensile strengths of hydrophilic PVAc and hydrophobic PP composites made with 1% loading of different GO fractions. Unlike modulus, the addition of GO doesn't affect strength values for hydrophobic PP but just hydrophilic PVAc. Polymer represents the control and % represents an increase of strengths relative to control.

Another important mechanical property of the polymer/GO composites is the tensile strength, which stands for the capacity of a material or structure to withstand loads tending to elongate. It is measured by the maximum stress that a material can

withstand while being stretched or pulled before breaking. Figure 5-9 shows the tensile strength values of the GO reinforced polymer composites. One interesting observation that differentiates tensile strength results from modulus results is that there is no effect of reinforcement on the tensile strength of PP composites, which has been observed the literature earlier as well.[132,134,135] This is because the strength values are closely related to the attraction of filler and matrix surfaces. Since PP and GO have little affinity between them, there is no increase the strength value.[73,130,136,137] This doesn't hold true in case of hydrophilic PVAc where the oxygen functionalities make a difference.[90,138,139]

5.6 Electrochemical Applications of Graphene Oxide

Lithium-ion batteries (LIBs) are one of the most popular rechargeable batteries for critical applications such as electric vehicles, electronic devices, locomotives, and aerospace.[52] However, the theoretical capacity limits with the conventional electrode materials impede its further applications. It is imperative to search novel LIB materials with high reversible capacity, long cycle life, and low cost. In this regard, elaborately designed GO-based materials exhibit superior performance in both anode and cathode materials.[140,141]

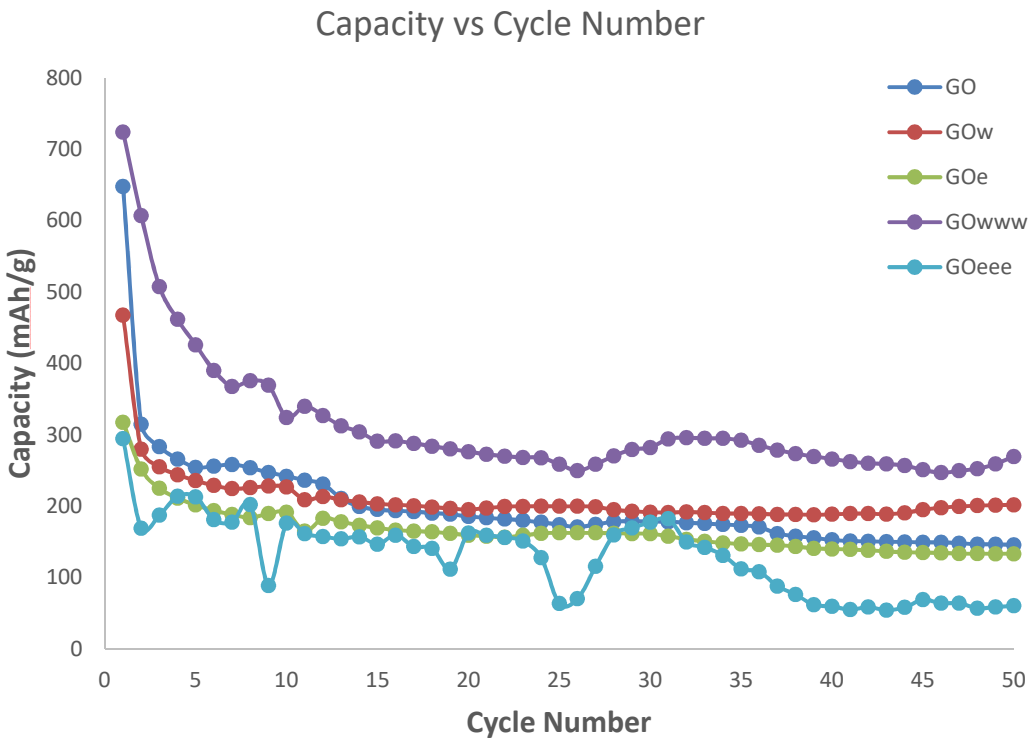

Figure 5-10. Comparison of loss of capacity with increasing cycle number for batteries containing different GO fraction samples.

Figure 5-10 shows the capacity of the battery (button cell) fabricated with materials containing the GO and its fractions (GOw, GOe, GOwww, and GOeee) for 50 cycles. The GO precursor used for fractionation here is oxidized by a modified Hummers' method for 2 hours. Each cycle represents a charging and discharging step. All the capacity results indicate that the GO material obtained from the water region of the fractionation (GOw and GOwww, refer Figure 3-3 and Appendix (Figure 10-3)) allow the diffusion of ions in the battery for higher number of cycles storing higher amount of energy (capacity) than that of GO fractions obtained from emulsions regions (GOe and GOeee). Capacity values of 50th charge-discharge cycle of each battery are

shown in Figure 5-11 Incorporation of extreme water fraction of GO shows a high capacity significantly more than that of emulsion fractions.

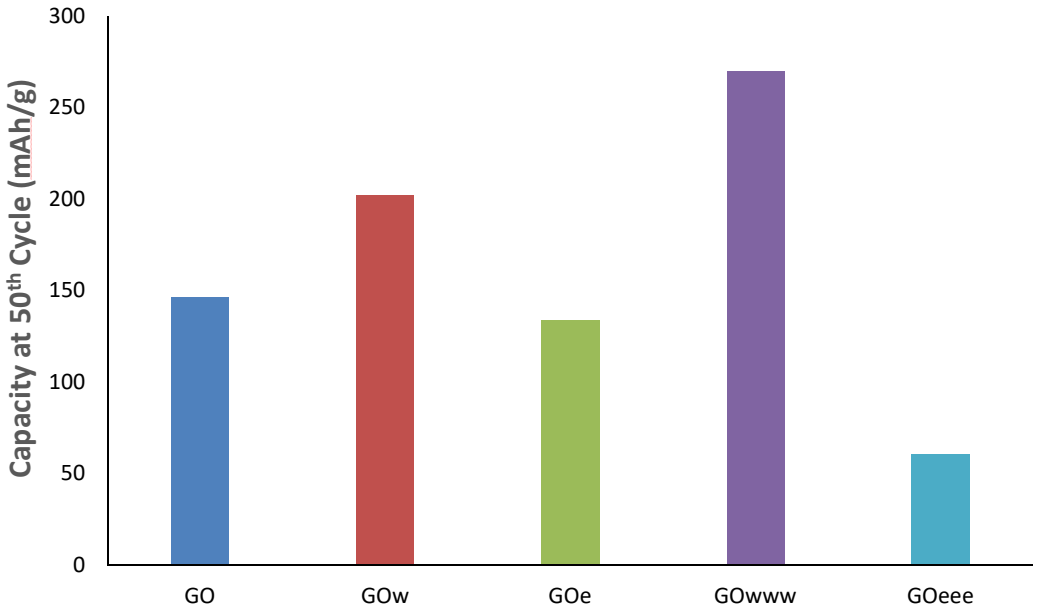

Figure 5-11. Capacity values for batteries containing different GO fraction samples.

In order to understand the variation due to original GO material, Appendix (Figure 10-10) shows the results obtained from batteries fabricated and tested identically to the same batteries used in the experiments shown in Figure 5-10 but with a different GO precursor that was synthesized by a modified Hummers' method for 1 hour. This electrochemical experiment proves that the oxygen functionalities play an important part in final capacity and consistency of a battery. Also, choosing the optimum synthesis methods for GO is also important for the final battery performance.

Chapter 6: New Generations of Graphene Oxide

6.1 Sonicated Graphene Oxide

The oxidation of graphite to GO starts with the oxidizing agents diffusing between the layers of the graphite.[142] In order to achieve faster diffusion during oxidation, we carried out the modified Hummers' reaction with bath sonication for 2 hours and we named the resulting product sonicated graphene oxide (SGO). The GO product that was synthesized with the same Hummers' method but without the use of bath sonication during the reaction is named as HGO.

The reaction used twenty-five milliliters of sulfuric acid (Fisher Scientific, ACS Plus) and 500 mg of sodium nitrate (Acros Organics, 99%+, ACS Reagent) added to a round bottom flask and stirred until dissolved. One gram of natural flake graphite (Asbury Mills, Grades 3243 and 2299) was then added to the flask and mixed until dispersed. When graphite is added, the solution turns black with a viscosity similar to that of water. Finally, 3 g of potassium permanganate (EM Sciences, GR ACS) is slowly added to the reaction flask to avoid overheating the system, but quickly enough so that the system does not thicken first. Addition of the oxidizing agent initially changes the solution to a dark red, which then rapidly converts to dark green with an increase in viscosity. The solution temperature can rise above 80 ˚C, and as the reaction continues past an hour, the temperature begins to drop slightly.

Once all reagents are combined, the reaction proceeds under constant stirring for two hours before it is quenched. Bath sonication is stopped after 2 hours and the oxidation reaction is complete. Immediately after the bath sonication is stopped, the reaction is quenched by the rapid addition of 200 mL of de-ionized (DI) water and 25 mL of hydrogen peroxide (Acros Organics, 35 wt. %). Adding the water causes the solution temperature to rise with a vigorous effervescence caused by the addition of the hydrogen peroxide. After the effervescence slows to a minor bubbling, 25 mL of hydrochloric acid (Sigma Aldrich, 37% A.C.S. reagent) was added to solubilize residual salts.

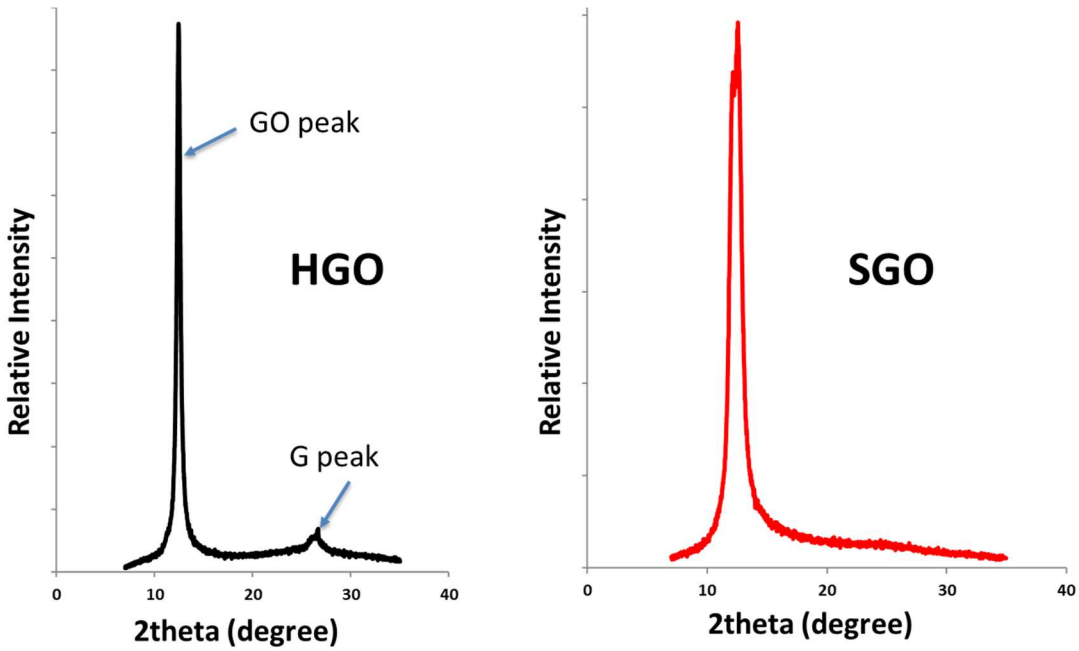

Figure 6-1. XRD patterns of graphene oxide produced by Modified Hummers' method and (HGO) and Bath Sonication Method (SGO).

After quenching the solution, it becomes a yellow suspension, in contrast to the black product of the Hummers method (without bath sonication) as shown in the

Appendix (Figure 10-11) and is further diluted with DI water. It should be noted that the product looks black for the same reaction without the use of bath sonication. Additional workup includes centrifugation at 4,000 rpm until the supernatant is clear. The supernatant is then removed, and fresh DI water is added to resuspend the graphite via bath sonication. The process is repeated until the solution attains a neutral pH. Cleaned graphite samples are then dried, ground into a powder, and stored in a vacuum oven to prevent absorption of water.

Figure 6-1 shows the XRD pattern of HGO and SGO. SGO does not show any G peak which is a sign of highly oxidized GO product. As opposed to SGO, HGO contains a significant intensity of G peak.

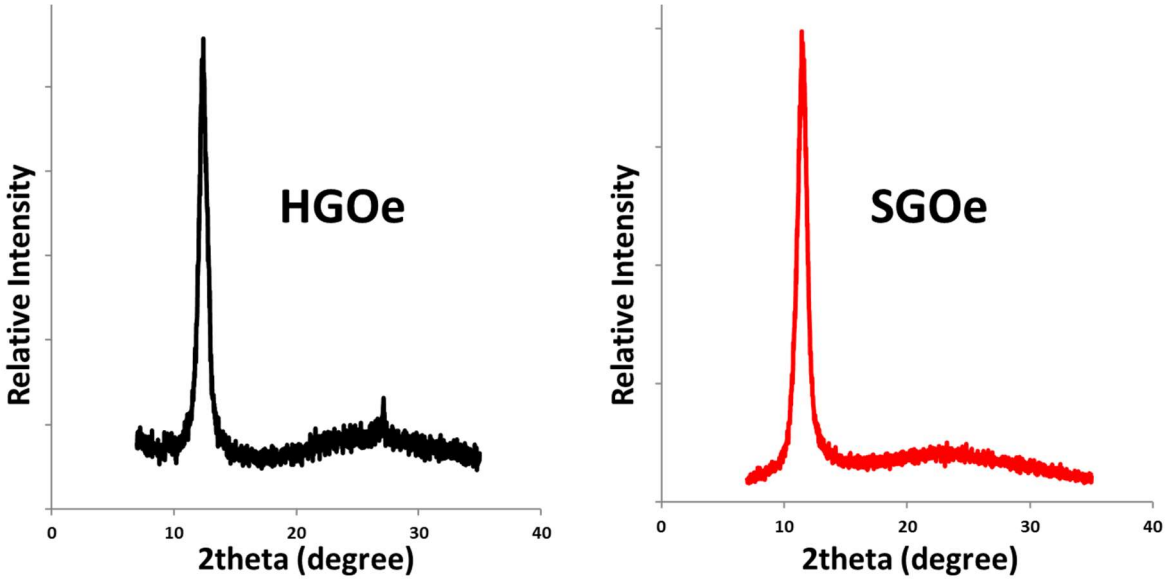

Figure 6-2. XRD patterns of HGOe and SGOe, the emulsion region fractions of HGO and SGO respectively.

In order to corroborate this phenomenon further, both these GO products are used for fractionation (refer Figure 3-3 for fractionation process). XRD patterns of emulsion region GO fractions (HGOe and SGOe) are compared as shown in Figure 6-2. HGOe and SGOe are the more graphitic (less oxidized) fractions of their corresponding original GO materials. Interestingly, the emulsion fraction of SGO, i.e. SGOe with comparatively lower degree of oxidation than SGO, does not show any G- peak. It shows that SGO is very highly oxidized. However, HGOe shows an intense G-peak corresponding to more graphitic nature than that of HGO. It also shows that HGO contains fewer oxidized sheets than SGO.

6.2 Under-oxidized Graphene Oxide

6.2.1 Method to produce uGO:

Fractionation of original GO (or GO) is carried out using chloroform and water as solvents. Forming an emulsion in the presence of GO creates two phases: a water phase containing highly oxidized GO and a lower oil-in-water emulsion phase containing uGO. The solvents used to form the emulsion are recycled. The final emulsion fraction after ‘n’ number of fractionation steps is called GOne.[109]

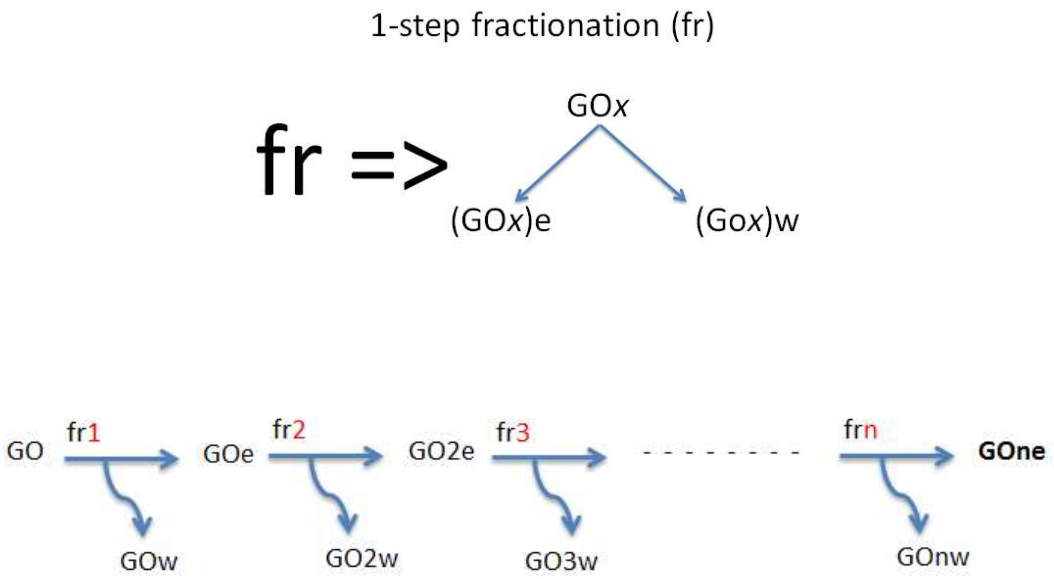

Figure 6-3. a) Schematic representation of the definition of 'fr.' 'fr' is 1-step fractionation of GOx into two of its fractions, the emulsion fraction GOxe and the water fraction- GOxw. b) Scheme for multiple fractionations. Here GOne is the fractionation products of n fractionations (x=n) of GO.[109]

For a particular GO/water/oil system, a particular value of x= n giving GOne is called uGO. Generally, it is when the XRD r ratio (area of GO peak divided by the area of graphite peak) is < 0.50 as shown in Figure 6-5.[109] The XRD r ratio is one way to determine the degree of oxidation of a GO sample. Higher 'r ratio' means a greater degree of oxidation. An example is shown in Figure 6-4.

6.2.2 X-Ray Diffraction characterization approach

Each fractionation step uses an oil/water-based emulsion to get an emulsion fraction (GOe) and water fraction (GOw) as explained in Figure 6-3a. After performing six fractionation steps, i.e., n=6 referring to Figure 6-3b, to get GO6e, the r ratio is 0.45 (Figure 6-5), and we assign it uGO from a 6-step fractionation using chloroform-water

emulsion system. XRD r value for GO is 0.94. This is the GO used for six fractionation steps to get the final fraction- uGO with XRD r value of 0.45.

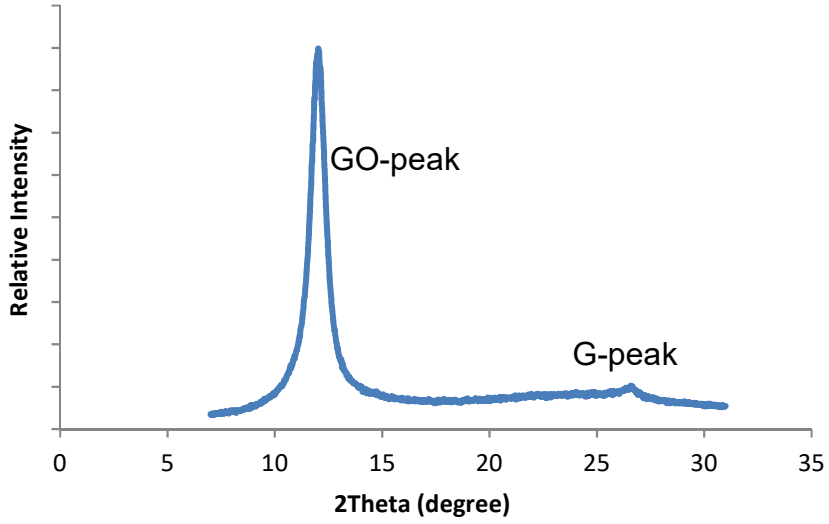

Figure 6-4. XRD diffraction pattern of original GO. XRD r ratio is 0.94.

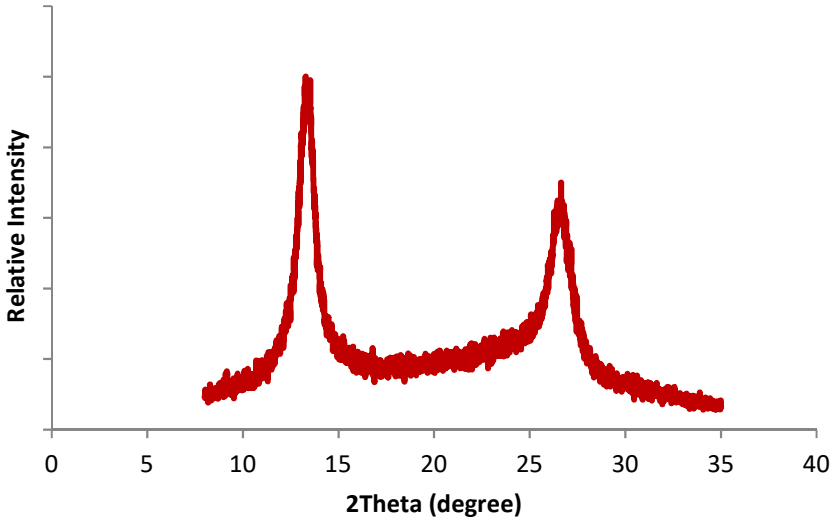

Figure 6-5. XRD diffraction pattern of uGO. XRD r ratio is 0.45.

6.2.3 Raman Spectroscopy characterization approach

Conversion of GO to rGO leads to a higher D peak intensity (relative to G peak intensity). This is a well-known indication of increased disorder in the system. A typical example is shown in Figure 6-6. Here, the I_D/I_G ratio is much higher for rGO as compared to the GO used to make that rGO.

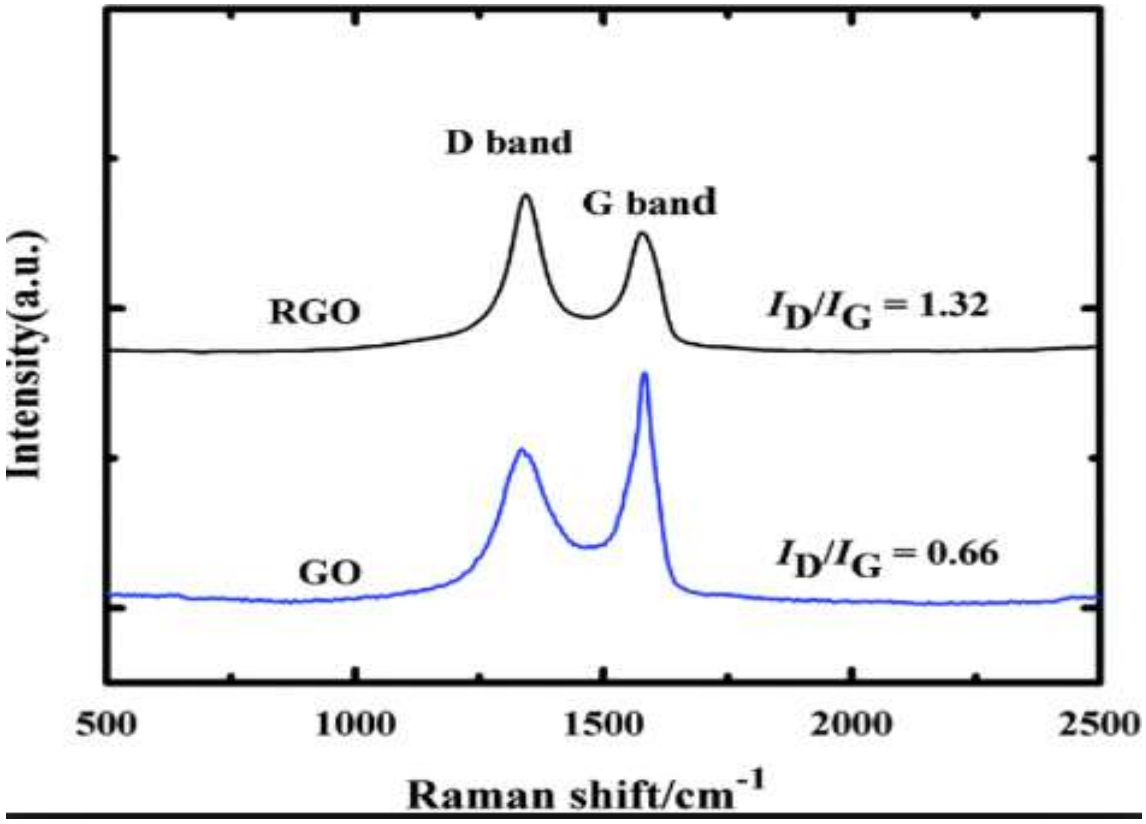

Figure 6-6. Comparison of I_D/I_G peak intensity ratio of rGO and GO peak.[97] (Taken from: *J. Mater. Chem. A*, 2014,2, 1332-1340.)

I_D/I_G ratio from the Raman spectrum of uGO decreases as compared to that of GO from which it was isolated as shown in Figure 6-7. It means that uGO doesn't contain all the defects that a corresponding rGO would contain due to reduction reactions. But

uGO is oxidized to a lower extent than GO and thereby exhibits more delocalization of electrons.

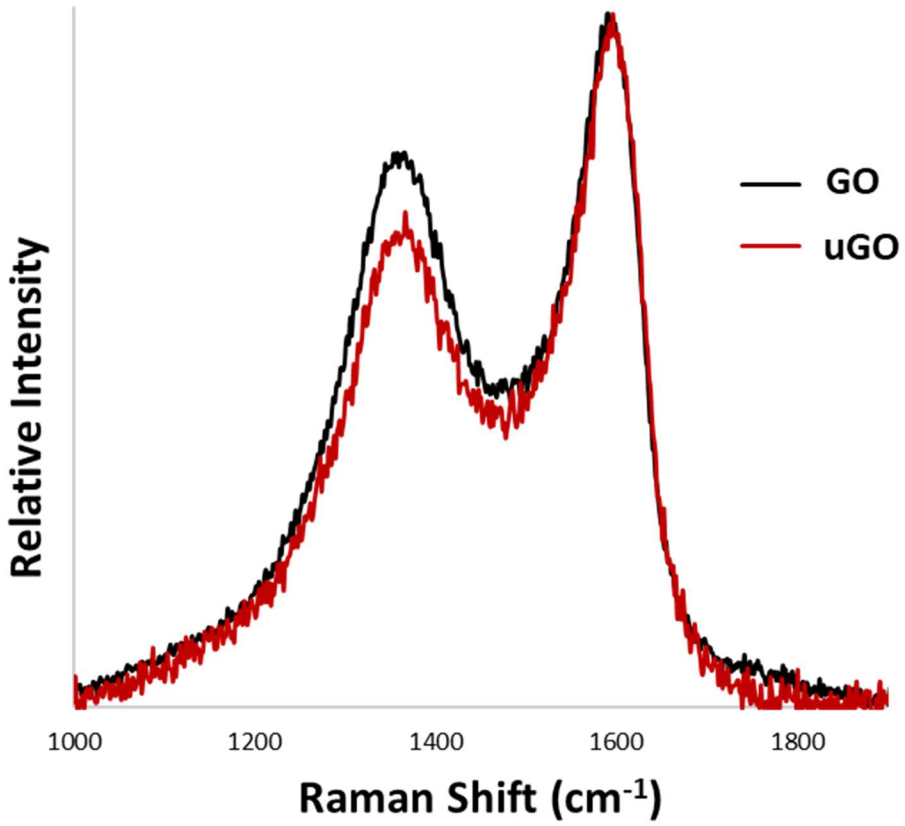

Figure 6-7. Raman spectrum of Original GO and uGO with I_D/I_G peak intensity ratio of 0.75 and 0.69 respectively.

Raman spectra results from Figure 6-6, and Figure 6-7 are the primary basis for identification of uGO, indicating that uGO has fewer defects than rGO, confirming the presence of a lesser degree of oxidation (i.e., more delocalization of electrons/C=C bonds), and one reason for the better properties of uGO as compared to rGO.

6.2.4 uGO Aging

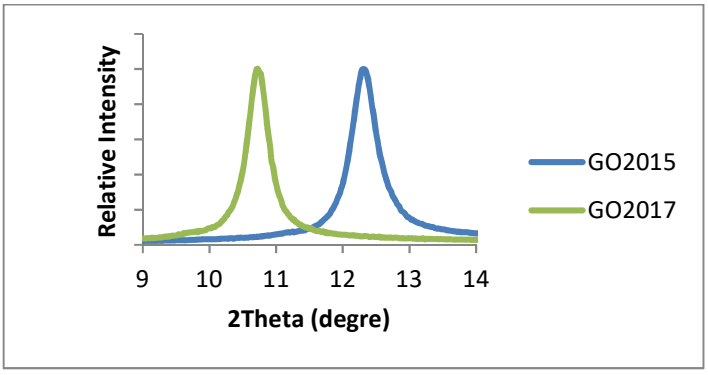

Figure 6-8. XRD experiment for same GO sample performed in the year 2015 and 2017. FWHM for GO2017 is 71% of FWHM for GO2015.

An increase in uGO crystallinity compared to GO is observed over time. The full width at half maximum value (FWHM) for an XRD pattern is a method to compare the crystallinity of various materials qualitatively.

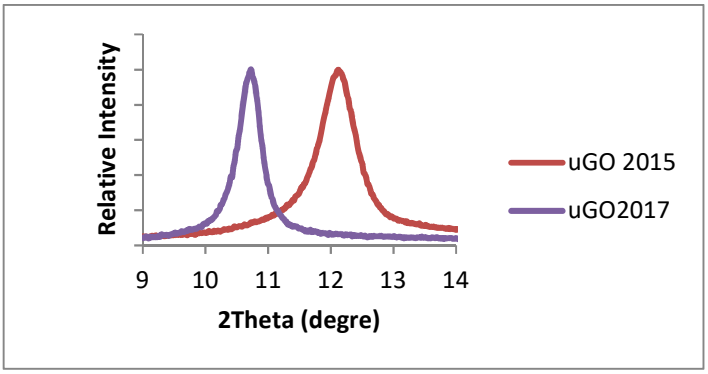

Figure 6-9. XRD experiment for same uGO sample performed in the year 2015 and 2017. FWHM for uGO2017 is 60% of FWHM for uGO2015.

The higher the FWHM value, the lower is the crystallinity.[143,144] XRD experiments were conducted by keeping GO and uGO coated glass slides for 2 years in a Petri dish. Figure 6-8and Figure 6-9 shows the XRD patterns for GO and uGO respectively.

Each figure further demonstrates the two types of patterns, one that was done in the year 2015 (larger FWHM) and another in the year 2017 (smaller FWHM). FWHM of GO peak in XRD pattern decreases to 71% in two years as opposed to uGO that decreases to a much lower value of 60%. It can be inferred that uGO goes on to be more crystalline with time than that of original GO.

6.2.5 uGO Hydrogels

Polymer hydrogel[145] was formed by mixing 6ml of DI water, 4ml of heptane, 0.5g HMA (hydroxymethylacrylamide), 6mg of N,N'-Methylenebisacrylamide crosslinker, 10mg of potassium peroxodisulfates (KPS), 5.5mg of N,N,N,N-tetramethylethylenediamine (TEMDA) = 5.5, and GO or uGO= 15mg.

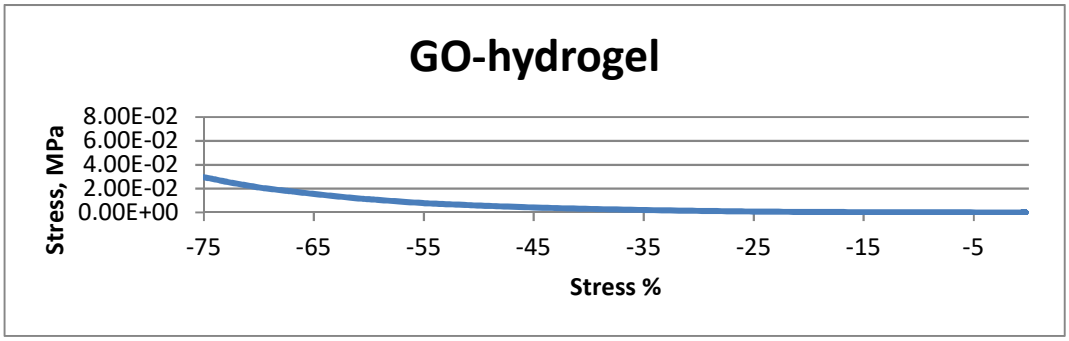

Figure 6-10. DMA stress vs. strain compression test for GO hydrogel.

Due to the presence of water and oil, the system gives rise to an emulsion stabilized by GO sheets.[108] This mixture is then kept at 40 °C overnight. The result is a GO hydrogel. The same procedure is used for uGO to produce a uGO hydrogel.

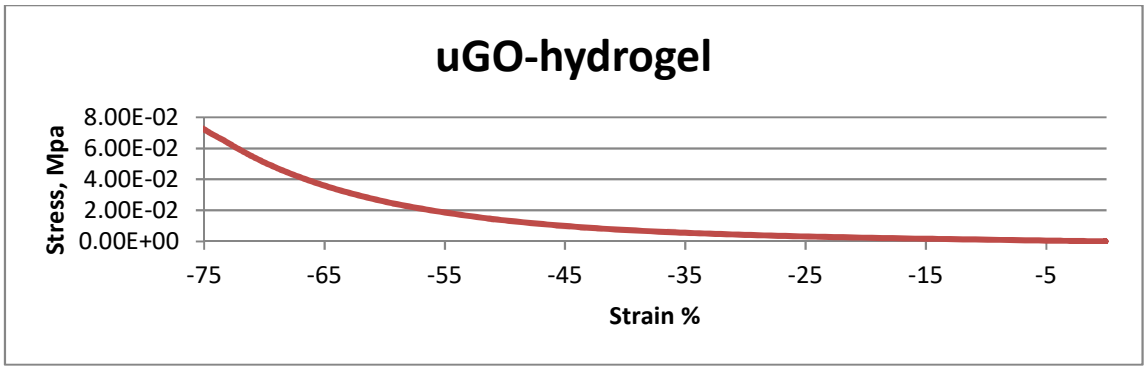

Figure 6-11. DMA stress vs. strain compression test for uGO hydrogel.

The stress sensitivity of hydrogels has been a topic of discussion in the past, but not many materials are available to improve this property.[146,147] DMA is performed on GO and uGO hydrogels. Negative strain % value indicate compression. dAs per Figure 6-10 and Figure 6-11, the advantage of uGO hydrogel is that it is more sensitive towards compression compared to original GO hydrogel as shown by the DMA results.

Table 6-1. Stress values obtained from DMA for GO and uGO hydrogels at -25, -50, and -75 %Strain.

Strain (%)	**Corresponding Stress (kPa)**	
	GO hydrogel	**uGO hydrogel**
-25	0.84	3.2
-50	5.9	13.8
-75	29.7	72.4

Chapter 7: Thermal Equilibrium State of Graphene Oxide

In the last/past decade, graphene oxide (GO) has emerged to be an most important two-dimensional materials because of its wide range of applications in the areas of environmental[110,140], medical devices and therapeutics[106,148], polymer nanocomposites[149], electrochemical[103], medicinal chemistry[150,148], energy[151], and electronics.[88,3] Our findings conclude that totally different GO materials become similar within a few years with identical defect densities. The majority of GO is synthesized using Modified Hummers' methods, and we have shown that, within a few years, storage leads to an identical GO. Factors responsible for the excellent properties of GO are its exfoliated nature and the oxygen functionalities on its surface and edges which make it easier to process.[152,81,153] There has been some effort to control and optimize these factors to make this material more promising for present and future advanced technologies.[24,25,152] Comparison of various studies on GO, e.g. XRD,[3,25,142,154–157], TGA,[81,158–163], etc. show that properties are sometimes very different as these studies do not mention whether the experiments were performed after a day or a month or a year. The presented research in this chapter proves that the analysis of aging is very important in the case of GO materials.

In recent years, there have been vast discrepancies in the properties of similar kind of GO materials[29,86,99,139,153,164]. To have better control, especially in case of extremely sensitive applications in neurology[141,99], biosensing[148], medicinal chemistry[150,148], etc., the properties of GO need to be consistent over time and in different environments.

There has been no investigation done to look at the changes that take place in GO with time, and this could be one of the reasons for inconsistencies in GO products.

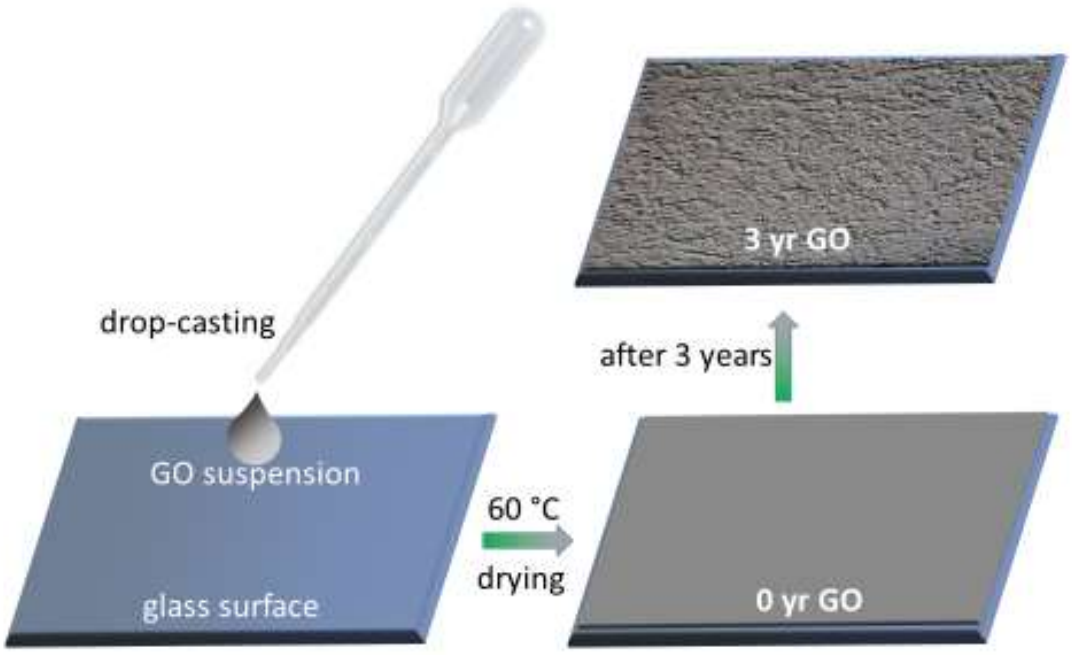

Figure 7-1. Procedure to form GO film on a glass surface through drop casting to obtain 0 yr GO and later, 3 yr GO samples.

We have investigated the effect that the passage of time has on the GO sheets, both when kept isolated, or under the influence of various environments, or when used in an application. A GO film is formed by drop-casting an aqueous GO suspension on a glass substrate as shown by illustration in Figure 7-1. This GO film sample is named as 0 yr GO. After storing the GO film for three years, the film sample is named as 3 yr GO. GO that is stored as a suspension in water (5mg/ml) for three years is 3 yr_W GO. GO1 is 2 hours oxidized, and GO2 is 3 hours oxidized graphene oxide material using Modified Hummers method.[29,86,99,153,164]

7.1 Constant Defect Density and the Interlayer Distance

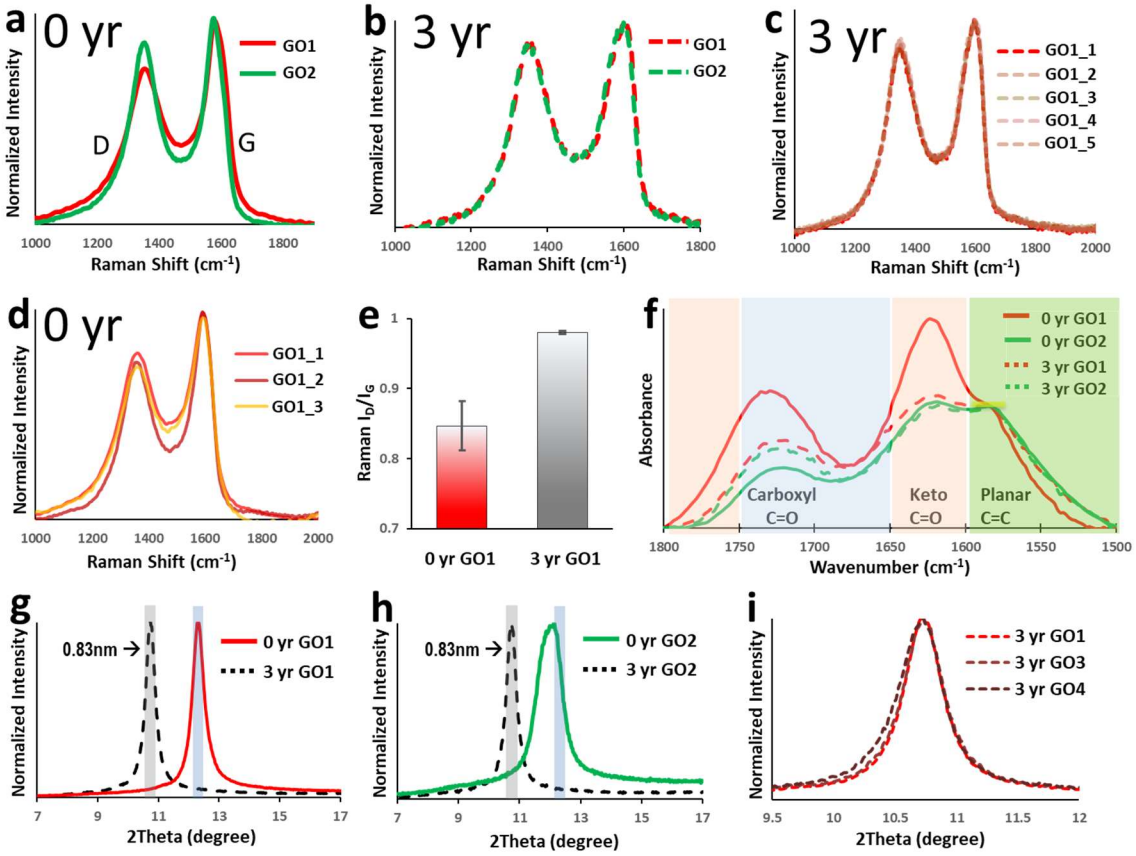

Figure 7-2. a) Raman spectra of o yr GO1 and GO2 (solid). b) Raman spectra of 3 yr GO1 and 3 yr GO2 (dotted), i.e., after three years of storage in dry conditions, showing similar defect density (I_D/I_G) irrespective of original GO1 and GO2 samples having varying defect densities (I_D/I_G). c) Raman spectra at five different spots of 3 yr GO1 showing constant defect density (I_D/I_G) value across the entire sample. d) Raman spectra at three different spots of 0 yr GO1 showing varying defect densities across the sample. e) Comparison of Raman I_D/I_G values for 0 yr and 3 yr GO1. Error bars show that the I_D/I_G value approaches a monodisperse defect density in three years. f) FTIR spectra of GO1 and GO2 for 0 years (solid) and 3 years (dotted) aging where GO1 and GO2 appear relatively similar (carboxyl C=O) after 3 years of storage irrespective of initial GO samples' peak intensities relative to C=C stretching band (1500-1600 cm^{-1}). Yellow mark shows the normalized C=C peak stretching. g-

h) X-Ray diffraction pattern showing “GO-peak” for GO1 and GO2 with no aging (solid) and after 3 year aging (dotted). The d-spacing in GO changes to a constant value of 0.83nm (10.6° 2θ value) after 3 years of storage as films on glass surface irrespective of the initial d-spacing of the GO samples. i) XRD patterns of GO1, GO3, and GO4 after 3 years of storage as films on a glass surface. These GO samples are synthesized by different oxidation methods.[1,3]

A typical Raman spectrum of GO shows two characteristic peaks, D peak (~1350 cm^{-1}) and G peak (~1590 cm-1). Raman spectroscopy allows us to monitor the disruption of the sp^2 carbon network in the GO samples with time. To characterize GO with Raman, comparing the D-band, with intensity I_D, that corresponds to a disrupted sp^2 network,[28] with the G-band, with intensity I_G, that corresponds to an intact sp^2 network, indicates the defects present in GO including but not limited to topological defects and functionalization.[86]

Figure 7-2a shows distinct Raman spectrum for 0 yr GO1 and 0 yr GO2 with I_D/I_G ratio of 0.86 and 0.93 respectively. After 3 years, the Raman spectra of these samples, i.e., 3 yr GO1 and 3 yr GO2 are shown in Figure 7-2b. The I_D/I_G ratio for both these samples becomes 0.98, and different Raman spectra of these two different GO materials (GO1 and GO2) appear near to identical after three years, the same spectra which were significantly different originally with no aging. This observation suggests that GO changes slowly to a certain defect density to approach the most stable thermal equilibrium state. In order to corroborate this similarity in the defect density of 3 yr GO samples further, various spots for Raman analysis are chosen on 3 yr GO1 as shown in Figure 7-2c. In general, Raman spectra from different regions of a GO sample (e.g., o yr GO1) shows a relatively broad range of I_D/I_G values.[165,166] As seen in Figure 7-2d,

within this single sample, unlike uniform I_D/I_G value for various spots on 3 yr GO1, some regions of 0 yr GO1 show more I_D/I_G value than others due to varying relative D-peak area and FWHM indicating that oxidation and defect density are not uniform on each sheet in GO without aging. In practice, Figure 7-3 shows the GO1 surface under a microscope for Raman analysis where various spots can be selected for experiment and I_D/I_G value calculation. It is important to note that this extent of monodispersed defect density at thermal equilibrium stage cannot be achieved by oxidation reactions, as there are variations in defect density value (I_D/I_G) at different GO regions in oxidized GO materials without aging.[166]

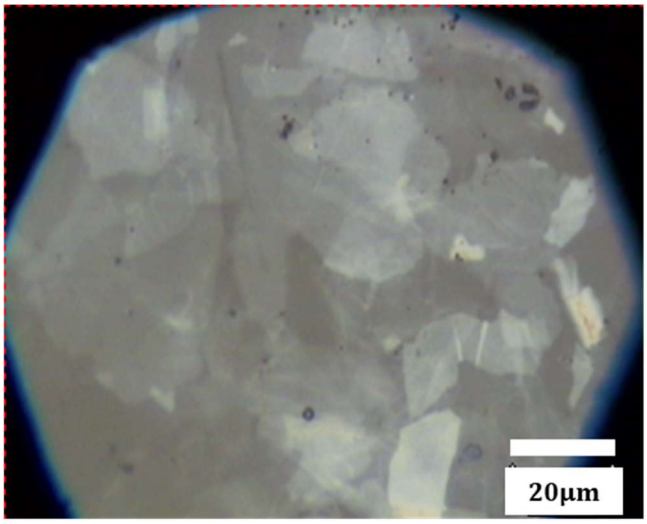

Figure 7-3. Original GO1 (o yr GO1) under the microscope showing characteristic laser spot and its size for each Raman experiment.

Figure 7-2**f** shows FTIR spectra for C=C in-plane, carboxylic carbonyl, and ketone vibrations, for various GO samples normalized by C=C in-plane peak.[47,167] GO FTIR contains numerous peaks,[168] and of those numerous peaks, we have concentrated on the three significant peaks- a peak at approximately 1550 cm^{-1} assigned to sp^2 hybridized C=C in-plane vibrations,[47] a peak at approximately 1730 cm^{-1} assigned to

carboxylic carbonyl stretching,[125,43] and a peak at approximately 1620 cm^{-1} assigned to ketone vibration.[125] 0 yr GO1 and 0 yr GO2 show a vast difference between C=O groups relatively.

Conversely, 3 yr GO1 and 3 yr GO2 tend to have a similar distribution of the three groups. FTIR results show that carboxylic C=O groups that are known to form the defect boundaries in GO,[26,59] become similar in their abundance (relative to C=C) after three years. This agrees with the Raman results showing uniform defect density with time.

Although changes in extent of oxygen functionalities take place during GO aging, GO reduction, and GO synthesis processes, 3 yr GO cannot be reproduced from GO reduction or oxidation reactions and it is a unique product of the aging phenomenon. The reason is because, while the relative extent of the oxygen functionalities becomes uniform in case of 3 yr GO, the same is not true in the process of functionality increase during GO oxidation or the loss during GO reduction, and the growth of oxidative islands on the GO plane and edges is not uniform.[28,29,88,142,169] This observation also suggests a state of GO material due to aging by attaining a thermodynamic minimum, a thermal equilibrium state.

A typical XRD of GO contains a GO peak (2θ= 10-13°) and sometimes a G peak (2θ= 26.8).[3] Figure 7-2g-h shows GO peaks (2θ= 10-13°) for two pairs of 0 yr GO and 3 yr GO samples. The differences in the 2θ values, and thus the interlayer spacing, between the 0 yr GO1 and 0 yr GO2 disappeared, and they attain similar interlayer distance of 0.83nm, corresponding to 2θ= 10.6°, after three years as observed in 3 yr GO. This phenomenon is further corroborated by two other types of GO sheets in

Figure 7-2i, Table 7-1 and Appendix (Figure 10-12), where four different GO samples attained a similar range of interlayer distance after three years (0.82-0.83nm). The change in interlayer distance after the passage of 3 years is about 13-17%. Figure 7-2i gives a closer look at the relative GO XRD peaks for all four samples where GO sheets approach this interlayer spacing of 0.83nm. High GO d-spacing means low oxidation degree (XPS results prove this later in this chapter) that gives rise to a reduced extent of hydrogen bonding, i.e., reduced number density of oxygen functionalities with time.[170,171]

More interestingly, the full width at half maximum (FWHM) value for the XRD GO peak goes down by 30-40% with time, and the GO peak becomes sharper for all 3 yr GO. This indicates more uniformity in d-spacing over time. Appendix (Figure 10-12) shows a broader diffraction pattern of the GO samples and includes the G peak, indicating that the 2θ value for the G peak (2θ= 26.8) remains the same after three years.[3] The 2θ value for the XRD GO peaks does not occur in 10.4-10.8 region but typically at 12.0 or higher in most of the cases including Figure 7-2g-h (XRD figure) XRD diffraction patterns depicted by the highlighted region. Multiple studies representing different times of GO oxidation stages do not show any major changes in the GO peak 2θ position, even in extreme oxidative conditions, at least not near the 10.6 degree region.[142,169] Also, generally GO shows polydisperse interlayer distance distribution for all kind of oxidation times[169] while the 3 yr GO shows a monodisperse value of the interlayer distance of 0.83nm, indicating minimum energy state indicated by monodispersed- spacing.

Table 7-1. XRD GO peak d-spacing and FWHM changes after two years of storage of graphene oxide samples.

Sample	GO peak d-spacing (nm)		3 yr GO FWHM relative to 0 yr
	0 yr	3 yr	
GO1	0.71	0.83	71%
GO2	0.72	0.83	75%
GO3	0.76	0.83	69%
GO4	0.69	0.82	60%

One of the characteristics to look for is the graphitic content in a GO material. This can be done by comparison of the intensities of the GO peak (2θ= 10-13°) and the G peak (2θ = 26.8). Appendix (Figure 10-12) shows that, although the GO peak position changes to a lower 2θ value, the relative intensity of GO peak to G peak, i.e. r value, (where $r = A_{GO}/(A_{GO}+A_G)$, where A_{GO} and A_G are GO and G peak areas respectively) remains same for o yr and 3 yr samples in the case of both GO1 and GO2, even though the GO d-spacing changes with time.[25] This means that the graphitic content doesn't change with time. Though the nature and extent of oxygen functional groups are changing on GO surface as per FTIR results, the XRD r value remains unchanged, indicating that graphite sheets remain graphitic, and GO sheets remain oxidized and

do not become rGO, for which a broad XRD peak appears between 22 and 25˚ 2θ value.[159] Also, due to this unchanging r value it can be concluded that exfoliation does not happen with time in a given dry GO film. This is further proof of minimum energy stage of GO where the interlayer distance between sheets changes without changing other inherent properties like GO extent relative to graphitic (r value) and the exfoliation profile.

7.2 Functionalities and Topology

Figure 7-4a-c shows the XPS spectrum for 0 yr GO1and 3 yr GO1 where the C1s spectra were compared by deconvoluting each spectrum into the peaks that correspond to carbon sp^2 (C=C, 284.8 eV), epoxy/hydroxyls (C-O, 286.2 eV), and carbonyl/carboxylate (C=O, 288.5 eV) functional groups. The C1s XPS spectra are normalized by the C=C peak. XPS shows that the overall extent of oxygen functionalities goes down after three years, but more importantly, the ratio of C-O and C=O in 0 yr GO and 3 yr GO remain similar (~2:1).

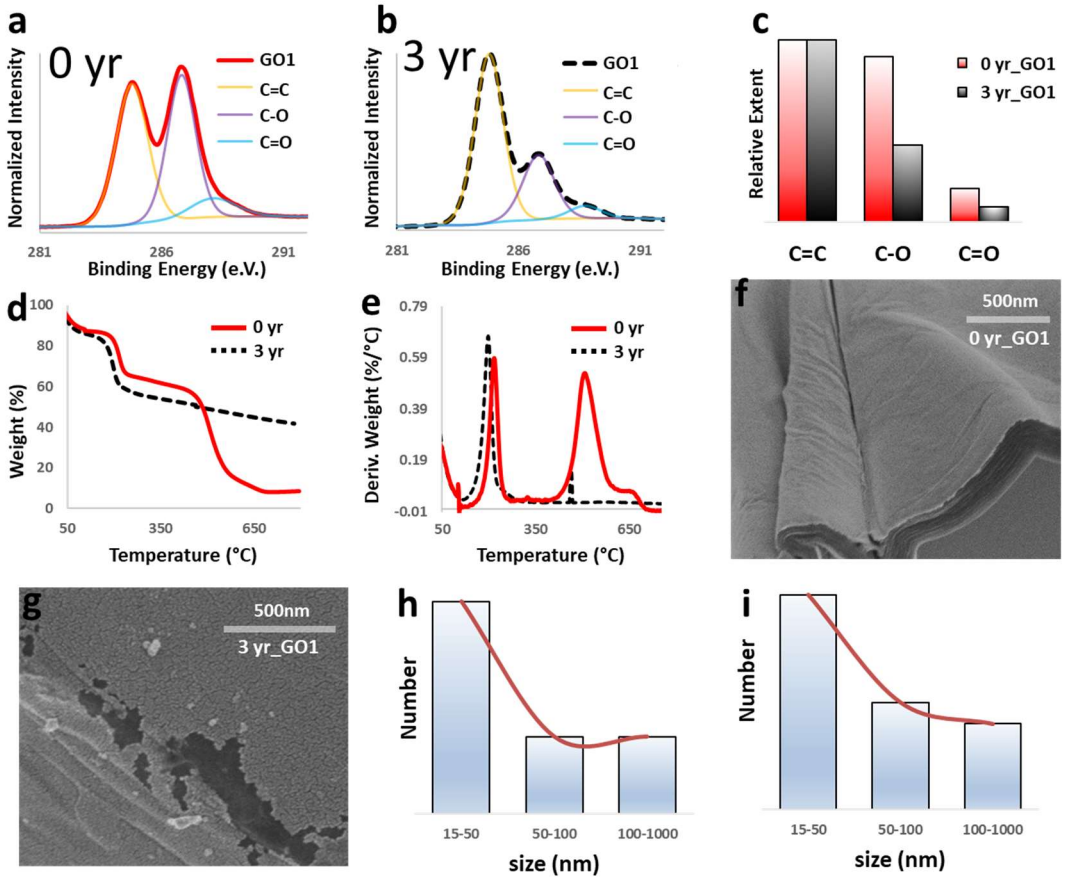

Figure 7-4. a,b) XPS of 0 yr GO1 and 3 yr GO1 with normalized C=C peak (at 284.6e.V.). c) Comparison of extent of C=C, C-O, and C=O, normalized by the C=C peak, where C-O and C=O group intensities go down with the passage of 3 years. d) TGA of 0 yr GO1 (dotted) and 3 yr GO1 (dotted) showing about 40% and 5% residual weight respectively, at 750 °C due to loss of overall functionalities in GO1 within 3 years. e) DTA of 3 yr GO1 (dotted) showing 20 °C left shift in degradation (at 200 °C) as compared to that of 0 yr GO1 (dotted). A very small degradation of strongly bonded functionalities is shown in 3 yr GO (after 425 °C) while GO showed a huge weight loss. f) SEM picture of 0 yr GO1 showing no visible topological defects. g) SEM image of 0 yr GO1 showing micro and nano-scale topological defects after 3 years of storage. h,i) Size distribution of two defect sites as observed in Appendices (

Figure 10-13 and Figure 10-14).

The most important effect of the reduced amount of oxygen functionalities appears in XRD patterns in Figure 7-2g-i. As discussed earlier, the possible reason for having a greater interlayer distance in 3 yr GO samples relative to 0 yr GO is the loss of oxygen functionalities. As suggested by FTIR and XRD results, the loss of functionalities responsible for hydrogen bonding between the two graphene planes result in reduced attraction between the two planes.

Figure 7-4d-e shows the extent of oxygen functionalities left in GO after three years by TGA and DTA analysis. This observation is in agreement with XPS results where it was shown that there a reduction of about 50% (2.2 Carbon to Oxygen functionalities as per XPS).

Topological defects in GO appear over time as per SEM pictures in Figure 7-4f-g and Appendices (

Figure 10-13 and Figure 10-14). 0 yr GO1 sample appears without any topological defects. However, in the case of 3 yr GO1, Appendix (Figure 10-14) SEM shows that defects start appearing at a few nanometers scale and then merge into each other to become microscale. Islands at a distance of about 15-30 nm are encircled in Appendix (Figure 10-14). No such defects were noticed in the case of 0 yr GO1. These defects contribute to the increased intensity of the D-peak in Raman spectroscopy. This is one

of the reasons for the appearance of higher Raman I_D/I_G values despite the extent of oxygen functionalities going down. It is similar to the case of reduced graphene oxide where the I_D/I_G value doesn't go down as much as the extent of functionalities due to the increased extent of structural defects. As per Ferrari *et. al.*[172], the intensity ratio of D and G bands (I_D/I_G) in the Raman spectra reflects the average distance between structural defects (L_D) in the graphene plane.[173] The I_D/I_G is positively correlated with L_D, given that the intensity ratio of 2D and G bands (I_{2D}/I_G) is conspicuously less than 1, which follows the criterion for defective graphene materials as per some studies.[174] Defect size distributions of 3 yr GO1 at two different defect sites in Figure 7-4h-I and Appendices (

Figure 10-13 and Figure 10-14) are similar.[172] This shows that these structural defect sites that appear to grow aging grow in a similar manner over time. It is also observed that defect islands grow bigger with oxidation reaction,[169,175] but in this case the aging process disturbs the delocalization of electrons in the GO plane due to the growth of defect islands with longer shelf life as shown by Raman results in Figure 7-2.

Figure 7-5a shows the variation of the Raman I_D/I_G values for GO1 with time. After 1 year, the defect density reaches almost 90% of its plateau value and then attains a stage where the graphene structure is more stable with time. The decreasing size of the error bars with the progress of time in dry storage signals the monodispersity of the Raman defect density. Increasing I_D/I_G values are a sign of disruption of

delocalization of electrons in the GO basal plane, which can be due to increasing functionalities or various types of morphological defects on the GO plane.[28]

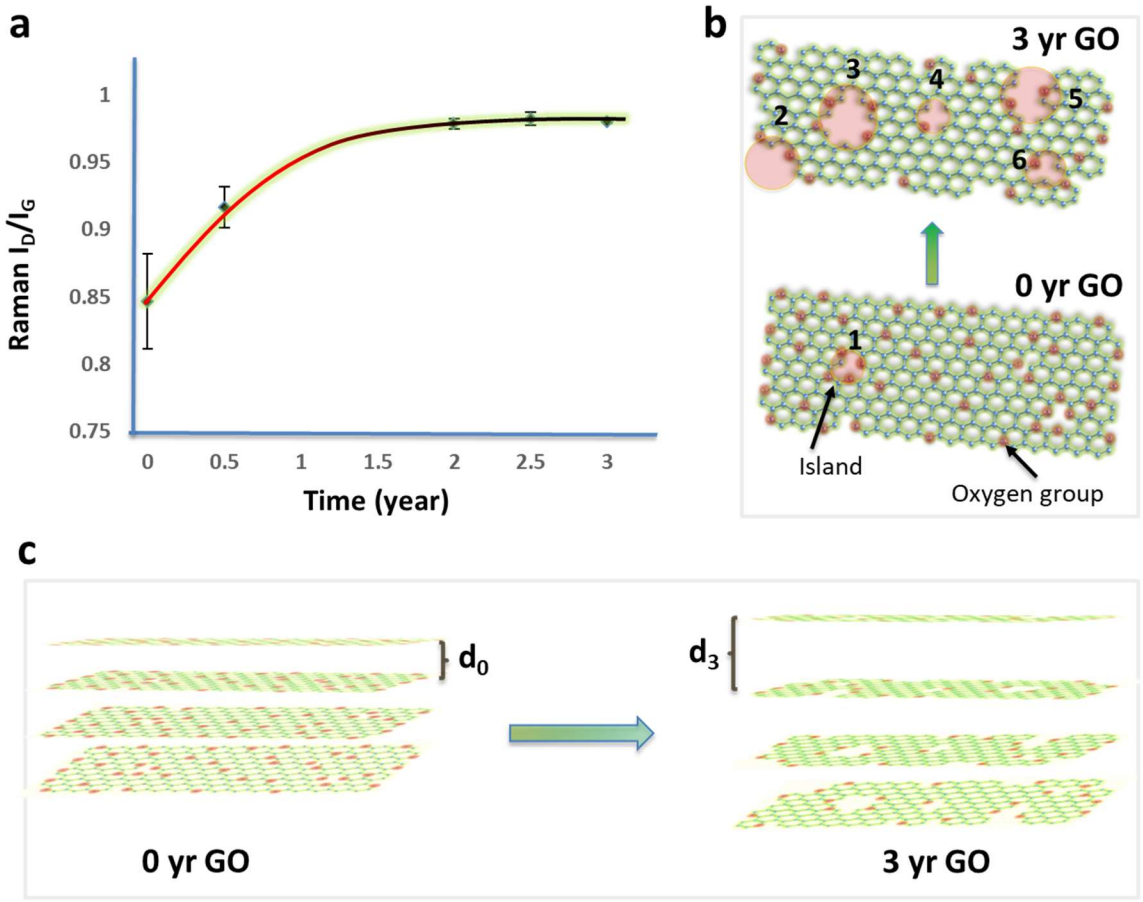

Figure 7-5. a) Variation of Raman defect density (I_D/I_G) of GO1 with time. The defect density starts approaching a thermal equilibrium state within one year of storage in the dry environment. b) Illustration showing the changes in GO sheets due to topological defects arising in 3 yr GO. Numbers (1-6) represent edge or in-plane islands[175], corresponding to the defect sites containing oxygen functional group clusters. c) Illustration showing the increase in GO sheet interlayer distance after the passage of 3 years due to the decreased amount of oxygen functionalities leading to a reduced extent of hydrogen bonding between GO sheets.[170]

However, the FTIR, XPS and TGA results have shown that the oxidation extent (i.e., oxygen functionalities) is decreasing with time. Also, SEM has shown a glimpse of micro and nano-scale defects appearing in the 3 yr GO surface. All of these observations lead to the conclusion that the morphological defects in GO are increasing with time as shown by an illustration in Figure 7-5b. These defects occur due to: the increasing size of oxidative islands present realative to original 0 yr GO (defect 2 growing to become 3), or the loss of basal carbon atoms in plane (defect 4), or on the edges (defects 1 and 5), or merger of two or more defect sites (defect 6).[28,29,142,169] Figure 7-5c illustrates that the interlayer distance in all the 0 yr GO samples increase to a constant value of 0.83nm after 3 years due to the loss of oxygen functionalities as suggested by XPS that leads to reduction in the extent of hydrogen bonding between two adjacent graphene sheets.[170]

We have also looked into the storage of GO materials in water. Studies in the past have examined the changes that occur while storing the GO samples in water for short periods, but do not examine any long-term changes.[176,177] Figure 7-6a shows the Raman spectra of GO1 that was stored as a suspension in water (5mg/ml) for three years (3 yr_W GO1). A moderate increase in the I_D/I_G value for 3 yr_W GO1 is seen from 0 yr GO1, but it is not as high as in the case of drier conditions. XRD patterns in Figure 7-6b suggests that 3 yr_W GO1 sheets attain the minimum energy interlayer spacing of 0.83nm whether stored in aqueous suspension or dry conditions. An important difference though is the FWHM of the 2θ peak, i.e., the distribution of oxidation that doesn't change much due to minimal loss of oxygen functionalities (as

shown by XPS later) leading to more polydisperse oxidation throughout different GO sheets than that of 3 yr GO1.

7.3 Effects of Aqueous Medium

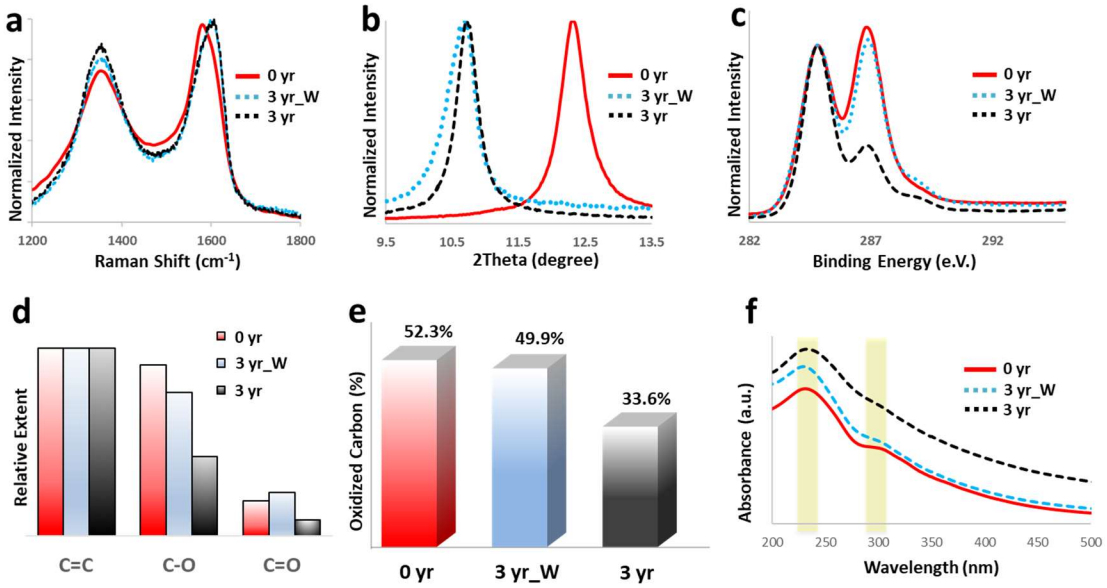

Figure 7-6. **Aqueous medium effect on GO1.** a) Raman spectra comparison of 3 yr_W GO1 (stored as 5mg/ml suspension in water at pH=6), 3 yr GO1 (stored for 3 years as a dry film on a glass surface), and 0 yr GO1 (no aging). Raman shows a moderate change in I_D/I_G ratio for 3 yr_W as compared to 0 yr GO1. b) XRD shows d spacing for 3 yr_W GO1 changing to a similar value as in the case of 3 yr GO1 but with higher FWHM value. c-d) XPS of 3 yr_W shows little change in oxygen functionalities as compared to 0 yr GO. e) The extent of oxidized carbon for different GO samples which only includes the molecules covalently bonded to the carbon plane and excludes all the trapped moieties within the GO sheets, e.g., H_2O, and thus gives a better estimate of how basal carbon functionalization is affected by time in different storage environments. f) UV-vis spectra show relative conjugation between GO samples with two characteristic peaks, between 227-234nm (pi-pi transition, C=C) and 300-310nm (n→pi transition, C=O).

Figure 7-6c-d shows the loss of C-OH covalent bonds in dry storage while there was only a 10% change in the case of solution storage. XPS shows that overall extent of oxygen functionalities went down after three years, but more importantly, the ratio of C-O and C=O in 0 yr, 3 yr, and 3 yr_W GO remained similar (~4.883 and 4.850, respectively). Figure 7-6e shows the changes in functionalization extent in GO, a factor that avoids the inclusion of intercalation of moisture into the calculations. It is important to note that there is not much change in the extent of functionalized carbons with GO stored in suspension. However, in dry condition aging, the extent of oxidized carbon is reduced by about 36% of original 0 yr GO1. That means that the oxygen functionalities are more stable in aqueous conditions (at pH=6) than in drier conditions. This result also suggests that the GO products or processes containing GO in aqueous conditions will be more consistent in performance than those in other environments.

The uv-vis spectrum in Figure 7-6f suggests that all GO samples show a λ_{max} at a 227-234 nm range (π-π transition, C=C) while 0 yr GO1 and 3 yr_W GO1 show a more pronounced shoulder with a λ_{max} at 300-310nm (n$\rightarrow\pi$ transition, C=O).[3] The presence of a π-π transition shows that all GO samples consist of C=C groups and also, 3 yr GO consists of more C=C groups after the loss of oxygen functionalities than 0 yr GO which has more oxygen functionalities. The very small shoulder at the 300-310 nm range shows a lack of n$\rightarrow\pi$ transition in 3 yr GO confirms that there is very small amount of carbonyl and carboxyl groups present after aging in dry conditions, confirming the XPS results.

7.4 Effects of encapsulation

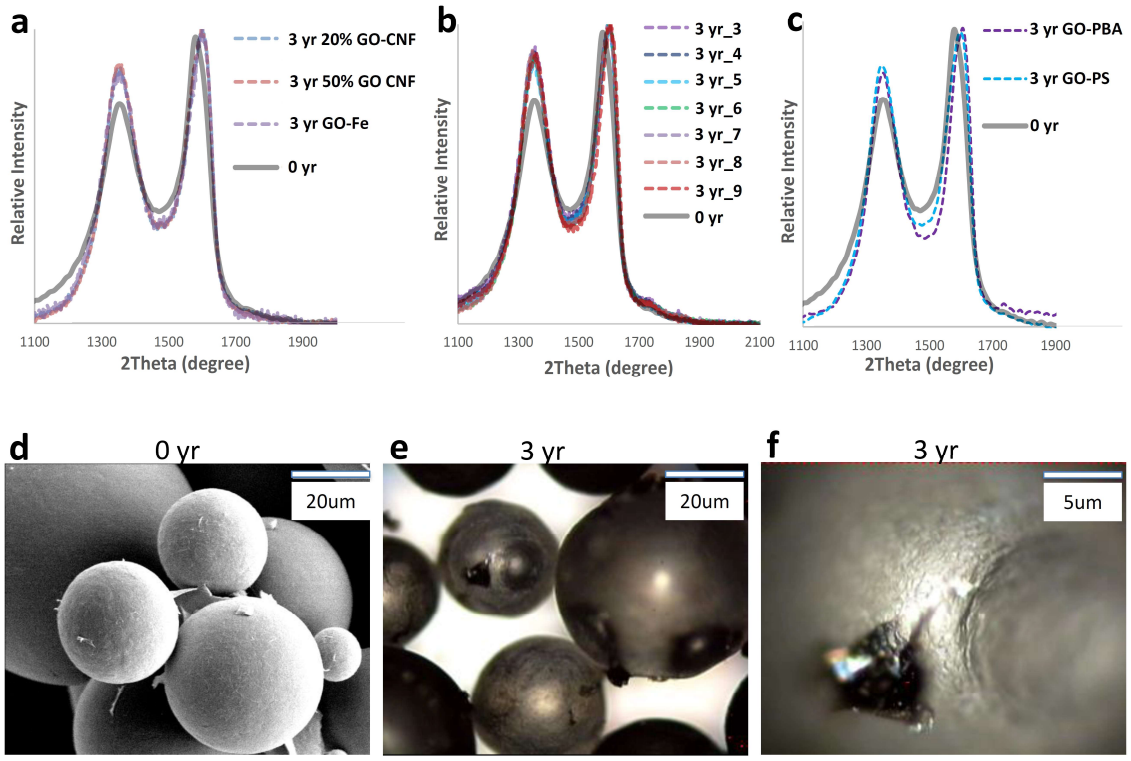

Figure 7-7. Effect of aging on GO in various chemical environments and when used in different applications. a) Raman spectra of graphene oxide that was used to make GO-cellulose films (3 yr GO-CNF) with 20% and 50% GO concentration[178] and 3 yr GO-Fe filtration membrane[179] after the passage of 3 years, showing an increased I_D/I_G ratio of the GO components of the films and membrane as compared with 0 yr unaged GO. b) 0 yr GO is used to obtain 5mg/ml suspensions in water at various pH (3 to 9), drop-casted onto glass surface, dried, and kept for 3 years to get 3 yr_'pH' ('pH'=3 to 9, dotted plots). Raman defect densities (I_D/I_G) of 0 yr GO change to a similar value irrespective of the pH environments. This study corroborates the changes occurring with time in GO when used for various

applications like biological, electrochemical, mechanical, etc. which contain GO in different pH environments.[52] c) Raman spectra obtained from GO-polystyrene[180,155] and GO-polybutylacrylate composites[181] after 3 years show similar changes in Raman defect density (I_D/I_G) after 3 years irrespective of different polymer material vicinity. d). SEM image of 0 yr GO-PS spheres showing clear defect-free GO templated PS spheres useful in various applications.[126,180] e,f). SEM images in different magnifications of 3 yr GO-PS spheres after 3 years containing various surface defects contributing partly to the increased Raman defect density in (c).

So far, our results suggest that GO is exhibiting changes to attain a specific structure over time. It is also important to investigate whether these effects are due to topological changes or oxidation degree variations and whether external environments like the types of encapsulating materials (polymers, metals, etc.), pH, moisture, etc. govern the fate of GO material. Also, it is imperative to know whether the nature of the GO material changes with time depending upon the external environment. It is also interesting to note that GO in all the different environments changes to attain a specific range of I_D/I_G ratio.[3]

GO encapsulation in different materials is done to understand the aging process that takes place in various environments and for some of the significant GO-based materials. The results are shown in Figure 7-7. Processing of GO-cellulose films (GO-CNF) with 20% and 50% GO concentration is done by a dispersion approach. In order to obtain a stable cellulose micro-network dispersion, we chose a highly polar solvent, formamide. Cellulose shows a stable colloid property in formamide as shown by the homogeneous Tyndall phenomenon.[182] The preparation of GO-CNF membranes is realized by the filtration of the mixed solution of cellulose (formamide solution, 5

mg/mL) and GO (aqueous solutions, 1.00 and 2.5mg/mL concentrations). Cellulose extracts GO from the water phase to the formamide phase (5 mL) although water and formamide are miscible. The resulting composite film is then dried to obtain a GO-CNF membrane with 20% and 50% GO concentration.[182]

Processing of GO-Fe filtration membrane was also done by a dispersion method. 15 mL of GO (2.7 mg/mL) was dispersed into 40 mL ethanol with stirring. 0.95 g of $FeCl_3.6H_2O$ (3.5 mmol) and 1.05 g of $FeSO_4.7H2O$ (3.78 mmol) were dissolved in 10 mL of distilled water under sonication, then the solution was injected dropwise into the GO suspension and stirred for 30 min. The resulting mixture was heated to 68 °C before buffer solution was added to adjust the pH to 10. The mixture was stirred at 68 °C for 2 h and then cooled to room temperature. The Fe-GO composite was separated from the mixture using filtration on a filter paper and rinsed three times with ethanol and distilled water respectively before being dried at 65 °C for 12 hours.

Processing GO samples with varying pH was also accomplished. 0 yr GO was used to obtain 5mg/ml suspensions in water at various pH (3 to 9) which contained GO in different pH environments. Buffer solutions (one with acidic and one with basic pH values) were obtained from Fisher Scientific (with CAS numbers- 6381-92-6 and 877-24-7). Six GO suspensions were obtained with pH values of 3, 4, 5, 6, 7, and 8 by varying the amounts and type of buffer solutions.

Processing of GO-polystyrene nanocomposite spheres is done by adding GO to DI water at a concentration of 4.0 mg/mL for the total solution, and suspended using a bath sonicator for 15 minutes to disperse the GO sheets. Emulsions were made with water/styrene ratios of 3/7 by volume. In the styrene phase, 9 mg

azobisisobutyronitrile (AIBN) and 0.375 mL of divinylbenzene (DVB) was added. The mixtures were hand- shaken for 10 seconds prior to blending for 30 seconds with a Kinematica Brinkmann Polytron Homogenizer (Model PT 10-35). The emulsion is then placed in an oven at 65 °C overnight to polymerize. After polymerization, the vials were placed in a second oven at 80 °C overnight to dry.[155,180]

Processing of GO-polybutylacrylate composites is done using a 250 mL Erlenmeyer flask loaded with 110 mg GO, 15 mL DI water, 10 mL butyl acrylate (Acros Organics, 99%), 100 µL divinylbenzene (Sigma-Aldrich, 80%), 30 mg azobisisobutyronitrile (AIBN) (Sigma- Aldrich, 98%), and a stir bar. The contents were then mixed for about 1 min on a stir plate. The stir bar was then removed, and the contents were mixed for 1 min, using a Silverson L5M-A high shear blender. After mixing, the contents were poured gently into a 100 mL glass jar. The jar was then sealed and placed into a convection oven (Blue M, Stabil-Therm) at 65 °C for 24 h to react. The jar was then broken to remove the composite sample, which was then placed in the same oven for four days.[181]

Despite its extensive use in various applications, nothing is known of the physical changes in GO-based products with time. It is important to study this to predict the changes in the properties and optimize the use of a particular GO for a specific application. Figure 7-7a shows the Raman spectra of GO-Cellulose films with 20 and 50% GO concentrations and GO-Fe filtration membranes with 10% GO concentration after the passage of three years. When compared by Raman, the defect density of the original GO (0 yr GO) show a lower level of defect peaks than the 3 yr results. Also, this increase in the defect density (relative Raman D peak intensity) is similar for

different samples to the extent that these spectra superimpose on each other. In recent years, GO in combination with cellulose has shown promising and economically viable applications in multiple areas.[178,182–186] GO in combination with Fe or with cellulose isn't significantly affected by these environments, but defects grow due to the passage of time to a similar extent. This is important as GO in combination with Fe has emerged to be an important area of investigation for various filtration and ion sieving membranes,[179,187,188] however there is no information available concerning the changes that occur in these membranes due to aging. Multiple electrochemical, biological, electronic, and mechanical applications use GO in various environments where pH is an important factor.[52,189,190] To investigate the effect of pH, GO suspensions (5mg/ml) with pH values from 3 to 9 were drop cast on a glass surface, and after three years of storage Figure 7-7b shows their Raman spectra. Similar to earlier films and membranes, defect density not only grows relative to 0 yr GO but is similar irrespective of the pH environment. GO/polystyrene composites have a decade long history and various types of composites for different functions have been obtained.[139,155,180] A similar study is done with GO-polystyrene composite spheres[180] and GO-polybutylacrylate sensor material[181,191,192] obtained similar observations of elevated I_D/I_G ratios as shown in Figure 7-7c. It is important to understand the origin of Raman defect density, I_D/I_G which is not only affected by changes in delocalization of electrons on the GO plane but also due to another kinds of defects as.[28] Figure 7-7d-f shows SEM images of GO-polystyrene spheres taken in 2015 (d) and 2018 (e,f). While GO-PS 2015 shows no sign of visible defects, GO-PS 2018 shows multiple

openings/fractures/micro-sized physical holes in the structure templated by GO sheets.

7.5 Conclusion

This study provides conclusive evidence that GO materiasl changes over time and thtat these changes are not limited to pure GO material but also GO contained in composite materials. Another important aspect of the variations of GO over time is that they appear to reach a thermodynamic minimum energy configuration which can be helpful in the qualitative and quantitative assessment of future GO materials. The **thermodynamic energy minimum** of GO, i.e., a plateau region in r value versus time curve, is achieved between the second and third year of aging with the majority (about 90%) of changes in GO taking place in the first year.

7.6 Methods

7.6.1 Graphene Oxide Synthesis

Graphene oxide is synthesized using a modified Hummers' method.[1,3,193] Twenty-five mL of concentrated sulfuric acid (Fisher Scientific, ACS Plus) and 500 mg of sodium nitrate (Acros Organics, 99%+, ACS Reagent) is added to a round bottom flask and stirred until dissolved. One gram (1 weight equivalent) of graphite is then added to the flask and mixed until dispersed. Finally, 3 g (3 weight equivalents) of

potassium permanganate (EM Sciences, GR ACS) is added to the reaction mixture. When graphite is added to the reaction flask, the solution immediately turns black and has a viscosity similar to that of water. The potassium permanganate is added slowly to avoid overheating the system, but quickly enough so that the system does not thicken before all of the oxidants can be added. Throughout the reaction process, the solution transitions from a low-viscosity liquid to a highly viscous slurry. Addition of the oxidizing agent initially changes the solution to a dark red. This initial thickening begins after five to ten minutes and coincides with an increase in the reaction temperature and a change in color from black to dark green/brown. The solution temperature rises near to 80 °C, and as the reaction continues past an hour, the temperature begins to drop slightly. To quench the reaction, 200 mL of de-ionized (DI) water and 25 mL of hydrogen peroxide (Acros Organics, 35 wt. %) are added to the reaction vessel. 25 mL of hydrochloric acid (Sigma Aldrich, 37% A.C.S. reagent) is then added to solubilize residual salts. Adding water causes the solution temperature to rise with a vigorous effervescence. The hydrochloric acid is not added until the effervescence slows to a minor bubbling.

Preparation of GO samples for storage is as follows. A GO film is formed by drop-casting an aqueous suspension onto a glass substrate (Glob Scientific Inc., 1380-10, plain). The 3 yr GO analysis was done on film sample after storing it for 3 years, and 0 yr GO signifies an analysis that was done on the GO film immediately after formation. If GO was stored as suspension in water (5mg/ml) for 3 years, it is denoted as 3 yr_W. GO1 is oxidized for 2 hours, and GO2 was oxidized for 3 hours to form modified Hummers GO.[29,86,99,153,164]

7.6.2 Analysis of Graphene Oxide

Field Emission Scanning Electron Microscopy (FESEM) was performed on a JEOL JSM-6445F/Thermo Noran System Six EDXS with an accelerating voltage of 10.0 kV and a 15 mm working distance. Samples were prepared by adhering dried GO powders to carbon tape on an SEM stub. Samples were then sputter-coated with a palladium/gold mixture using a Polaron Instruments SEM coating unit E5100 for 30 seconds.

X-Ray Diffraction (XRD) was performed using a Bruker D2 Phaser. For each sample, the graphite powder was tightly packed in order to generate a smooth surface.

Raman spectroscopy was done using a Renishaw 2000 Raman Spectrometer, operating at a wavelength of 514.5 nm. Powder samples were placed on a clean glass slide and scanned three times for ten seconds to minimize fluorescence background over a Raman shift of 1000 to 3200 cm^{-1}.

Thermal Gravimetric Analysis (TGA) was performed on a TA Instruments TGA Q-500. Samples were placed inside a platinum DSC pan with small holes punched in the lid. This was done to prevent loss of material during heating. The samples were heated in a nitrogen atmosphere at a rate of 10 °C per minute to a final temperature of 600 °C.

Fourier Transform Infrared Spectroscopy (FTIR) samples were prepared by mixing 1 wt. % GO samples with 99 wt.% KBr (Fisher Scientific, IR Grade) pellets. Spectra were collected on a Nicolet Magna-IR 560 spectrometer. Elemental Analysis samples were completed in-house on an Elementar vario Micro cube, where oxygen content was calculated by subtraction.

X-ray photoelectron spectra (XPS) characterization of the synthesized materials were done on a PHI model Quantum 2000 spectrometer with scanning ESCA multiprobe (F Physical Electronics Industries Inc.), using Al Ka radiation (I=1486.6 eV) as the radiation source. The spectra were recorded in the fixed analyzer transmission mode with pass energies of 187.85 eV and 29.35 eV for recording survey and high-resolution spectra, respectively. The thin film samples were pinned to a sample stage with a washer and screw then placed in the analysis chamber. The main chamber is pumped down to ultrahigh vacuum (1x10-9 torr) before data acquisition commences. Binding energies (BE) were measured for C KLL, C 1s, and O 1s. The XPS spectra obtained were analyzed and fitted using CasaXPS software (version 2.3.16). Measurements take account only top 5nm depth of the samples. Beam diameter is 100μm.

Chapter 8: Summary and Future Work

8.1 Summary

A fractionation method was successfully developed to produce various GO fractions from from an original material (initial GO precursor). This method does not use any physical or chemical reactions and hence avoids any kind of incorporation of undesirable structural defects. The different GO fractions vary in terms of oxidation and size.

Further, a number, DO, (Dispersity of oxidation) for GO is defined that universally describes the GO oxidation distribution. The statistical studies were performed for corroborating the dispersity of GO further and development of various fitting models for the same.

Various properties of GO fractions are explored, and a route for easier optimization of GO-based products was developed. GO fractions were used, and their performance was analyzed in a number of applications in the areas of biocompatible materials, polymer nanocomposites, and electrochemistry.

Methods to produce a new generation of GO materials are explained. SGO is produced with the same effort as Modified Hummers' GO is produced but with enhanced properties. Another reduced graphene oxide like material, uGO, was obtained. This material has the low extent of oxidation found in rGO, but its Raman defect density is much lower.

An in-depth study of aged graphene oxide in dry, aqueous, and encapsulated environments was done. The results showed that GO establishes a minimum energy stage after a couple of years and originally different GO materials become similar. This study proves that the GO used in various applications changes with time, and so the performance of the products it is being used in will change over time. Understanding these effects quantitatively will enable optimizing the performance of such GO products.

8.2 Future Work

GO fractionation results in GO materials varying in terms of oxidation and size. Using additional characterization approaches, such as HR-TEM, could reveal other important feature that can be crucial in understanding its nanostructure and defects sites and oxidation islands. These studies might provide useful information about the topological features of that GO fractions that lead to stabilization of emulsion systems.

Further work should be carried out to find the details about the distribution of oxygen functionalities on individual sheets. Present research only provides the details of oxidation on bulk GO material and distribution on individual sheets is considered random. This dissertation has suggested routes to produce different types of GO materials, i.e., uGO and SGO. But they were only used in few applications. Use of these materials can be explored in various fields due to their unique and significant properties.

Minimum energy structures of various other GO materials should be studied to establish a universal method for prediction of properties over time. Knowing whether

all GO materials show a reduction in their oxidation extent and give rise to a common structure could lead to an approach for aging-resistant GO materials.

Chapter 9: References

1. Hummers, W. S. *et al.* Preparation of Graphitic Oxide. *J. Am. Chem. Soc.* **80**, 1339–1339 (1958).
2. SHAHRIARY, LEILA; ATHAWALE, A. A. Graphene Oxide Synthesized by using Modified Hummers Approach. **02**, (2014).
3. Marcano, D. C. *et al.* Improved Synthesis of Graphene Oxide. *ACS Nano* **4**, 4806–4814 (2010).
4. Fasolino, A., Los, J. H. & Katsnelson, M. I. Intrinsic ripples in graphene. *Nat. Mater.* **6**, 858–861 (2007).
5. Meyer, J. C. *et al.* The structure of suspended graphene sheets. *Nature* **446**, 60–63 (2007).
6. Geim, A. K. & Novoselov, K. S. The rise of graphene. *Nat. Mater.* **6**, 183 (2007).
7. Novoselov, K. S. *et al.* Electric Field Effect in Atomically Thin Carbon Films. *Science (80-.).* **306**, 666–669 (2004).
8. Lee, C., Wei, X., Kysar, J. W. & Hone, J. Measurement of the Elastic Properties and Intrinsic Strength of Monolayer Graphene. *Science (80-.).* **321**, 385–388 (2008).
9. Balandin, A. A. *et al.* Superior Thermal Conductivity of Single-Layer Graphene. *Nano Lett.* **8**, 902–907 (2008).
10. Peigney, A., Laurent, C., Flahaut, E., Bacsa, R. R. & Rousset, A. Specific surface area of carbon nanotubes and bundles of carbon nanotubes. *Carbon N. Y.* **41**, 507–514 (2001).
11. Orlita, M. *et al.* Approaching the Dirac Point in High-Mobility Multilayer Epitaxial Graphene. *Phys. Rev. Lett.* **101**, (2008).
12. Radovic, L. R. & Bockrath, B. On the Chemical Nature of Graphene Edges: Origin of Stability and Potential for Magnetism in Carbon Materials. *J. Am. Chem. Soc.* **127**, 5917–5927 (2005).
13. Robinson, J. T., Perkins, F. K., Snow, E. S., Wei, Z. & Sheehan, P. E. Reduced graphene oxide molecular sensors. *Nano Lett.* **8**, 3137–3140 (2008).

14. Wang, X., Zhi, L. & Müllen, K. Transparent, Conductive Graphene Electrodes for Dye-Sensitized Solar Cells. *Nano Lett.* **8**, 323–327 (2008).
15. Eda, G. *et al.* Transparent and conducting electrodes for organic electronics from reduced graphene oxide. *Appl. Phys. Lett.* 233305 (2008).
16. Kim, K. S. K. S. K. S. *et al.* Large-scale pattern growth of graphene films for stretchable transparent electrodes. *Nature* **457**, 706–10 (2009).
17. Zhao, J., Pei, S., Ren, W., Gao, L. & Cheng, H.-M. Efficient Preparation of Large-Area Graphene Oxide Sheets for Transparent Conductive Films. *ACS Nano* **4**, 5245–5252 (2010).
18. Zhang, L. L., Zhou, R. & Zhao, X. S. Graphene-based materials as supercapacitor electrodes. *J. Mater. Chem.* **20**, 5983 (2010).
19. Choi, B. G., Yang, M., Hong, W. H., Choi, J. W. & Huh, Y. S. 3D Macroporous Graphene Frameworks for Supercapacitors with High Energy and Power Densities. *ACS Nano* **6**, 4020–4028 (2012).
20. Sarker, A. K. & Hong, J.-D. Layer-by-Layer Self-Assembled Multilayer Films Composed of Graphene/Polyaniline Bilayers: High-Energy Electrode Materials for Supercapacitors. *Langmuir* **28**, 12637–12646 (2012).
21. Lin, Y., Ding, F. & Yakobson, B. I. Hydrogen storage by spillover on graphene as a phase nucleation process. *Phys. Rev. B* **78**, (2008).
22. Parambhath, V. B., Nagar, R. & Ramaprabhu, S. Effect of Nitrogen Doping on Hydrogen Storage Capacity of Palladium Decorated Graphene. *Langmuir* **28**, 7826–7833 (2012).
23. Fowler, J. D. *et al.* Practical Chemical Sensors from Chemically Derived Graphene. *ACS Nano* **3**, 301–306 (2009).
24. Loh, K. P., Bao, Q. L., Eda, G. & Chhowalla, M. Graphene oxide as a chemically tunable platform for optical applications. *Nat. Chem.* **2**, 1015–1024 (2010).
25. Kumar, H. V., Woltornist, S. J. & Adamson, D. H. Fractionation and Characterization of Graphene Oxide by Oxidation Extent Through Emulsion Stabilization. *Carbon N. Y.* **98**, 491–495 (2016).
26. He, H., Klinowski, J., Forster, M. & Lerf, A. A new structural model for graphite oxide. *Chem. Phys. Lett.* **287**, 53–56 (1998).

27. Gao, W., Alemany, L. B., Ci, L. & Ajayan, P. M. New insights into the structure and reduction of graphite oxide. *Nat. Chem.* **1**, 403–408 (2009).
28. Gómez-Navarro, C. *et al.* Atomic structure of reduced graphene oxide. *Nano Lett.* **10**, 1144–1148 (2010).
29. Bagri, A. *et al.* Structural evolution during the reduction of chemically derived graphene oxide. *Nat. Chem.* **2**, 581–587 (2010).
30. Buchsteiner, A., Lerf, A. & Pieper, J. Water Dynamics in Graphite Oxide Investigated with Neutron Scattering. *J. Phys. Chem. B* **110**, 22328–22338 (2006).
31. Sun, X. *et al.* Nano-graphene oxide for cellular imaging and drug delivery. *Nano Res.* **1**, 203–212 (2008).
32. Eda, G. & Chhowalla, M. Graphene-based Composite Thin Films for Electronics. *Nano Lett.* **9**, 814–818 (2009).
33. Cai, W. *et al.* Synthesis and Solid-State NMR Structural Characterization of 13C-Labeled Graphite Oxide. *Science (80-.).* **321**, 1815–1817 (2008).
34. Eda, G., Fanchini, G. & Chhowalla, M. Large-area ultrathin films of reduced graphene oxide as a transparent and flexible electronic material. *Nat. Nanotechnol.* **3**, 270–274 (2008).
35. Blake, P. *et al.* Making graphene visible. *Appl. Phys. Lett.* **91**, 1063124 (2007).
36. Deshpande, A. & LeRoy, B. J. Scanning probe microscopy of graphene. *Phys. E Low-dimensional Syst. Nanostructures* **44**, 743–759 (2012).
37. Paredes, J. I., Villar-Rodil, S., Solís-Fernández, P., Martínez-Alonso, A. & Tascón, J. M. D. Atomic Force and Scanning Tunneling Microscopy Imaging of Graphene Nanosheets Derived from Graphite Oxide. *Langmuir* **25**, 5957–5968 (2009).
38. PANDEY, D., REIFENBERGER, R. & PINER, R. Scanning probe microscopy study of exfoliated oxidized graphene sheets. *Surf. Sci.* **602**, 1607–1613 (2008).
39. Ferrari, a. C. *et al.* Raman Spectrum of Graphene and Graphene Layers. *Phys. Rev. Lett.* **97**, 187401-1–4 (2006).
40. Ferrari, A. C. & Basko, D. M. Raman spectroscopy as a versatile tool for studying the properties of graphene. *Nat. Nanotechnol.* **8**, 235–246 (2013).

41. Graf, D. *et al.* Spatially Resolved Raman Spectroscopy of Single- and Few-Layer Graphene. *Nano Lett.* **7**, 238–242 (2007).
42. Islam, S. S. *et al.* Raman study on single-walled carbon nanotubes with different laser excitation energies. *Bull. Mater. Sci.* **30**, 295–299 (2007).
43. Hontoria-Lucas, C., López-Peinado, a. J., López-González, J. d. D., Rojas-Cervantes, M. L. & Martín-Aranda, R. M. Study of oxygen-containing groups in a series of graphite oxides: Physical and chemical characterization. *Carbon N. Y.* **33**, 1585–1592 (1995).
44. Kim, S. *et al.* Room-temperature metastability of multilayer graphene oxide films. *Nat. Mater.* **11**, 544–9 (2012).
45. Yan, J. *et al.* Functionalized graphene oxide with ethylenediamine and 1,6-hexanediamine. *New Carbon Mater.* **27**, 370–376 (2012).
46. Kumar, P. V *et al.* Scalable enhancement of graphene oxide properties by thermally driven phase transformation. *Nat. Chem.* **6**, 151–8 (2014).
47. Acik, M. *et al.* Unusual infrared-absorption mechanism in thermally reduced graphene oxide. *Nat. Mater.* **9**, 840–845 (2010).
48. Chen, W., Yan, L. & Bangal, P. R. Preparation of graphene by the rapid and mild thermal reduction of graphene oxide induced by microwaves. *Carbon N. Y.* **48**, 1146–1152 (2010).
49. Sutter, P., Cortes, R., Lahiri, J. & Sutter, E. Interface Formation in Monolayer Graphene-Boron Nitride Heterostructures. *Nano Lett.* **12**, 4869–4874 (2012).
50. B.C., B. On the Atomic Weight of Graphite. *Philos. Trans. R. Soc. London.* **149**, 249–259 (1859).
51. Staudenmaier, L. Verfahren sur Darstellung der Graphitsaure. *Berichte der Dtsch. Chem. Gesellschaft* **31**, 1481–1487 (1898).
52. Zhu, Y. *et al.* Graphene and graphene oxide: Synthesis, properties, and applications. *Adv. Mater.* **22**, 3906–3924 (2010).
53. Boehm, H. P., Clauss, A., Fischer, G. O. & Hofmann, U. Dünnste kohlenstoff-folien. *Zeitschrift für Naturforsch.* **17**, 150–153 (1961).
54. Geim, A. K. Graphene prehistory. *Phys. Scr.* **T146**, 014003 (2012).
55. Boukhvalov, D. W. & Katsnelson, M. I. Modeling of graphite oxide. *J. Am. Chem.*

Soc. **130**, 10697–10701 (2008).

56. Lahaye, R. J. W. E., Jeong, H. K., Park, C. Y. & Lee, Y. H. Density functional theory study of graphite oxide for different oxidation levels. *Phys. Rev. B* **79**, 125435 (2009).
57. Szab, T. *et al.* Evolution of surface functional groups in a series of progressively oxidized graphite oxides. *Chem. Mater.* **18**, 2740–2749 (2006).
58. Hofmann, U. & Holst, R. Über die Säurenatur und die Methylierung von Graphitoxyd. *Ber. Dtsch. Chem. Ges. B* **72**, 754 (1939).
59. Lerf, A., He, H., Forster, M. & Klinowski, J. Structure of Graphite Oxide Revisited. *J. Phys. Chem. B* **102**, 4477–4482 (1998).
60. Ruess, G. On the structure of the gloss carbon. *Monatshefte für Chemie* **76**, 253–256 (1947).
61. Clauss, A., Plass, R., Boehm, H. P. & Hofmann, U. Untersuchungen zur Struktur des Graphitoxyds. *Zeitschrift für Anorg. und Allg. Chemie* **291**, 205–220 (1957).
62. Scholtz, W. & Boehm, H. P. Untersuchungen am Graphitoxid. VI. Betrachtungen zur Struktur des Graphitoxids. *Zeitschrift für Anorg. und Allg. Chemie* **369**, 327–340 (1969).
63. Nakajima, T. & Matsuo, Y. Formation process and structure of graphite oxide. *Carbon N. Y.* **32**, 469–475 (1994).
64. Stankovich, S. *et al.* Synthesis of graphene-based nanosheets via chemical reduction of exfoliated graphite oxide. *Carbon N. Y.* **45**, 1558–1565 (2007).
65. Rourke, J. P. *et al.* The real graphene oxide revealed: Stripping the oxidative debris from the graphene-like sheets. *Angew. Chemie - Int. Ed.* **50**, 3173–3177 (2011).
66. Dimiev, A., Kosynkin, D. V., Alemany, L. B., Chaguine, P. & Tour, J. M. Pristine graphite oxide. *J. Am. Chem. Soc.* **134**, 2815–2822 (2012).
67. Si, Y. & Samulski, E. Synthesis of Water Soluble Graphene. *Nano Lett.* **8**, 1679–1682 (2008).
68. Dua, V. *et al.* All-organic vapor sensor using inkjet-printed reduced graphene oxide. *Angew. Chemie - Int. Ed.* **49**, 2154–2157 (2010).
69. Yang, J. *et al.* Facile Synthesis and Characterization of Graphene Nanosheets.

J. Phys. Chem. C **112**, 8192–8195 (2008).

70. Schniepp, H. C. *et al.* Functionalized single graphene sheets derived from splitting graphite oxide. *J. Phys. Chem. B* **110**, 8535–8539 (2006).
71. Stankovich, S. *et al.* Stable aqueous dispersions of graphitic nanoplatelets via the reduction of exfoliated graphite oxide in the presence of poly(sodium 4-styrenesulfonate). *J. Mater. Chem.* **16**, 155–158 (2006).
72. Stankovich, S., Piner, R. D., Nguyen, S. T. & Ruoff, R. S. Synthesis and exfoliation of isocyanate-treated graphene oxide nanoplatelets. *Carbon N. Y.* **44**, 3342–3347 (2006).
73. Suk, J. W., Piner, R. D., An, J. & Ruoff, R. S. Mechanical properties of monolayer graphene oxide. *ACS Nano* **4**, 6557–6564 (2010).
74. Becerril, H. A. *et al.* Evaluation of solution-processed reduced graphene oxide films as transparent conductors. *ACS Nano* **2**, 463–470 (2008).
75. Liu, H. *et al.* Reduction of graphene oxide to highly conductive graphene by Lawesson's reagent and its electrical applications. *J. Mater. Chem. C* **1**, 3104 (2013).
76. Yan, J.-A. A., Xian, L. & Chou, M. Y. Structural and electronic properties of oxidized graphene. *Phys. Rev. Lett.* **103**, 086802 (2009).
77. Hu, W. *et al.* Graphene-based antibacterial paper. *ACS Nano* **4**, 4317–4323 (2010).
78. Liu, Z., Robinson, J. T., Sun, X. & Dai, H. PEGylated Nanographene Oxide for Delivery of Water-Insoluble Cancer Drugs. *J. Am. Chem. Soc.* **130**, 10876–10877 (2008).
79. Yang, X. *et al.* Multi-functionalized graphene oxide based anticancer drug-carrier with dual-targeting function and pH-sensitivity. *J. Mater. Chem.* **21**, 3448 (2011).
80. Zedan, A. F., Moussa, S., Terner, J., Atkinson, G. & El-Shall, M. S. Ultrasmall gold nanoparticles anchored to graphene and enhanced photothermal effects by laser irradiation of gold nanostructures in graphene oxide solutions. *ACS Nano* **7**, 627–636 (2013).
81. Dikin, D. A. *et al.* Preparation and characterization of graphene oxide paper.

Nature **448**, 457–460 (2007).

82. Zhu, Y., Cai, W., PINER, R., Velamakanni, A. & RUOFF, R. Transparent self-assembled films of reduced graphene oxide platelets. *Appl. Phys. Lett.* **95**, 103104 (2009).
83. Nicolosi, V., Chhowalla, M., Kanatzidis, M. G., Strano, M. S. & Coleman, J. N. Liquid Exfoliation of Layered Materials. *Science (80-.).* **340**, 1226419-1–18 (2013).
84. Francis, P. S.; Cooke R. C.; Elliott, J. H. Fractionation of Polyethylene. *J. Polym. Sci. A Polym. Chem.* **31**, 453–466 (1958).
85. Stepto, R. F. T. Dispersity in polymer science (IUPAC Recommendations 2009). *Pure Appl. Chem.* (2009). doi:10.1351/PAC-REC-08-05-02
86. Dimiev, A. M. *et al.* Mechanism of Graphene Oxide Formation. *ACS Nano* **8**, 3060–3068 (2014).
87. Sydlik, S. A., Jhunjhunwala, S. & Webber, M. J. In Vivo Compatibility of Graphene Oxide with Differing Oxidation States. *ACS Nano* **9**, 3866–3874 (2015).
88. Wei, Z. *et al.* Nanoscale Tunable Reduction of Graphene Oxide for Graphene Electronics. *Science (80-.).* **328**, 1373–1377 (2010).
89. Robinson, J. T. *et al.* Wafer-scale reduced graphene oxide films for nanomechanical devices. *Nano Lett.* **8**, 3441–3445 (2008).
90. Putz, K. W., Compton, O. C., Palmeri, M. J., Nguyen, S. T. & Brinson, L. C. High-nanofi ller-content graphene oxide-polymer nanocomposites via vacuum-assisted self-assembly. *Adv. Funct. Mater.* **20**, 3322–3329 (2010).
91. Dreyer, D. R. & Bielawski, C. W. Carbocatalysis: Heterogeneous carbons finding utility in synthetic chemistry. *Chem. Sci.* **2**, 1233 (2011).
92. Gao, W. *et al.* Direct laser writing of micro-supercapacitors on hydrated graphite oxide films. *Nat. Nanotechnol.* **6**, 496–500 (2011).
93. Woltornist, S. J., Oyer, A. J., Carrillo, J.-M. Y., Dobrynin, A. V & Adamson, D. H. Conductive thin films of pristine graphene by solvent interface trapping. *ACS Nano* **7**, 7062–6 (2013).
94. Woltornist, S. J., Carrillo, J.-M. M. Y., Xu, T. O., Dobrynin, A. V & Adamson, D.

H. A. Polymer/Pristine Graphene Based Composites: From Emulsions to Strong, Electrically Conducting Foams. *Macromolecules* **48**, 687–693 (2015).

95. Kim, J. *et al.* Graphene oxide sheets at interfaces. *J. Am. Chem. Soc.* **132**, 8180–6 (2010).
96. Jung, I., Dikin, D. a., Piner, R. D. & Ruoff, R. S. Tunable electrical conductivity of individual graphene oxide sheets reduced at 'Low' temperatures. *Nano Lett.* **8**, 4283–4287 (2008).
97. Das, A. K. *et al.* Iodide-mediated room temperature reduction of graphene oxide: a rapid chemical route for the synthesis of a bifunctional electrocatalyst. *J. Mater. Chem. A* **2**, 1332–1340 (2014).
98. Krishnan, D. *et al.* Energetic graphene oxide: Challenges and opportunities. *Nano Today* **7**, 137–152 (2012).
99. Chung, C. *et al.* Biomedical applications of graphene and graphene oxide. *Acc. Chem. Res.* **46**, 2211–2224 (2013).
100. Sudeep, P. M. *et al.* Covalently Interconnected Three-Dimensional Graphene Oxide Solids. *ACS Nano* **7**, 7034–7040 (2013).
101. Wang, W. *et al.* An efficient thermoelectric material: preparation of reduced graphene oxide/polyaniline hybrid composites by cryogenic grinding. *Rsc Adv.* **5**, 8988–8995 (2015).
102. Potts, J. R., Dreyer, D. R., Bielawski, C. W. & Ruoff, R. S. Graphene-based polymer nanocomposites. *Polymer (Guildf).* **52**, 5–25 (2011).
103. Chen, D., Feng, H. & Li, J. Graphene oxide: Preparation, functionalization, and electrochemical applications. *Chem. Rev.* **112**, 6027–6053 (2012).
104. Yoo, D. Y. *et al.* Graphene Oxide Nanosheet Wrapped White-Emissive Conjugated Polymer. (2014).
105. Bourgeat-Lami, E., Faucheu, J. & Noël, A. Latex routes to graphene-based nanocomposites. *Polym. Chem.* **6**, 5323–5357 (2015).
106. Feng, L., Wu, L. & Qu, X. New horizons for diagnostics and therapeutic applications of graphene and graphene oxide. *Adv. Mater.* **25**, 168–186 (2013).
107. Jin, M. *et al.* Graphene oxide thin film field effect transistors without reduction. *J. Phys. D. Appl. Phys.* **42**, 135109 (2009).

108. Cote, L. J. *et al.* Graphene oxide as surfactant sheets. *Pure Appl. Chem.* **83**, 95–110 (2010).
109. Adamson, D. H. & Kumar, H. V. Fractionation of Graphene Oxide Through Emulsion Stabilization and Graphene Oxide Produced Thereby. U.S. Patent 20180127275A1. (2018).
110. Perreault, F., Fonseca De Faria, A. & Elimelech, M. Environmental applications of graphene-based nanomaterials. *Chem. Soc. Rev.* **44**, 5861–5896 (2015).
111. Yu, C. *et al.* Creation of Reduced Graphene Oxide Based Field Effect Transistors and Their Utilization in the Detection and Discrimination of Nucleoside Triphosphates. *ACS Appl. Mater. Interfaces* 150506164724005 (2015). doi:10.1021/acsami.5b00155
112. Atkins, P. W. (Peter W., De Paula, J. & Keeler, J. *Atkins' Physical chemistry*. (Oxford University Press, 2010).
113. Francis Galton. Opening Address by Francis Galton. *Nature* **32**, 507–510 (1885).
114. Algina, J. & Keselman, H. J. Comparing squared multiple correlation coefficients: Examination of a confidence interval and a test significance. *Psychol. Methods* **4**, 76–83 (1999).
115. Mann, H. B. & D. R. Whitney. On a test of whether one of two random variables is stochastically larger than the other. *Ann. Math. Stat.* **18**, 50–60 (1947).
116. Wenzel, R. N. Resistance of solid surfaces to wetting by water. *Ind. Eng. Chem.* **28**, 988–994 (1936).
117. Voiry, D. *et al.* High-quality graphene via microwave reduction of solution-exfoliated graphene oxide. *Science (80-.).* **3398**, 1–7 (2016).
118. Zhu, Y., Cai, W., Piner, R. D., Velamakanni, A. & Ruoff, R. S. Transparent self-assembled films of reduced graphene oxide platelets. *Appl. Phys. Lett.* **95**, 10–12 (2009).
119. Nair, R. R. *et al.* Fine Structure Constant Defines Visual Transparency of Graphene. doi:10.1126/science.1156965
120. Dickinson, W. W., Kumar, H. V., Adamson, D. H. & Schniepp, H. C. High-throughput optical thickness and size characterization of 2D materials.

Nanoscale **10**, 14441–14447 (2018).

121. Dimiev, A. M. *et al.* Terms of Use Mechanism of Graphene Oxide. 3060–3068 (2014).
122. Roddaro, S., Pingue, P., Piazza, V., Pellegrini, V. & Beltram, F. The optical visibility of graphene: Interference colors of ultrathin graphite on SiO2. *Nano Lett.* **7**, 2707–2710 (2007).
123. Nel, A. E. *et al.* Understanding biophysicochemical interactions at the nano-bio interface. *Nat. Mater.* **8**, 543–557 (2009).
124. Luo, N. *et al.* PEGylated graphene oxide elicits strong immunological responses despite surface passivation. *Nat. Commun.* **8**, 1–10 (2017).
125. Trusovas, R. *et al.* Recent Advances in Laser Utilization in the Chemical Modification of Graphene Oxide and Its Applications. *Adv. Opt. Mater.* **4**, 37–65 (2016).
126. Kassaee, M. Z., Motamedi, E. & Majdi, M. Magnetic Fe3O4-graphene oxide/polystyrene: Fabrication and characterization of a promising nanocomposite. *Chem. Eng. J.* **172**, 540–549 (2011).
127. Che Man, S. H., Thickett, S. C., Whittaker, M. R. & Zetterlund, P. B. Synthesis of polystyrene nanoparticles 'armoured' with nanodimensional graphene oxide sheets by miniemulsion polymerization. *J. Polym. Sci. Part A Polym. Chem.* **51**, 47–58 (2013).
128. Dittrich, B., Wartig, K.-A., Hofmann, D., Mülhaupt, R. & Schartel, B. Flame retardancy through carbon nanomaterials: Carbon black, multiwall nanotubes, expanded graphite, multi-layer graphene and graphene in polypropylene. *Polym. Degrad. Stab.* **98**, 1495–1505 (2013).
129. Huang, Y. *et al.* Polypropylene/Graphene Oxide Nanocomposites Prepared by In Situ Ziegler−Natta Polymerization. *Chem. Mater.* **22**, 4096–4102 (2010).
130. Yun, Y. S. *et al.* Reinforcing effects of adding alkylated graphene oxide to polypropylene. *Carbon N. Y.* **49**, 3553–3559 (2011).
131. Wang, D. *et al.* Dielectric properties of reduced graphene oxide/polypropylene composites with ultralow percolation threshold. *Polymer (Guildf).* **54**, 1916–1922 (2013).

132. Yuan, B. *et al.* Preparation of functionalized graphene oxide/polypropylene nanocomposite with significantly improved thermal stability and studies on the crystallization behavior and mechanical properties. *Chem. Eng. J.* **237**, 411–420 (2014).
133. Liu, M., Guo, B., Du, M., Chen, F. & Jia, D. Halloysite nanotubes as a novel β-nucleating agent for isotactic polypropylene. *Polymer (Guildf).* **50**, 3022–3030 (2009).
134. Nguyen, D. A. *et al.* Morphological and physical properties of a thermoplastic polyurethane reinforced with functionalized graphene sheet. *Polym. Int.* **58**, 412–417 (2009).
135. Cai, D., Yusoh, K. & Song, M. The mechanical properties and morphology of a graphite oxide nanoplatelet/polyurethane composite. *Nanotechnology* **20**, 085712 (2009).
136. Xu, Y., Hong, W., Bai, H., Li, C. & Shi, G. Strong and ductile poly(vinyl alcohol)/graphene oxide composite films with a layered structure. *Carbon N. Y.* **47**, 3538–3543 (2009).
137. Song, P. *et al.* Fabrication of exfoliated graphene-based polypropylene nanocomposites with enhanced mechanical and thermal properties. *Polymer (Guildf).* **52**, 4001–4010 (2011).
138. Lee, J. *et al.* Graphene oxide nanoplatelets composite membrane with hydrophilic and antifouling properties for wastewater treatment. *J. Memb. Sci.* **448**, 223–230 (2013).
139. Compton, O. C. & Nguyen, S. T. Graphene oxide, highly reduced graphene oxide, and graphene: Versatile building blocks for carbon-based materials. *Small* **6**, 711–723 (2010).
140. Chen, L. *et al.* Ion sieving in graphene oxide membranes via cationic control of interlayer spacing. *Nature* **550**, 1–4 (2017).
141. Kuzum, D. *et al.* Transparent and flexible low noise graphene electrodes for simultaneous electrophysiology and neuroimaging. *Nat. Commun.* **5**, 1–10 (2014).
142. Morimoto, N. *et al.* Real-Time, in Situ Monitoring of the Oxidation of Graphite:

Lessons Learned. (2017). doi:10.1021/acs.chemmater.6b04807

143. Mariconda, A. *et al.* Synthesis of ruthenium catalysts functionalized graphene oxide for self-healing applications. *Polym. (United Kingdom)* **69**, 330–342 (2015).
144. Acocella, M. R. *et al.* Graphene oxide as a catalyst for ring opening reactions in amine crosslinking of epoxy resins. *RSC Adv.* **6**, 23858–23865 (2016).
145. Casolaro, M. & Casolaro, I. Polyelectrolyte Hydrogel Platforms for the Delivery. *Gels* **2**, (2016).
146. Jaspers, M. *et al.* Ultra-responsive soft matter from strain-stiffening hydrogels. *Nat. Commun.* **5**, 5808 (2014).
147. Deshpande, S. R., Hammink, R., Nelissen, F. H. T., Rowan, A. E. & Heus, H. A. A biomimetic stress sensitive hydrogel controlled by DNA nanoswitches. (2017). doi:10.1021/acs.biomac.7b00964
148. Yu, X. *et al.* Graphene-based smart materials. *Nat. Rev. Mater.* **2**, 1–14 (2017).
149. Stankovich, S. *et al.* Graphene-based composite materials. *Nature* **442**, 282–286 (2006).
150. Chow, E. K. & Ho, D. Cancer Nanomedicine- From Drug Delivery to Imaging.pdf. *ScienceTranslationalMedicine* **5**, 1–13 (2013).
151. Li, H. *et al.* Ultrathin, Molecular-Sieving Graphene Oxide Membranes for Selective Hydrogen Separation. *Science (80-.).* **342**, 95–98 (2013).
152. Li, D. & Kaner, R. B. Graphene-Based Materials. *Science (80-.).* **320**, 1170–1171 (2008).
153. Li, D., Müller, M. B., Gilje, S., Kaner, R. B. & Wallace, G. G. Processable aqueous dispersions of graphene nanosheets. *Nat. Nanotechnol.* **3**, 101–105 (2008).
154. Gudarzi, M. M. & Sharif, F. Self assembly of graphene oxide at the liquid–liquid interface: A new route to the fabrication of graphene based composites. *Soft Matter* **7**, 3432 (2011).
155. Kumar, H. V., Huang, K. Y.-S., Ward, S. P. & Adamson, D. H. Altering and investigating the surfactant properties of graphene oxide. *J. Colloid Interface Sci.* **493**, 365–370 (2017).

156. Xu, Y., Bai, H., Lu, G., Li, C. & Shi, G. Flexible Graphene Films via the Filtration of Water-Soluble. 5856–5857 (2008).
157. Guo, P., Song, H. & Chen, X. Hollow graphene oxide spheres self-assembled by W/O emulsion. *J. Mater. Chem.* **20**, 4867 (2010).
158. Yang, S., Feng, X., Ivanovici, S. & Müllen, K. Fabrication of Graphene-Encapsulated Oxide Nanoparticles: Towards High-Performance Anode Materials for Lithium Storage. *Angew. Chemie Int. Ed.* **49**, 8408–8411 (2010).
159. Park, S. *et al.* Hydrazine-reduction of graphite- and graphene oxide. *Carbon N. Y.* **49**, 3019–3023 (2011).
160. Najafi, F. & Rajabi, M. Thermal gravity analysis for the study of stability of graphene oxide–glycine nanocomposites. *Int. Nano Lett.* **5**, 187–190 (2015).
161. Song, J., Wang, X. & Chang, C.-T. Preparation and Characterization of Graphene Oxide. *J. Nanomater.* **2014**, 1–6 (2014).
162. Wojtoniszak, M. *et al.* Synthesis, dispersion, and cytocompatibility of graphene oxide and reduced graphene oxide. *Colloids Surfaces B Biointerfaces* **89**, 79–85 (2011).
163. Abdolhosseinzadeh, S., Asgharzadeh, H. & Seop Kim, H. Fast and fully-scalable synthesis of reduced graphene oxide. *Sci. Rep.* **5**, 10160 (2015).
164. Dreyer, D. R., Sungjin, P., Bielawski, W. & Ruo, R. S. The chemistry of graphene oxide. *Chem. Soc. Rev.* **39**, 228–240 (2010).
165. Eigler, S., Dotzer, C. & Hirsch, A. Visualization of defect densities in reduced graphene oxide. *Carbon N. Y.* **50**, 3666–3673 (2012).
166. Mohanta, Z., Atreya, H. S. & Srivastava, C. Correlation between defect density in mechanically milled graphite and total oxygen content of graphene oxide produced from oxidizing the milled graphite. *Sci. Rep.* **8**, 15773 (2018).
167. Acik, M. *et al.* The Role of Oxygen during Thermal Reduction of Graphene Oxide Studied by Infrared Absorption Spectroscopy. *J. Phys. Chem. C* **115**, 19761–19781 (2011).
168. Khanra, P. *et al.* 7,7,8,8-Tetracyanoquinodimethane-assisted one-step electrochemical exfoliation of graphite and its performance as an electrode material. *Nanoscale* **6**, 4864–4873 (2014).

169. Jeong, H. K., Jin, M. H., So, K. P., Lim, S. C. & Lee, Y. H. Tailoring the characteristics of graphite oxides by different oxidation times. *J. Phys. D. Appl. Phys.* **42**, 065418 (2009).
170. Chen, J. *et al.* Water-enhanced oxidation of graphite to graphene oxide with controlled species of oxygenated groups. *Chem. Sci.* (2016). doi:10.1039/c5sc03828f
171. Qiu, Y., Collin, F., Hurt, R. H. & Külaots, I. Thermochemistry and kinetics of graphite oxide exothermic decomposition for safety in large-scale storage and processing. *Carbon N. Y.* **96**, 20–28 (2016).
172. Cançado, L. G. *et al.* Quantifying defects in graphene via Raman spectroscopy at different excitation energies. *Nano Lett.* **11**, 3190–3196 (2011).
173. Lucchese, M. M. *et al.* Quantifying ion-induced defects and Raman relaxation length in graphene. *Carbon N. Y.* (2010). doi:10.1016/j.carbon.2009.12.057
174. Childres, I., Jauregui, L. A., Tian, J. & Chen, Y. P. Effect of oxygen plasma etching on graphene studied using Raman spectroscopy and electronic transport measurements. *New J. Phys.* (2011). doi:10.1088/1367-2630/13/2/025008
175. Weitz, R. T. *et al.* Electronic transport of chemically reduced graphene oxide. *Nano Lett.* **7**, 3499–3503 (2007).
176. Dimiev, A. M., Alemany, L. B. & Tour, J. M. Graphene oxide. Origin of acidity, its instability in water, and a new dynamic structural model. *ACS Nano* (2013). doi:10.1021/nn3047378
177. Eigler, S., Dotzer, C., Hof, F., Bauer, W. & Hirsch, A. Sulfur species in graphene oxide. *Chem. - A Eur. J.* **19**, 9490–6 (2013).
178. Chook, S. W. *et al.* Antibacterial hybrid cellulose–graphene oxide nanocomposite immobilized with silver nanoparticles. *RSC Adv.* **5**, 26263–26268 (2015).
179. He, G. *et al.* Fe3O4@graphene oxide composite: A magnetically separable and efficient catalyst for the reduction of nitroarenes. *Mater. Res. Bull.* **48**, 1885–1890 (2013).
180. Li, L. *et al.* Polystyrene sphere-assisted one-dimensional nanostructure arrays:

Synthesis and applications. *J. Mater. Chem.* **21**, 40–56 (2011).

181. Woltornist, S. J. *et al.* Controlled 3D Assembly of Graphene Sheets to Build Conductive, Chemically Selective and Shape-Responsive Materials. *Adv. Mater.* **29**, (2017).
182. Fang, Q., Zhou, X., Deng, W., Zheng, Z. & Liu, Z. Freestanding bacterial cellulose-graphene oxide composite membranes with high mechanical strength for selective ion permeation. *Sci. Rep.* **6**, 33185 (2016).
183. Yao, Q. *et al.* 3D assembly based on 2D structure of Cellulose Nanofibril/Graphene Oxide Hybrid Aerogel for Adsorptive Removal of Antibiotics in Water. *Sci. Rep.* **7**, 45914 (2017).
184. Thakur, V. K. & Voicu, S. I. Recent advances in cellulose and chitosan based membranes for water purification: A concise review. *Carbohydr. Polym.* **146**, 148–165 (2016).
185. Wilson, N. R. *et al.* Graphene Oxide: Structural Analysis and Application as a Highly Transparent Support for Electron Microscopy. *ACS Nano* **3**, 2547–2556 (2009).
186. Liang, H.-W. *et al.* Robust and Highly Efficient Free-Standing Carbonaceous Nanofiber Membranes for Water Purification. *Adv. Funct. Mater.* **21**, 3851–3858 (2011).
187. Dong, Y. *et al.* Graphene oxide–Fe3O4 magnetic nanocomposites with peroxidase-like activity for colorimetric detection of glucose. *Nanoscale* **4**, 3969 (2012).
188. Su, J., Cao, M., Ren, L. & Hu, C. Fe_3O_4–Graphene Nanocomposites with Improved Lithium Storage and Magnetism Properties. *J. Phys. Chem. C* **115**, 14469–14477 (2011).
189. Chen, L., Tang, Y., Wang, K., Liu, C. & Luo, S. Direct electrodeposition of reduced graphene oxide on glassy carbon electrode and its electrochemical application. *Electrochem. commun.* **13**, 133–137 (2011).
190. Song, Y., Qu, K., Zhao, C., Ren, J. & Qu, X. Graphene Oxide: Intrinsic Peroxidase Catalytic Activity and Its Application to Glucose Detection. *Adv. Mater.* **22**, 2206–2210 (2010).

191. Zhang, R., Hu, Y., Xu, J., Fan, W. & Chen, Z. Flammability and thermal stability studies of styreneebutyl acrylate copolymer/graphite oxide nanocomposite. doi:10.1016/j.polymdegradstab.2004.01.020
192. Li, G. L. *et al.* Organo- and Water-Dispersible Graphene Oxide−Polymer Nanosheets for Organic Electronic Memory and Gold Nanocomposites. *J. Phys. Chem. C* **114**, 12742–12748 (2010).
193. Shao, G. *et al.* Graphene oxide: The mechanisms of oxidation and exfoliation. *J. Mater. Sci.* **47**, 4400–4409 (2012).

Chapter 10: Appendix:

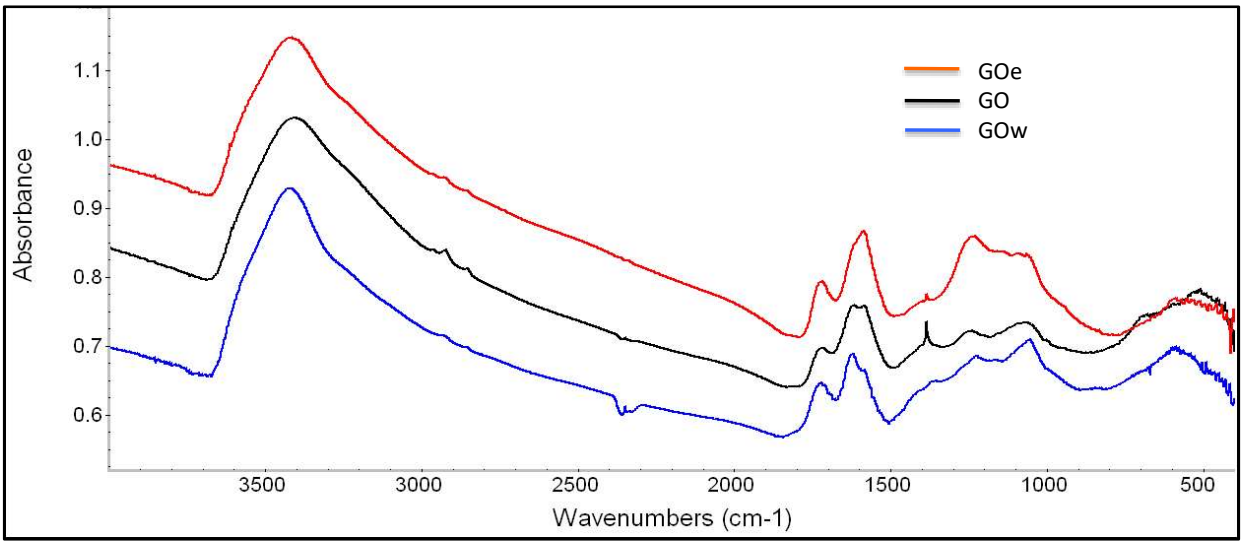

Figure 10-1. FTIR spectra of original GO, its emulsion fraction (GOe), and its water fraction (GOw).

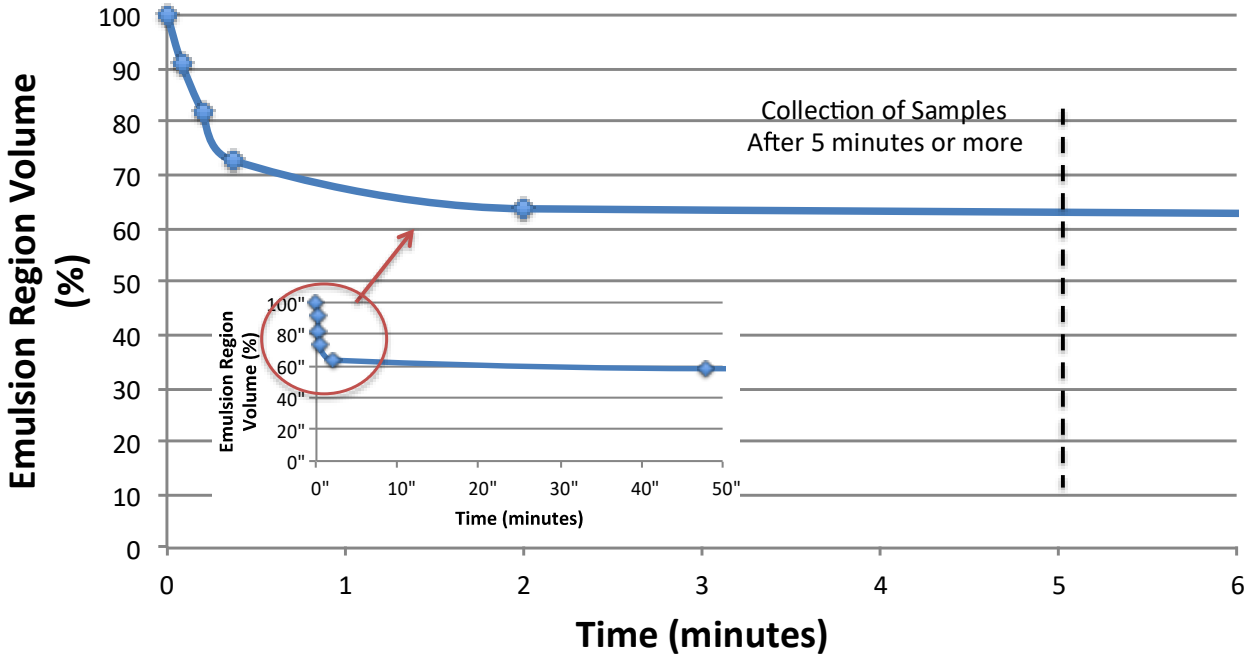

Figure 10-2. Plot of emulsion phase volume versus settling time.

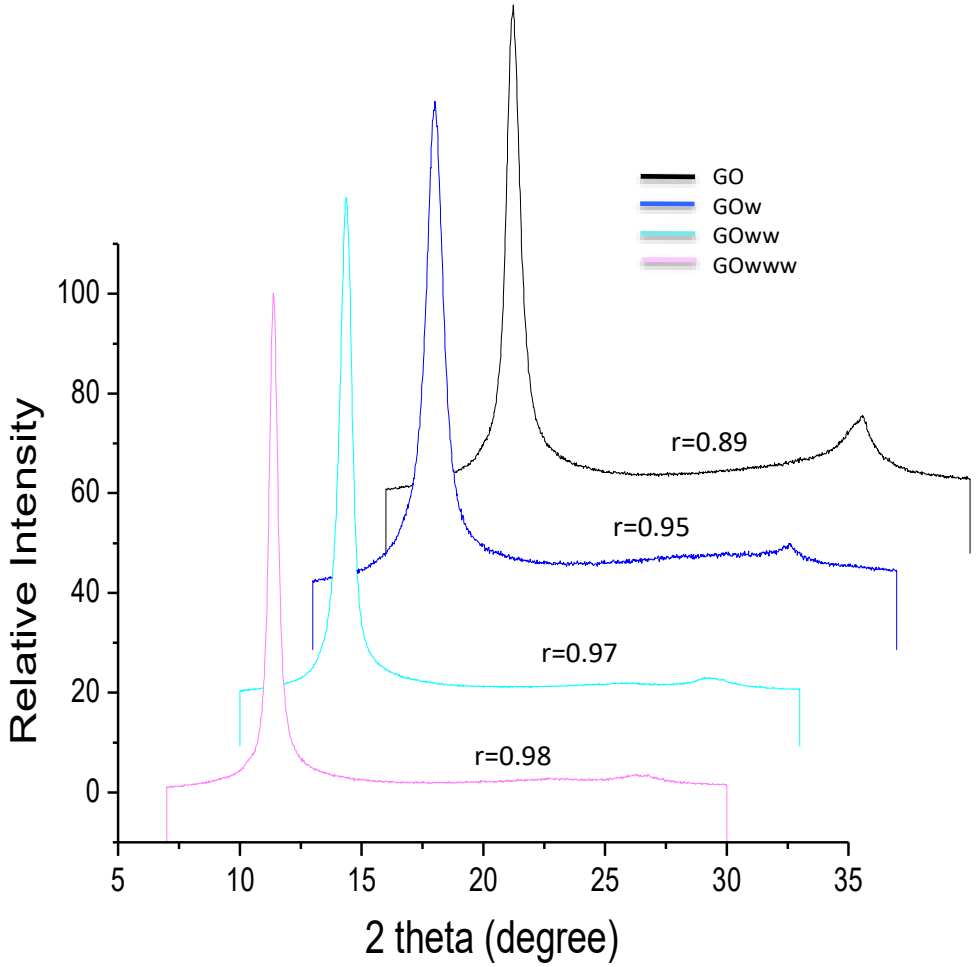

Figure 10-3. XRD of water region GO fractions with the corresponding r values. Increasing fraction resulting in a small, but significant, increase in the oxidation level of the material.

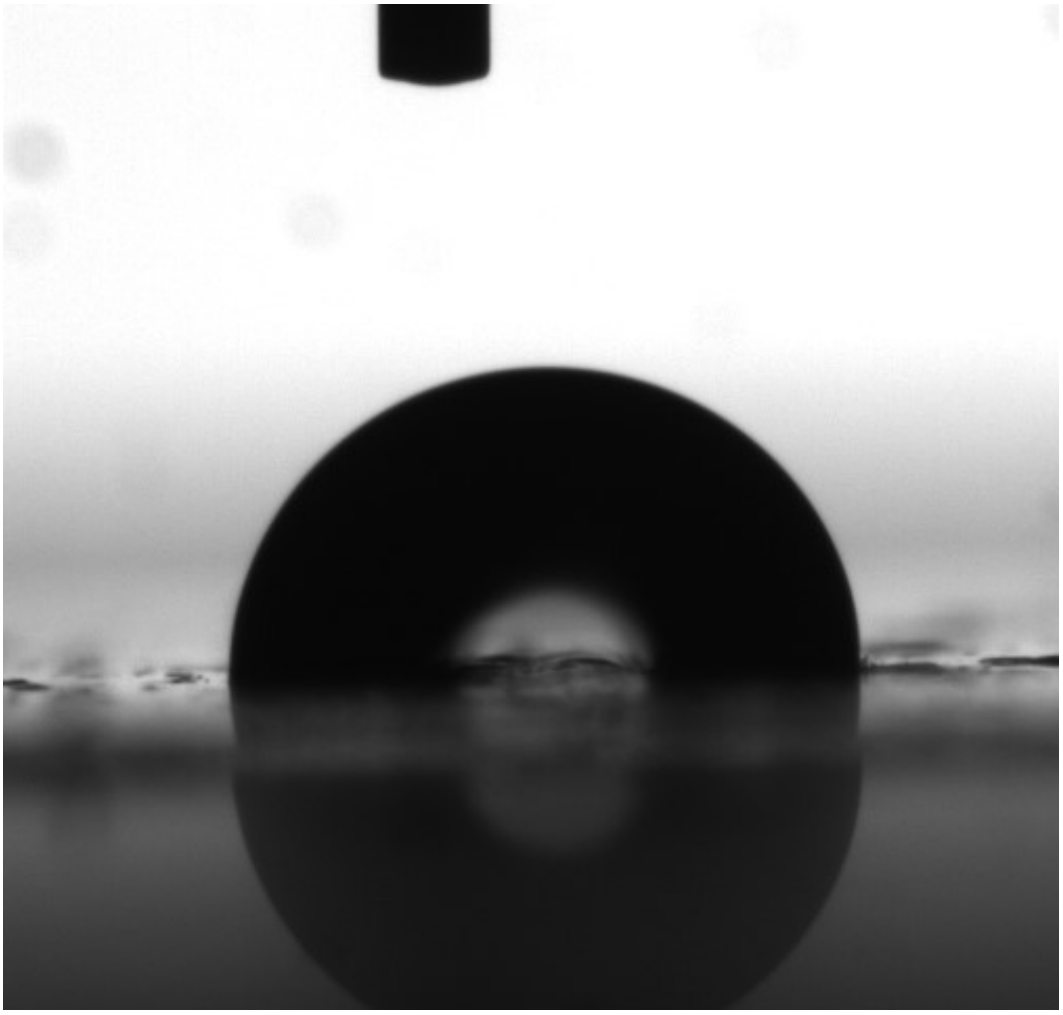

Figure 10-4. Water droplet picture for contact angle measurement.

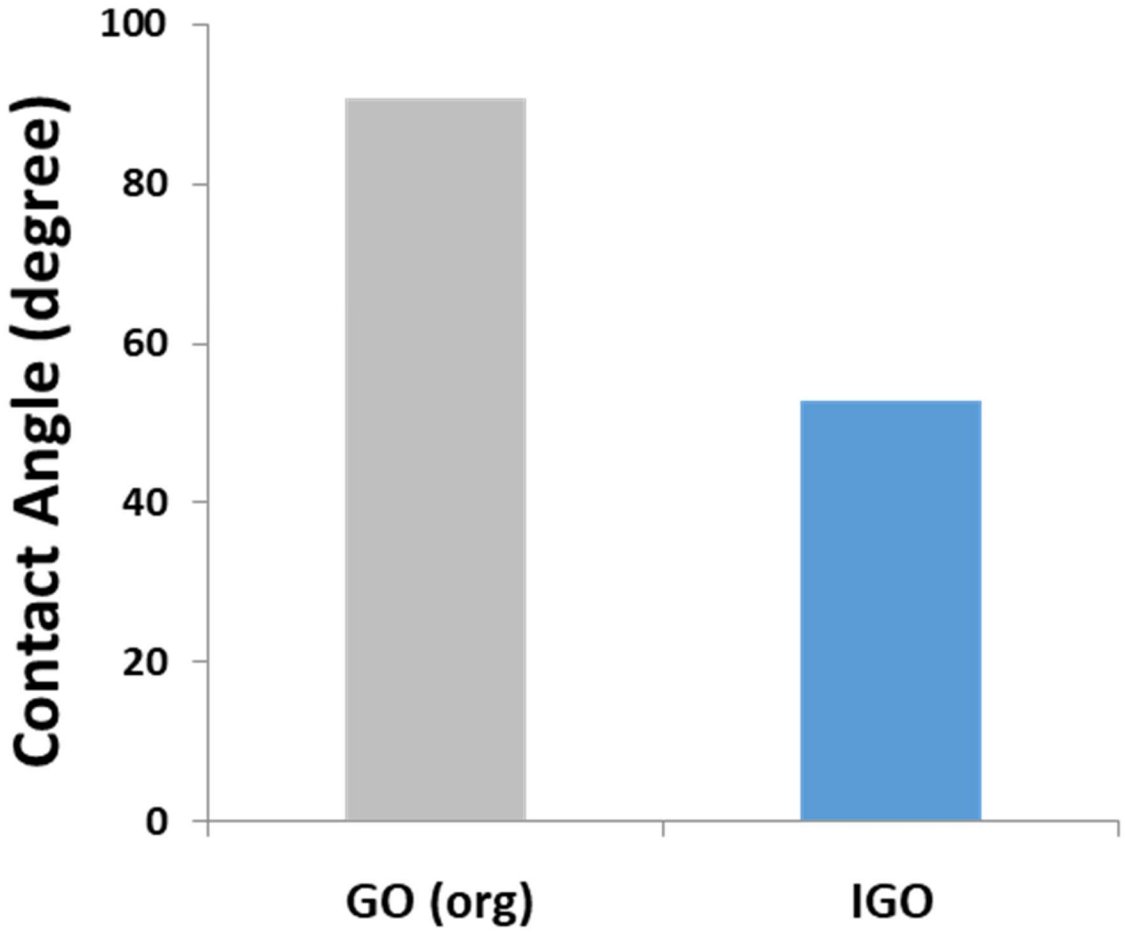

Figure 10-5 Contact angle values for original graphene oxide (GO (org)) and IGO.

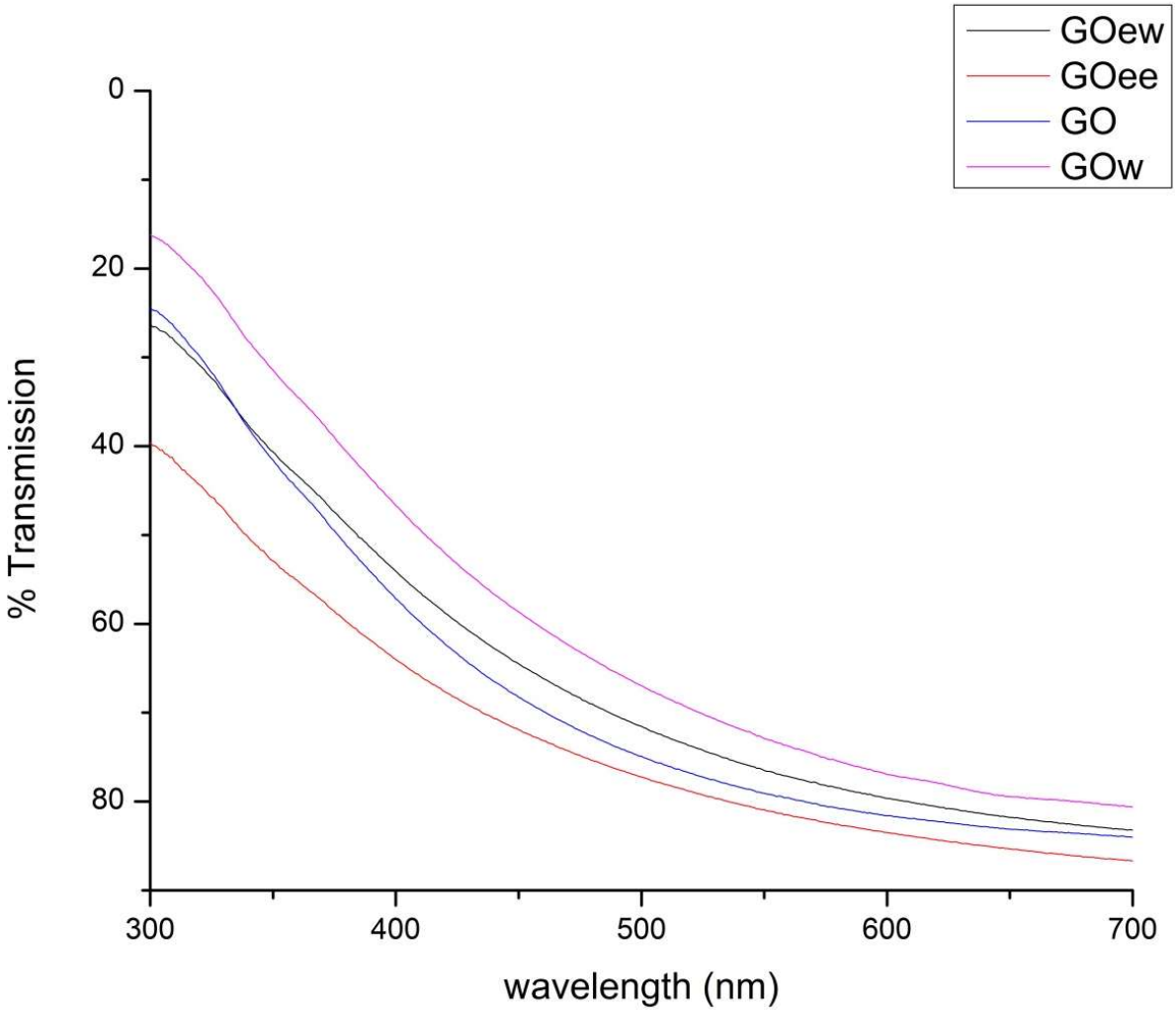

Figure 10-6. UV-vis plots for film-2t made from different GO fractions with a surface density of 0.24mg/cm^2.

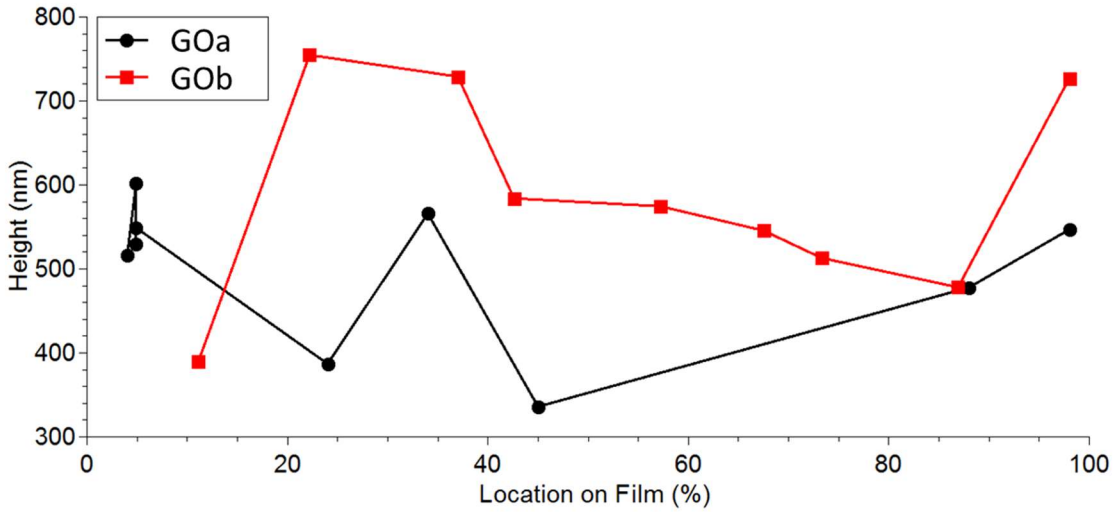

Figure 10-7. GO film thickness distribution as determined by AFM studies. The GO films are made from 0.24mg/cm^2 surface density of GO material on a glass substrate. Synthesis methods for GOa[1] and GOb[3] are different with mean thickness distribution of 501nm and 588nm.

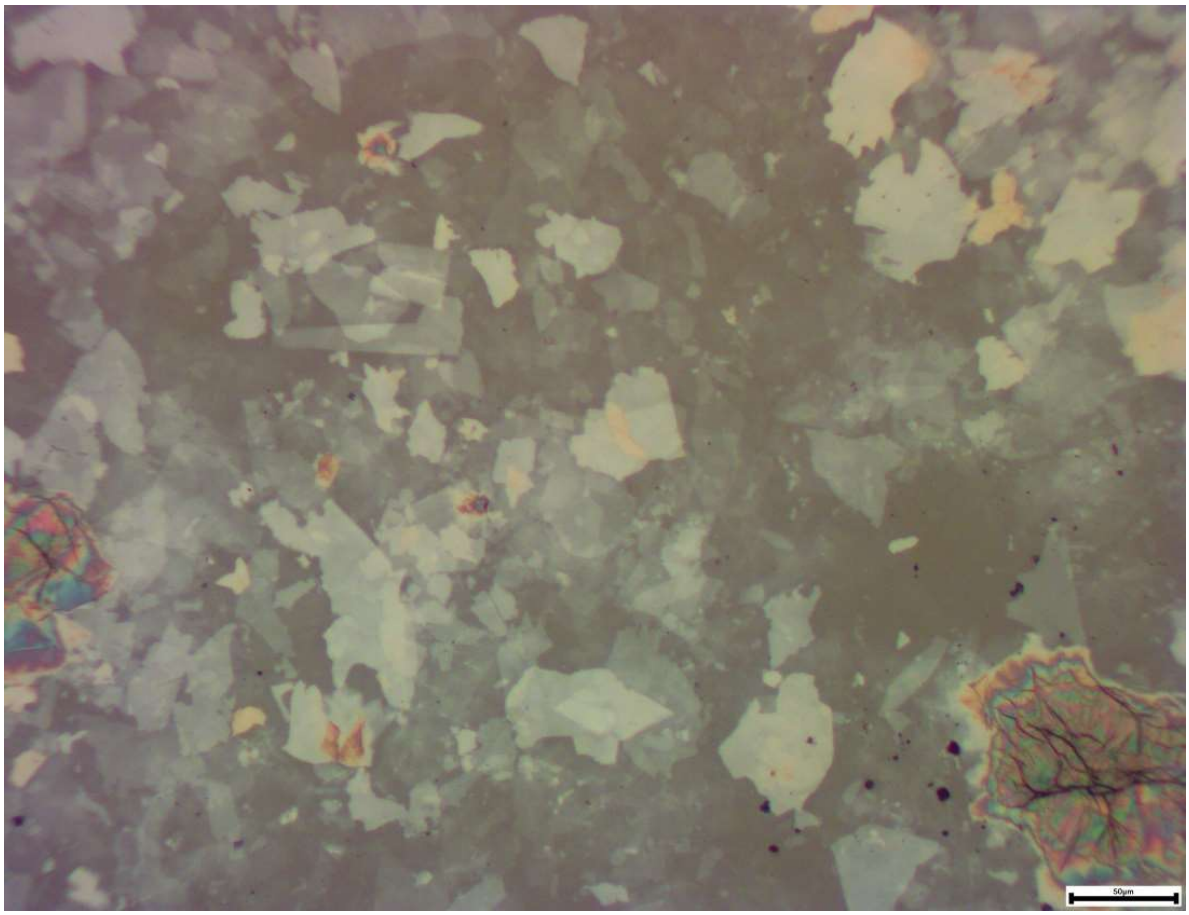

Figure 10-8. GO sheets on a glass slide using optical microscopy. Scalebar size is 50 µm.

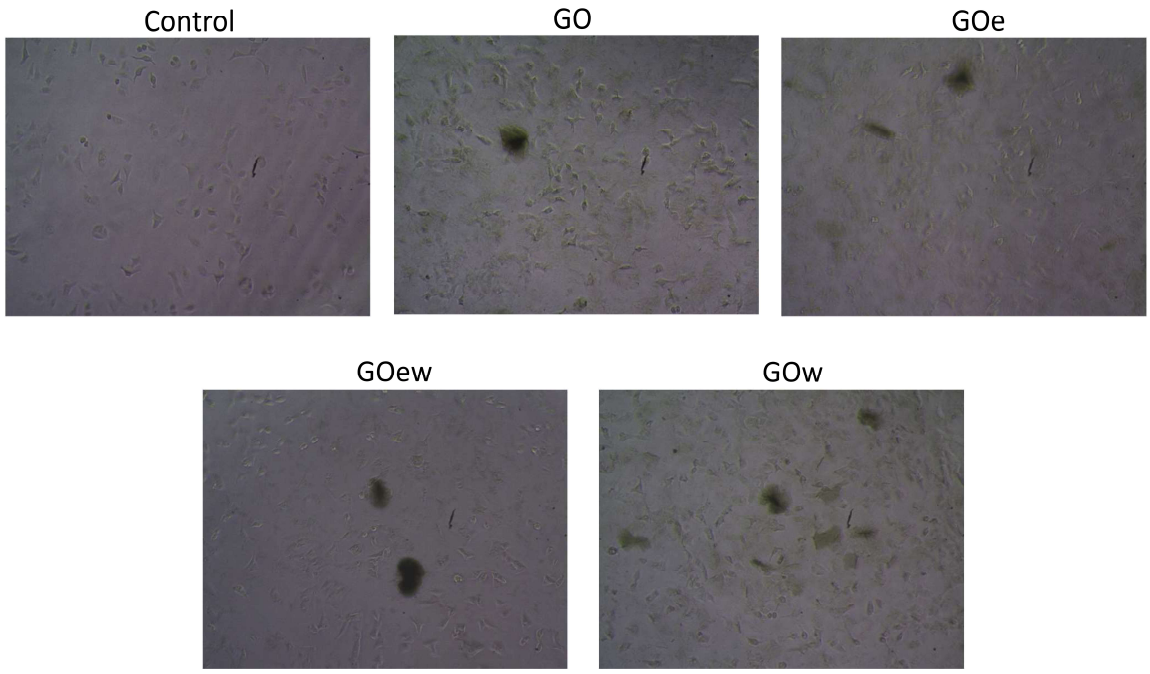

Figure 10-9. A549 cells exposed to PEG-GO samples (dilution 1/400) for 24 hours.

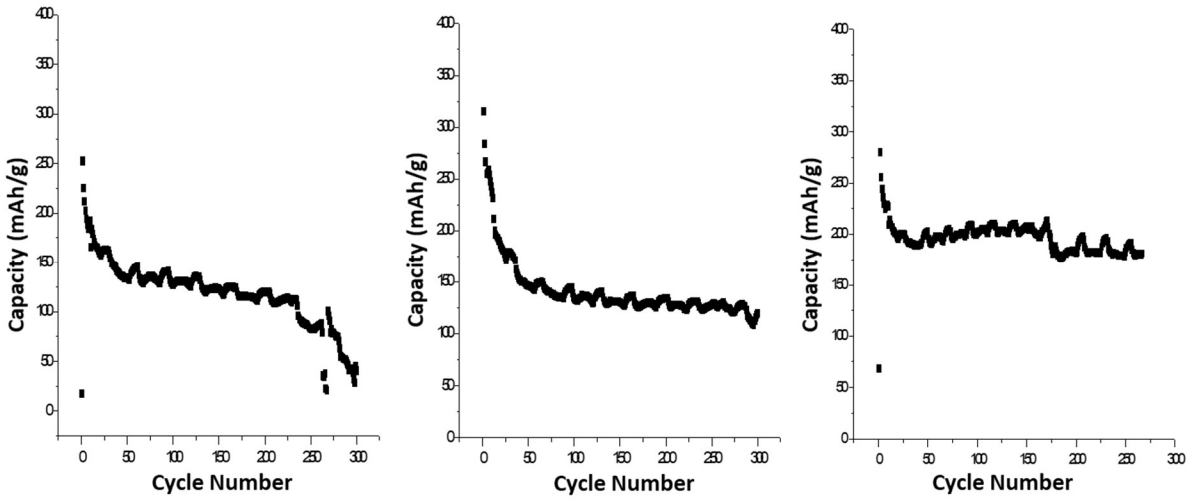

Figure 10-10. Comparison of loss of capacity with increasing cycle number for batteries containing GOe, GO, and GOw.

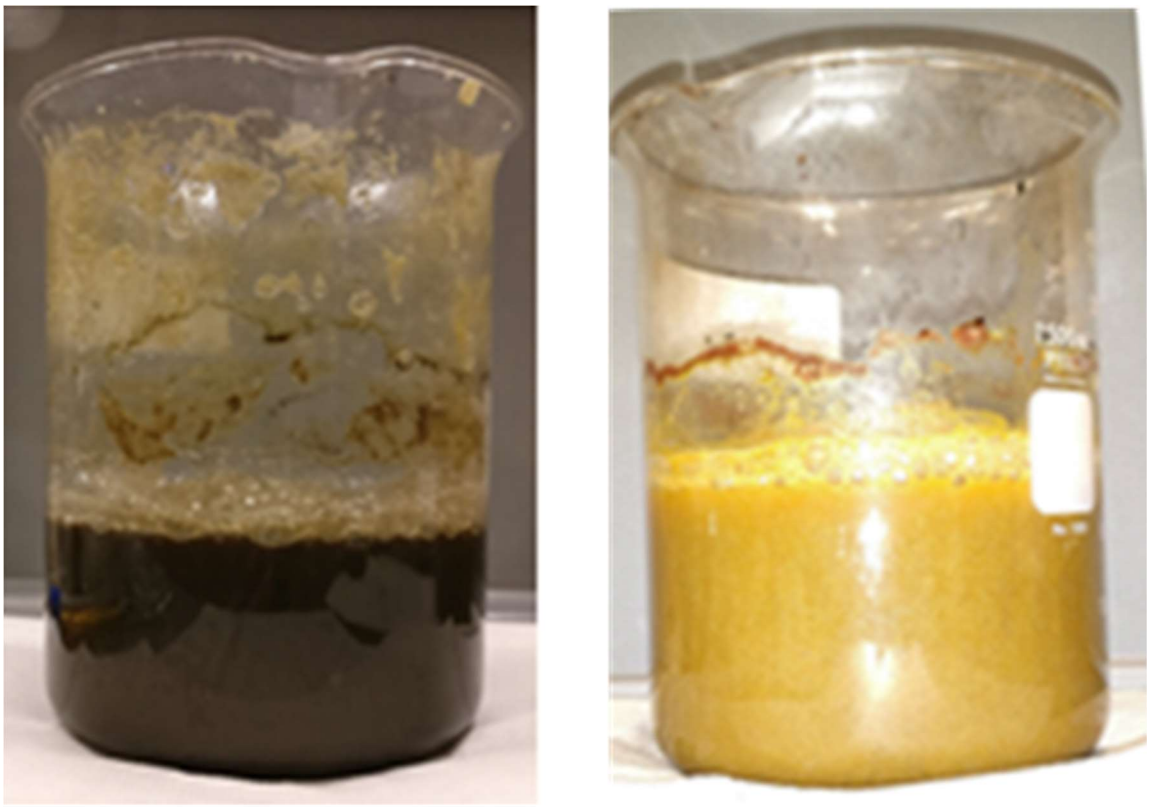

Figure 10-11. Picture of quenched HGO (black color in the left) and SGO (yellow color in the right) reaction products.

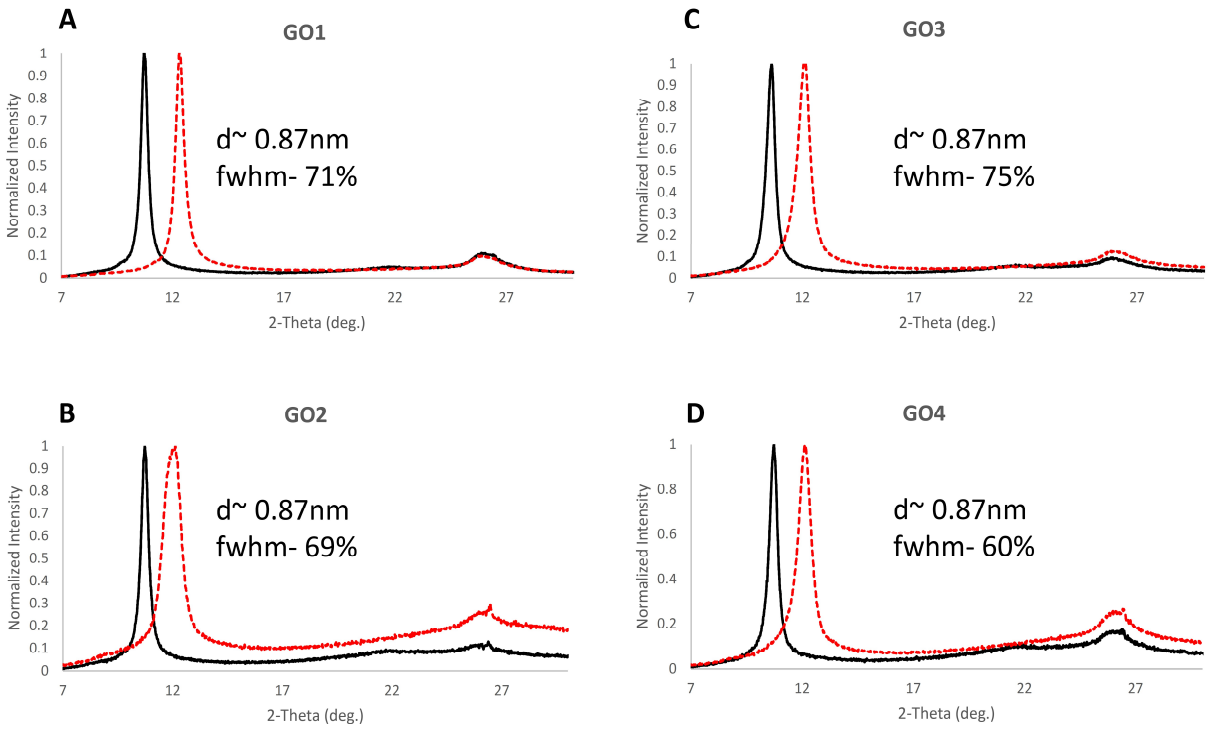

Figure 10-12. XRD patterns of four GO samples GO1, GO2, GO3, and GO4 done in 2015 (dotted line) and in 2018 (solid line). Typically, GO peak lies in 10-13 2θ range, and G peak lies in the 26-27 2θ value range.

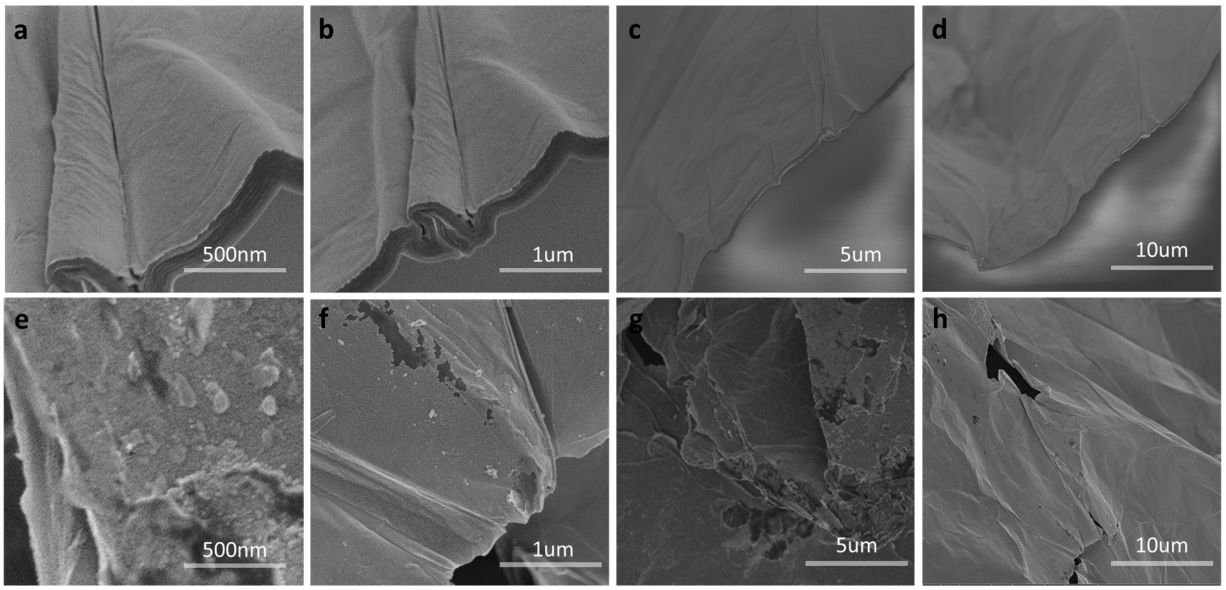

Figure 10-13. a-d) SEM of 0 yr GO sheets, and e-h) SEM of 3 yr GO sheets.

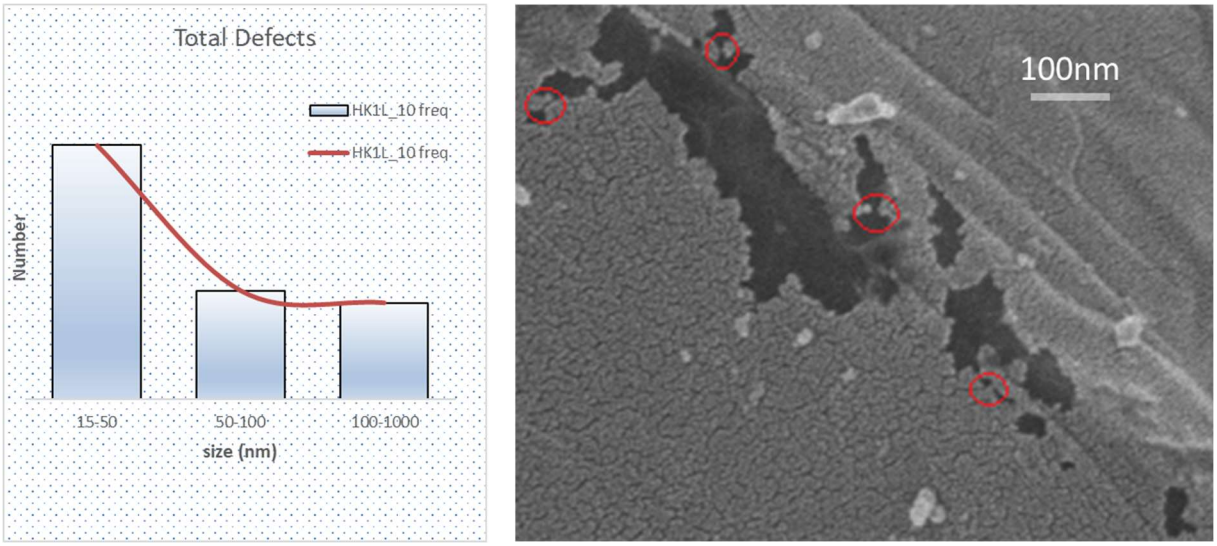

Figure 10-14. Size distribution of defect sites calculated from SEM picture of 3 yr GO sample. The scale of SEM picture- 100nm.